The clustered nucleus—cluster structures in stable and unstable nuclei

IOP PUBLISHING REPORTS ON PROGRESS IN PHYSICS

Rep. Prog. Phys. **70** (2007) 2149–2210 doi:10.1088/0034-4885/70/12/R03

The clustered nucleus—cluster structures in stable and unstable nuclei

Martin Freer

School of Physics and Astronomy, University of Birmingham, Edgbaston, Birmingham B15 2TT, UK

Received 13 August 2007, in final form 4 October 2007
Published 16 November 2007
Online at stacks.iop.org/RoPP/70/2149

Abstract

The subject of clustering has a lineage which runs throughout the history of nuclear physics. Its attraction is the simplification of the often uncorrelated behaviour of independent particles to organized and coherent quasi-crystalline structures. In this review the ideas behind the development of clustering in light nuclei are investigated, mostly from the stand-point of the harmonic oscillator framework. This allows a unifying description of alpha-conjugate and neutron-rich nuclei, alike. More sophisticated models of clusters are explored, such as antisymmetrized molecular dynamics. A number of contemporary topics in clustering are touched upon; the 3α-cluster state in ^{12}C, nuclear molecules and clustering at the drip-line. Finally, an understanding of the ^{12}C + ^{12}C resonances in ^{24}Mg, within the framework of the theoretical ideas developed in the review, is presented.

(Some figures in this article are in colour only in the electronic version)

This article was invited by Professor W Nazarewicz.

Contents

1. Introduction

The propensity for objects to congregate on all physical scales is striking. Underpinning this must be some significant reduction in potential energy or gain in stability. On the largest scale known to man, the universe, the survey of the 2dF galaxy redshift [1] shows matter congregates into filament-like structures. In this case, these are gravitationally assembled structures which grew from inhomogeneities post 'Big Bang'. The assemblage of stars into galaxies or the gravitational binding of planets within the solar system involve further reductions in scale, but yet more clustering. On the more human level, many biological systems have developed strategies which recognize that some organization into collective type behaviour offers some evolutionary advantage. For example, fish shoal to distract predators and predators hunt in packs to maximize success rates in kills. Subatomic systems also recognize the importance of order and symmetry. Atoms form molecules in the liquid or gas phase and crystals in the solid. Quarks find themselves confined within hadrons with only particular numbers of constituents (2 or 3). It would, therefore, be highly surprising if such a phenomenon did not extend to the nuclear domain.

Unlike the essentially pictorial view of a rather static collection of protons and neutrons in a spherical nuclear droplet, the nucleus is a highly dynamic collection of nucleons whose velocities can reach an appreciable fraction of the speed of light. In their dynamics, these nucleons possess correlations. In order to minimize the repulsion originating from the Pauli exclusion principle (PEP) like-nucleons pair with spins anti-aligned and in orbitals with maximal overlap, leaving a spin-zero entity. Of course, it is possible for both pairs of protons and neutrons to repeat exactly the same dance resulting in a maximally correlated quartet (2p + 2n) known as the α-particle. These correlations provide the subunits with their energetic advantage and for this reason the α-particle has one of the highest binding energies per nucleon amongst the light nuclei. Moreover, just as noble gases, the ^{4}He nucleus has a closed shell and is rather inert. It has a first excited state close to 20 MeV, whereas the average binding energy per nucleon across the whole of nuclei is less than 8 MeV per nucleon. This implies that the α-particle can propagate within the nucleus relatively unperturbed for a significant time. More precisely, it has been shown that the nuclear surface plays a critical role in the formation of clusters. When the nuclear density falls to one third of normal nuclear matter density, there is expected to be a phase change and nucleons condense into α-particles [2]. Such correlations may be witnessed in heavy nuclei in the form of significant preformation probabilities in α-decaying systems—essentially a measure of the degree of clusterization.

For this reason it has largely been the α-particle which has dominated the spectrum of cluster states throughout the history of the subject. Though other closed shell systems, e.g. ^{16}O and ^{12}C (which has a closed sub-shell) offer some possibilities. Some of the possible cluster candidates are illustrated in figure 3. However, both ^{16}O and ^{12}C have relatively low energy first excited states and decay thresholds which results in their limited resistance against the destabilizing influence of other dynamics within the nucleus. Herein lies the competition between the cluster and the mean-field.

Most interactions in nature serve to create a minimum in some variable. If this variable happens to be a spatial arrangement then geometric patterns emerge. If, for the purpose of illustration, the system is restricted to two dimensions then the types of patterns that emerge may be readily recognized. Figure 1 shows a calculation using an α-cluster model (section 6.1) for a range of light nuclei in which the α-particle constituents have been constrained to lie within a plane [3]. The particles arrange themselves to maximize the number of interactions with their neighbours, optimizing the binding energy. As a result an interlocking hexagonal pattern is produced. Such patterns arise naturally in two-dimensional systems elsewhere, for

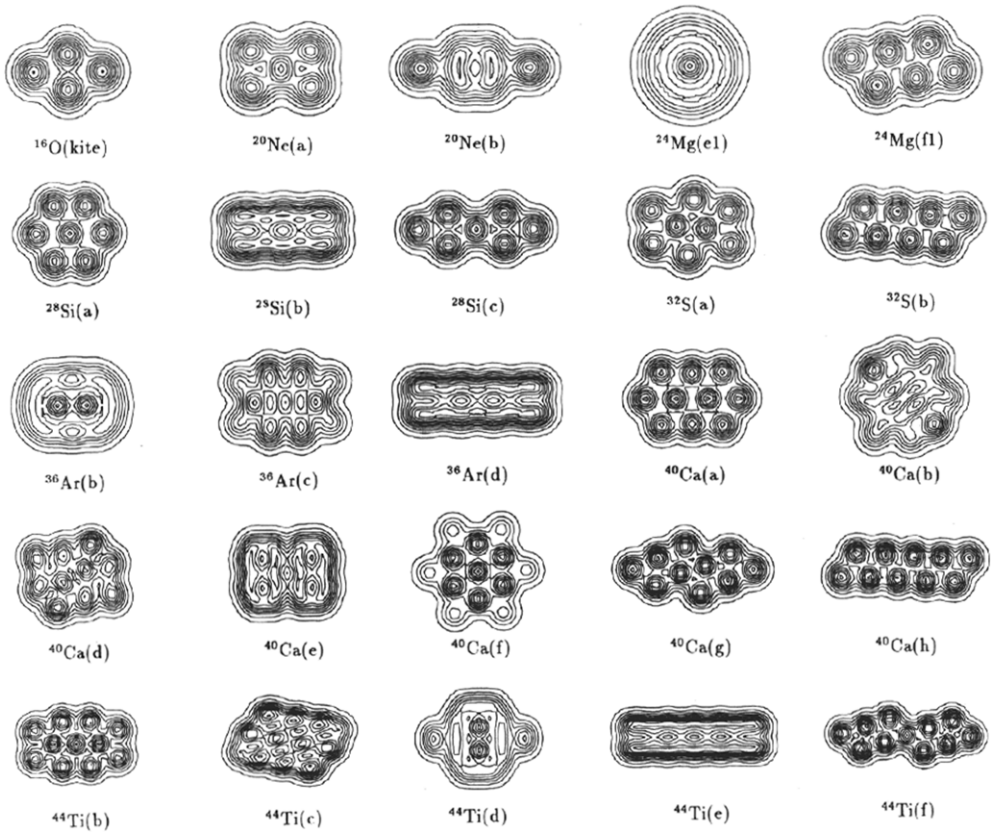

Figure 1. Alpha cluster model (ACM) calculation for 2D structures in a range of light nuclei [3]. The α-particles, which are explicitly defined in this model, arrange themselves into interlocking hexagonal structures.

example, the overlapping planes of the carbon atoms in graphite, or in the solution arrived at by the honeybee in determining the optimal structure which permits the minimum use of wax whilst maximizing honey storage.

The appearance of clusters out of a mean-field, constructed from the nucleon–nucleon interaction, is an interesting problem indicating that eventually the mean-field itself must be shaped by the emergence of the clusters. This we examine in the following section. Evidence for the ability of the mean-field to recognize the importance of the cluster comes from surprising sources. For example, the *ab initio* Greens function Monte Carlo (GFMC) calculations of ^{8}Be [4]. These calculations are *ab initio* in the sense that they predict the structure of nuclei based upon a starting point which is the nucleon–nucleon interaction expressed in terms of all two-body and three-body components. In this manner the interaction is not an effective interaction. It is somewhat remarkable that such an approach yields a ^{8}Be ground state, figure 2, that is clearly clustered. At this point it is thus tempting to assert that the nucleus ^{8}Be corresponds to an α–α cluster structure in the ground state.

There have been many recent developments in the field of nuclear clusters including the ability to perform *ab initio* calculations of the light nuclei, such as the GFMC methods and antisymmetrized molecular dynamics (AMD) (section 6.3), the appearance of both experimental and theoretical evidence for molecular structures (section 7.2) and the renewed

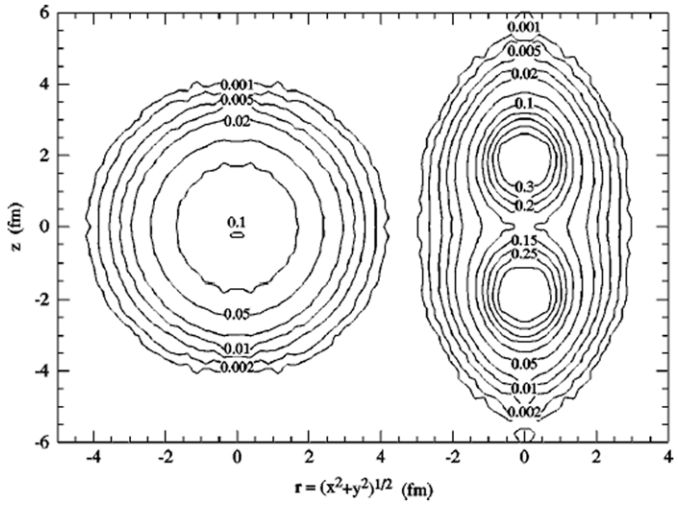

Figure 2. The GFMC calculations of the density of ^{8}Be. The left- and right-hand images are the densities calculated in the laboratory and intrinsic frames, respectively [4]. The 2α cluster structure is clearly evident. Reprinted with permission from [4]. Copyright 2000 by the American Physical Society.

focus on cluster states in nuclear synthesis, in particular the return to the Hoyle-state which may possess an α-condensate structure (section 7.1). This article provides both a review of the underlying principles behind the formation of clusters, and also the very recent advances in the field.

2. Appearance of the nuclear cluster from the mean-field

The possibility that the α-particles could be rearranged in some geometric fashion was realized even in the earliest days of the subject. An examination of the binding energy per nucleon of the light nuclei (figure 3) shows that the nuclei which have even, and equal, numbers of protons and neutrons (so-called α-conjugate nuclei) are particularly stable (related to the correlations discussed earlier), ^{8}Be, ^{12}C, ^{16}O, ^{20}Ne, ... These systems were examined by Hafstad and Teller [5], who charted the evolution of the binding energy with number of 'bonds' or connections between the α-particles (figure 4). The rather linear relationship pointed to an apparently constant α–α interaction and the resilience of the α-particle in the ground states of these nuclei. It should be noted that this view is not one which is currently held, where the cluster structure is believed to be eroded in most ground states. Nevertheless, these ideas were rather crucial in paving the way for what was to follow: the geometrical model was in fact employed for the excited states of these nuclei by Brink (figure 5). Earlier Morinaga had postulated, in a rather extreme prediction for the time, that it should be possible for the α-particles to arrange themselves in a linear fashion [7]. The idea that the cluster should not be manifest in the ground state but emerges as the internal energy of the nucleus is increased was realized to be key in the 1960s [8]. For a nucleus to develop a cluster structure it must be energetically allowed. Asymptotically, when the nucleus is separated into its cluster components an energy equivalent to the mass difference between the host and the clusters must be provided. Thus, close to the point at which the clusters are in contact within the host a similar energy (modulo the interaction energy between the clusters) is required. In other words, the cluster structure would expect to be manifest close to, and probably slightly below, the cluster decay threshold.

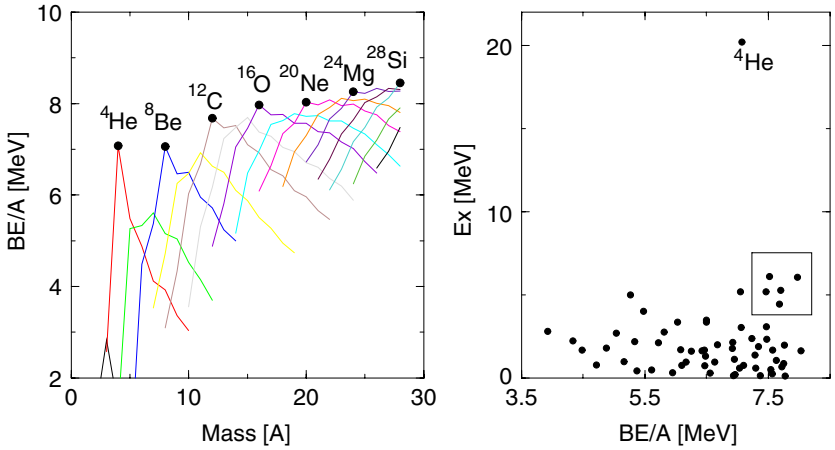

Figure 3. (Left) Binding energy per nucleon of light nuclear systems (up to $A = 28$), the lines connect isotopes of each element. The 'α-particle nuclei' are marked by the circles. (Right) Excitation energy of first excited states plotted versus binding energy per nucleon for nuclei up to $A = 20$. Good clusters should have both high binding energies and first excited states. The nucleus ^{4}He is clearly an outstanding cluster candidate. The box drawn includes nuclei which may also form clusters; ^{12}C, ^{14}O, ^{14}C, ^{15}N and ^{16}O.

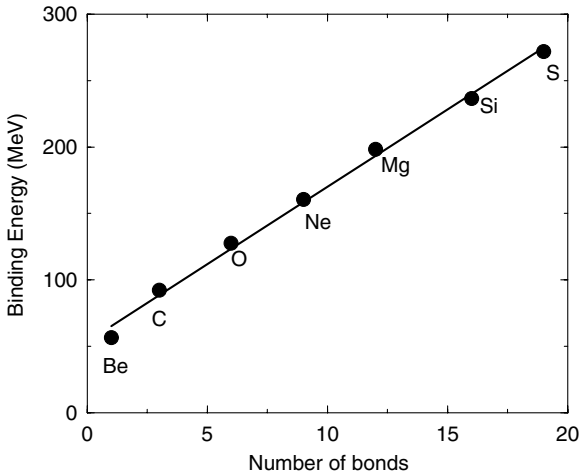

Figure 4. Binding energy per nucleon of $A = 4n$ nuclei versus the number of α–α bonds. The analysis by Hafstad and Teller [5] suggested that the ground states of $A = 4n$, α-conjugate, nuclei could be described by a constant interaction energy scaled by the number of bonds. For ^{8}Be there is one bond, ^{12}C—3, ^{16}O—6, ^{20}Ne—9, ^{24}Mg—12 and for structural reasons (the geometric packing of the α-particles) ^{28}Si—16.

This was the view reached by Ikeda, and is summarized in his diagram (figure 6). The diagram illustrates that each new cluster degree of freedom arises as the cluster decay threshold is approached, or crossed. Thus, there is the gradual transition from the compact ground state to the full liberation of the $N\alpha$ structure. Schematically, the diagram shows a linear arrangement of α-particles at the $N\alpha$-limit, though this need not be the most stable configuration. In fact, it may be argued that the linear structure has an inherent instability [84], though many have interpreted this limit as representing a linear structure.

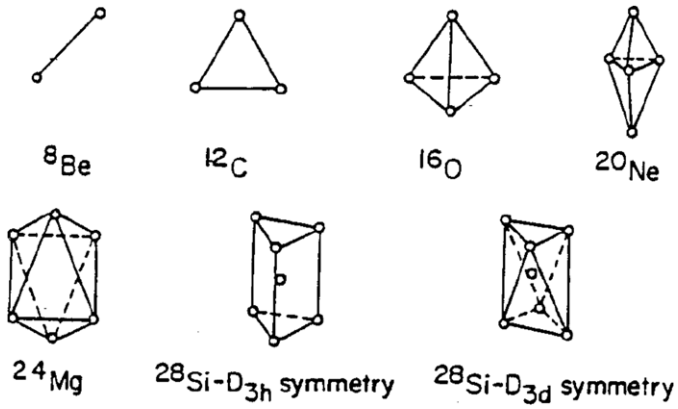

Figure 5. Geometric α-particle structures predicted by Brink [63]. Note that the arrangements reflect the number of possible bonds between α-particles predicted by Hafstad and Teller [5].

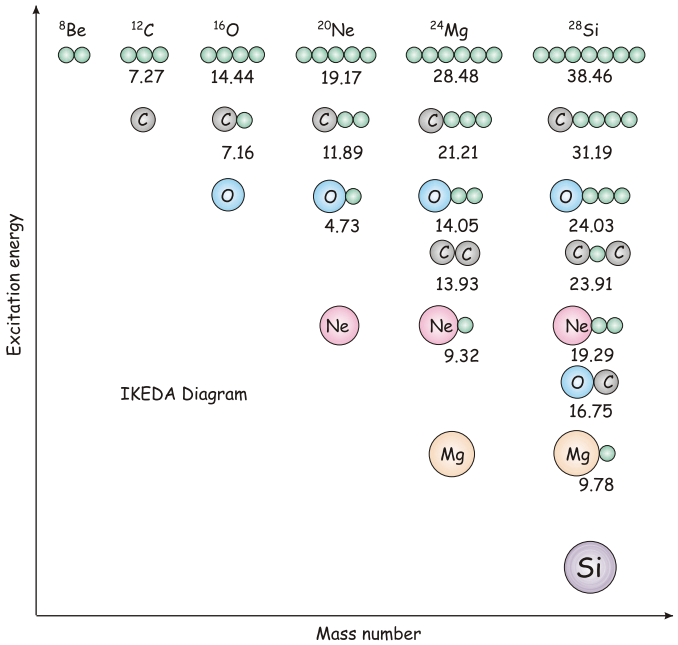

Figure 6. The Ikeda picture [8], from [85]. The diagram shows how the cluster degree of freedom evolves as the excitation energy increases. The important concept relayed by this diagram is that a cluster degree of freedom is only liberated close to a cluster decay threshold. Thus, for heavy systems the $N\alpha$ degree of freedom only appears at the highest energies.

It is clear that energetics are crucial in driving the system towards a particular cluster configuration. Without the inherent stability of the α-particle no cluster structure would be manifest. Moreover, the appropriate conditions for the formation of the cluster must be achieved, i.e. sufficient internal energy.

However, there is a second key ingredient whose role greatly influences the possible geometric arrangements of the clusters—and that is symmetries. Symmetries of course impact upon the collective excitations of the nucleus, but via their influence on the mean-field of light

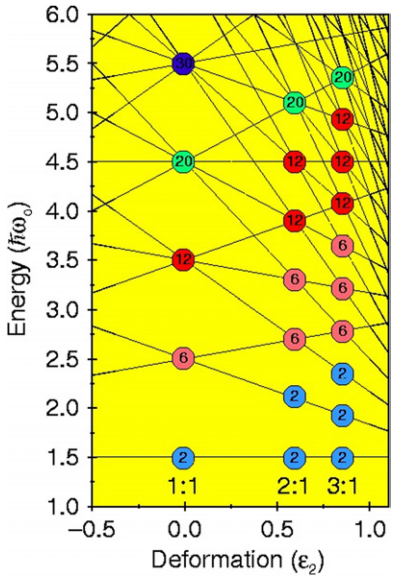

Figure 7. The deformed harmonic oscillator. The shell structure which appears at $\epsilon_2 = 0$ vanishes as the potential is deformed, but reappears at deformations of 2 : 1, 3 : 1, etc. It is at these shell closures that cluster structure appears. The numbers in the circles indicate the degeneracy of the level scheme at the crossing points, from [15].

systems, they guide the formation of the clusters themselves. In fact, there is a rather curious interaction between the mean-field and cluster degree of freedom. In order to illustrate this, we start with an analysis of a rather simple and schematic approach to the nuclear mean-field, but one which is nevertheless rather powerful. In the application of the harmonic oscillator (HO) to the nuclear problem, it is assumed that each nucleon moves within a parabolic potential (i.e. a linear restoring force) created by the mean-interaction of all of the other constituents. The solution of the Schrödinger equation then yields the well-known energy levels

$$E = \hbar\omega(n + 3/2) \tag{1}$$

for the three-dimensional nucleus, where oscillations can be along any of the three cartesian coordinate axes and n is the number of oscillator quanta. If the nucleus/potential is deformed, for example stretched along the z-axis, then the size of the potential in the x- and y-directions must shrink in order to conserve the nuclear volume. The extended potential in the z-direction lowers the oscillation frequency and, for an axially symmetric potential, is increased in the perpendicular direction. Thus, the degeneracy implicit in equation (1), is removed and

$$E = \hbar\omega_\perp n_\perp + \hbar\omega_z n_z + \frac{3}{2}\hbar\omega_0, \tag{2}$$

where the characteristic oscillator frequencies for oscillations perpendicular ($\perp$) and parallel (z) to the deformation axis are now required. These are constrained such that $\omega_0 = (2\omega_\perp + \omega_z)$, and the quadrupole deformation is given by

$$\epsilon = \epsilon_2 = (\omega_\perp - \omega_z)/\omega_0. \tag{3}$$

The total number of oscillator is now the sum of those on the parallel and perpendicular axes ($n_\perp + n_z$).

The characteristic energy levels of the deformed harmonic oscillator are shown in figure 7 [9]. The striking feature is the crossings of levels (regions of high degeneracy)

which occur for axial deformations of ($\omega_\perp$: ω_z) 2 : 1 and 3 : 1. In fact such degeneracies occur whenever the ratios ω_x : ω_y : ω_z = a : b : c where a, b and c are simple integers. Here shell structure is generated and corresponding *deformed* magic numbers emerge. In fact the magic numbers reveal some particularly interesting behaviour. If rather than examining the magic numbers the sequence of degeneracies is explored, then the sequence of spherical degeneracies (2, 6, 12, 20, ...) is repeated twice at a deformation of 2 : 1 and three times at 3 : 1. This pattern would indicate two interacting spherical harmonic oscillator potentials at 2 : 1 and three at 3 : 1, etc. Here the symmetry appears within the magic numbers. These ideas were articulated mathematically by Nazarewicz and Dobaczewski [10]. The connection with other models has also been noted. For example, in the Skyrme–Hatree–Fock approach, if a zero range interaction is employed then the potential energy becomes independent of the deformation. In this instance the resulting nuclear deformation is obtained by minimizing the kinetic energy only. It has been pointed out by Ripka [11] that this leads to the Mottelson conditions [12] which determine the oscillator frequencies ω_x, ω_x and ω_z;

$$\hbar\omega_x = \hbar\omega_0(\Sigma_x\Sigma_y\Sigma_z)^{1/3}/\Sigma_x, \tag{4}$$

$$\hbar\omega_y = \hbar\omega_0(\Sigma_x\Sigma_y\Sigma_z)^{1/3}/\Sigma_y, \tag{5}$$

$$\hbar\omega_z = \hbar\omega_0(\Sigma_x\Sigma_y\Sigma_z)^{1/3}/\Sigma_z, \tag{6}$$

where Σ_x is the sum over (N_x + 1/2) for occupied states, N_x being the number of nodes in the x-direction. So for example, with four nucleons in the $[n_x, n_y, n_z] = [0, 0, 0]$ state $\Sigma_x = \Sigma_y = \Sigma_z = 2$ and a further four nucleons in the $[n_x, n_y, n_z] = [0, 0, 1]$ state $\Sigma_x = \Sigma_y = 2$ and $\Sigma_z = 6$. Thus,

$$\epsilon = (\Sigma_x\Sigma_y\Sigma_z)^{1/3}(1/\Sigma_x - 1/\Sigma_z), \tag{7}$$

which for the particular case, ^{8}Be, gives ϵ=0.63, i.e. prolate and superdeformed.

However, it is also apparent that the symmetries extend beyond simply the numbers and are echoed in the densities of the nucleons located in the deformed orbits. We examine the rather trivial case of forming the first $N\alpha$-cluster nucleus at a deformation of 2 : 1, ^{8}Be. The levels which are labelled with degeneracy 2 are those with the oscillator quantum numbers $[n_\perp, n_z]$ = [0,0] and [0,1]. Each of these levels would be occupied by pairs of protons and pairs of neutrons with their spins coupled to zero. The density distributions of the particles is, of course, given by the square of the corresponding wave-functions, $\varphi_{0,0}$ and $\varphi_{0,1}$. The overall ^{8}Be density is given by $|\varphi_{0,0}|^2 + |\varphi_{0,1}|^2$. These three components are shown in figure 8. The feature which emerges is one in which the density is double humped corresponding to the localization of the protons and neutrons within two 'α-particles'. Here, arises the dichotomy in this approach. The observed distribution is generated by particles moving in an axially deformed potential, and this generates a clustered density distribution which in turn creates the mean-field in which the particles move. This latter field is not identical to the first. Clearly, to provide stable solutions, self consistent approaches are required. Some of these are described later (e.g. AMD).

Nevertheless, it is tempting to ask how much the density corresponds to free α-particle wave-functions? This can be achieved by computing

$$\phi_{\alpha(\pm)} = \frac{1}{\sqrt{2}}\left(\varphi_{0,0} \pm \varphi_{0,1}\right), \tag{8}$$

which corresponds projecting out the point symmetry of the two clusters. The overlap of an isolated α-particle, $\phi_\alpha = \exp(-\omega^2 r^2/2)/\sqrt{\pi}$, is found to be >90% [15]. The overlap of the two α-particle wave-functions in the interior results in a small distortion of the spherical

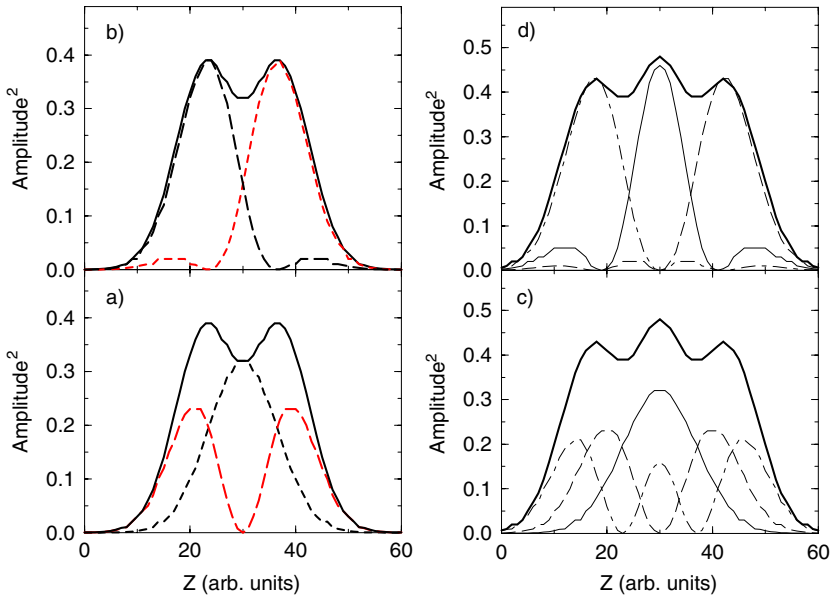

Figure 8. The density corresponding to the HO configurations for (*a*) ^{8}Be and (*c*) ^{12}C. In (*a*) the square of the $(n_x, n_y, n_z) = (0, 0, 0)$ and $(0, 0, 1)$ orbits are plotted as is their sum (——). The square of the $(0, 0, 0)$, $(0, 0, 1)$ and $(0, 0, 2)$ orbits together with their sum (——) are shown in (*c*). Parts (*b*) and (*d*) show the separation into the two and three centred components, respectively. These show the individual α-particle densities, and is performed in accordance with equations (8) and (5)–(11).

α-particle, introducing a p-state contribution. This may be viewed as a polarization, or distortion, of the free α-particle.

The symmetries in the HO found in the densities serve to enhance the probability of finding two protons and two neutrons in close proximity, and thus enhancing the preformation of the α-cluster within the nuclei. Thus, in this way the mean-field encourages the formation of the clusters themselves.

The above operation can be also applied to the 3 : 1 deformed shell closure, where we consider the three lowest orbits which are labelled with degeneracy 2. These are the $[n_\perp, n_z]$=[0,0], [0,1] and [0,2] HO levels. Figures 8 and 9 shows the densities which correspond to these three orbits. What can be clearly observed is that at the deformation of 3 : 1 there is a three humped structure. In other words, it is possible to see the evidence for the systems division into three centres. As with the ^{8}Be case, it is possible to project out the 'α-particles' by appealing to the point symmetries of a three centred systems. If we employ the wave-functions which are derived from the Hückel method (see section 5.1) we can equate the number of nodes in the multi-centred wave-functions with those in the harmonic oscillator wave-functions under consideration;

$$\psi_{0,0} = \frac{1}{2}\phi_{\alpha(-)} + \frac{1}{\sqrt{2}}\phi_{\alpha(0)} + \frac{1}{2}\phi_{\alpha(+)}, \tag{9}$$

$$\psi_{0,1} = \frac{1}{\sqrt{2}}\phi_{\alpha(-)} - \frac{1}{\sqrt{2}}\phi_{\alpha(+)}, \tag{10}$$

$$\psi_{0,2} = -\frac{1}{2}\phi_{\alpha(-)} + \frac{1}{\sqrt{2}}\phi_{\alpha(0)} - \frac{1}{2}\phi_{\alpha(+)}. \tag{11}$$

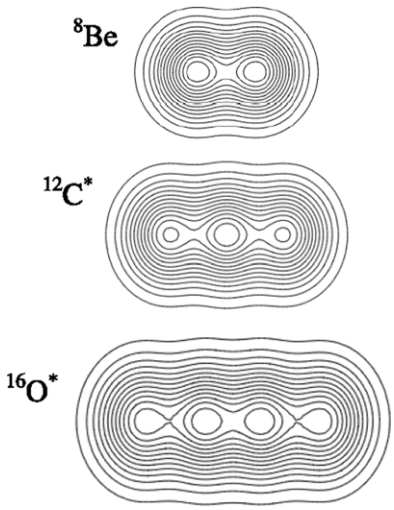

Figure 9. The density of the three HO configurations associated with placing α-particles (pairs of protons and neutrons) in the orbits in figure 7 with degeneracy 2, at deformations of 2 : 1, 3 : 1 and 4 : 1. The densities correspond to the linear structures in the 2α, 3α and 4α systems ^{8}Be, ^{12}C and ^{16}O, respectively. In each case the presence of the α-particles is clear.

These can be solved for the three α-particle like wave-functions $\phi_{\alpha(-,0,+)}$ The resulting α-particle densities are shown in figures 8 and 9. The greater overlap of the 'α-particles' means that the central α-particle has additional higher order components (quantified in [15]).

Such an analysis may be performed universally across the deformed harmonic oscillator and similar conclusions emerge; namely 2-fold clustering at a deformation at 2 : 1 and 3 at 3 : 1, etc. What is evident is that the cluster symmetries which are found in the HO are present *both* in degeneracies and densities. Figure 9 shows these symmetries for the first α-particle states appearing at deformations of 2 : 1, 3 : 1 and 4 : 1. Given the influence of the harmonic oscillator on more sophisticated nuclear models these cluster symmetries might be expected to be pervasive. The competition between the mean-field and clustering degrees of freedom is of great interest if the tendency of nuclei to fall either a shell-model or cluster-like description is to be probed. Itagaki and co-workers have recently explored this partition for a range of nuclei, e.g. [96–98].

Returning to the symmetries, these have been explored elsewhere in detail in order to identify particular cluster partitions. Building on some of the earlier work of Bengtsson [13], Rae [14] focussed on the details of the deformed magic numbers in order to probe explicitly the cluster decompositions. These are shown in table 1. Rae demonstrated that the deformed magic numbers could be expressed as the sums of spherical ones. This description locates at each deformation the associated cluster structure. At a deformation of 2 : 1 the superdeformed cluster states should be found in ^{8}Be ($\alpha + \alpha$), ^{20}Ne (^{16}O + α), ^{32}S (^{16}O + ^{16}O)... and at 3 : 1—hyperdeformation—^{12}C ($\alpha + \alpha + \alpha$), ^{24}Mg ($\alpha + {}^{16}$O + α), etc. Thus, the combination of the ideas of Rae and the Ikeda-picture permit the excitation energy, deformation and single-particle configuration of cluster states to be determined. Although more sophisticated models (section 6) allow a more realistic description of the nucleus to be arrived at, the ideas developed here remain the leading order terms in our understanding these nuclear states.

It should be noted that in the case of deformed states discussed here there exist two reference frames. The first is the intrinsic frame in which the coordinate system may be

Table 1. Relationship between the deformed magic numbers at deformations of 2 : 1 and 3 : 1 and spherical cluster decompositions from [14]. For example, at a deformation of 2 : 1 the neutron and proton magic numbers 4, 10 and 16 can be decomposed into the spherical neutron and proton magic numbers 2 + 2, 8 + 2 and 8 + 8. Thus, one would expect that at a deformation of 2 : 1 the cluster structures $\alpha + \alpha$, $\alpha + {}^{16}\mathrm{O}$ and ${}^{16}\mathrm{O} + {}^{16}\mathrm{O}$ to appear.

$\omega_\perp : \omega_z = 2:1$			$\omega_\perp : \omega_z = 3:1$		
Magic numbers at 2 : 1	Spherical magic numbers	Associated cluster configuration	Magic numbers at 3 : 1	Spherical magic numbers	Associated cluster configuration
4	2 + 2	$\alpha + \alpha$	6	2 + 2 + 2	$\alpha + \alpha + \alpha$
10	8 + 2	${}^{16}\mathrm{O} + \alpha$	12	2 + 8 + 2	$\alpha + {}^{16}\mathrm{O} + \alpha$
16	8 + 8	${}^{16}\mathrm{O} + {}^{16}\mathrm{O}$	18	8 + 2 + 8	${}^{16}\mathrm{O} + \alpha + {}^{16}\mathrm{O}$
28	20 + 8	${}^{40}\mathrm{Ca} + {}^{16}\mathrm{O}$	24	8 + 8 + 8	${}^{16}\mathrm{O} + {}^{16}\mathrm{O} + {}^{16}\mathrm{O}$
40	20 + 20	${}^{40}\mathrm{Ca} + {}^{40}\mathrm{Ca}$	36	8 + 20 + 8	${}^{16}\mathrm{O} + {}^{40}\mathrm{Ca} + {}^{16}\mathrm{O}$

aligned with the deformation axis. In this case angular momentum of individual nucleons is not a good quantum number, only its projection onto the deformation axis. The second frame is the laboratory frame, which is the reference frame of the shell model—here angular momentum is a good quantum number. In calculations such as Hartree–Fock (HF) or Hartee–Fock–Bogoliubov (HFB), the latter including pairing, it is necessary to project out from the intrinsic states, states of good angular momentum (projection after variation). In the HF case this projection is performed using the Peierls–Yoccoz procedure [20] and for the more complex case a technique introduced by Blatt [21]. The majority of the cluster structures presented in the present review correspond to intrinsic states. It is of course within this framework in which collective rotational energies have a natural description. In the case of light nuclei in which $SU(3)$ symmetry is respected it is often possible to deduce the relationship between the intrinsic and laboratory descriptions, i.e. the shell-model limit corresponding to various cluster structures.

As a further observation, it should be pointed out that the cluster structures generated within the harmonic oscillator basis correspond to 'single' Slater determinant wave-functions. That is to say the cluster structure arises due to the density patterns of the HO wave-functions themselves. An alternate description would be to employ a framework in which the system explicitly recognizes the cluster partition by forming a 'multi' Slater determinant description. Examples of both approaches are presented in the present review. For example, the AMD approach (see section 6.3) uses a single Slater determinant, whereas the resonating group method (RGM) (see section 6.2) employs a Slater determinant for each cluster.

3. Evidence for cluster structures in selected light nuclei

In this section the cluster structure of a few light nuclei is reviewed in order to illustrate that the predictions made by Ikeda *et al* [8] (figure 6) are borne out be more detailed calculations and indeed have some correspondence to experimental observations. The structure of the ground state of ${}^{8}\mathrm{Be}$ has already been discussed, and the character of ${}^{12}\mathrm{C}$ is explored in section 7.1. The next possible α-conjugate cluster nucleus is ${}^{16}\mathrm{O}$.

3.1. ${}^{16}O$

Interest in the cluster structure of ${}^{16}\mathrm{O}$ goes back to the earliest days of the subject. In the model of Hafstad and Teller [5], it was represented by a tetrahedral arrangement of α-particles. In the Ikeda picture, this would be associated with a compact ground state. At an energy of

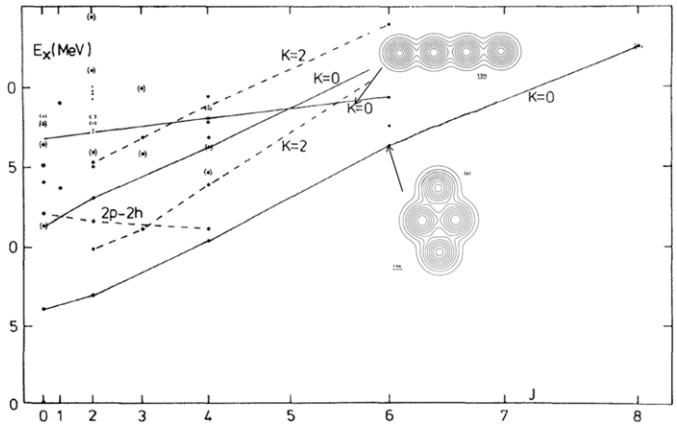

Figure 10. The experimental rotational bands assigned to states in ^{16}O, adapted from [22]. The density contour plots correspond to the structures found in the ACM calculations [22] associated with ^{12}C + α and 4α cluster structures. Original figure reprinted with permission from [22]. Copyright 1984 by the American Physical Society.

7.16 MeV the ^{12}C + α cluster structure should be manifest and a 4α-structure at 14.44 MeV. Several attempts have been made to collate the experimentally observed states in ^{16}O into rotational bands (e.g. [22,23], and references therein). The classification made in [22] is fairly representative and is shown in figure 10.

A whole variety of theoretical approaches have been brought to bear on the structure of ^{16}O including HF [24,25], Nilsson–Strutinksy (NS) [23], ACM [22] or a simple core + α potential model [26]. Importantly, some universal features and themes appear. The first excited state in ^{16}O lies at 6.05 MeV and possesses spin and parity $J^{\pi} = 0^{+}$. This state lies very close to the α-decay threshold. This state is associated with a 4p–4h structure in both the NS and HF calculations, i.e. an excitation of an α-particle to the sd-shell. In the NS calculations the 4p–4h structure is associated with a shell gap which appears for oblate deformations. Similarly, the HF studies find a structure which is closely linked with trial harmonic oscillator wave-functions in which all of the oscillator quanta lie on just two axes. The α-cluster model also associates the 6.05 MeV state with a quasi-planar structure (the corresponding density is shown in figure 10). The rotational characteristics of this state and the quadrupole moment corresponding to the gamma-width of the 2^{+} (6.92 MeV) transition to the 0^{+} excited state [22] agree well with most of the calculations. It should be noted that, both from the perspective that the state corresponds to a 4p–4h excitation and the characteristic intrinsic density which is shown in figure 10, that this state should have a ^{12}C + α cluster structure. Indeed, the core + α potential model constructed from this perspective reproduces the experimental characteristics of this band rather well, including the α-decay widths [26].

The next cluster configuration which is predicted by the Ikeda diagram corresponds to the 4α-state, drawn as a linear arrangement of α-particles. In the NS calculations this structure is associated with an 8p–8h structure in which two α-particles are removed from the ^{16}O core and placed in Nilsson orbitals from the sd- and fp-shells most strongly aligned with the prolate deformation. As a consequence a linear 4α arrangement results. Such a structure is also found in the ACM calculations (see figure 10) [22]. The experimental perspective is less clear. The evidence for the linear structure comes from measurements of the ^{12}C(α,^{8}Be) reaction [27,28]. A linear chain might be expected to break into two smaller chains, which would be associated with the ^{8}Be ground state. The final state of the above reaction contains two ^{8}Be nuclei. A series of resonances were observed in this final-state, but in particular a sequence of resonances with

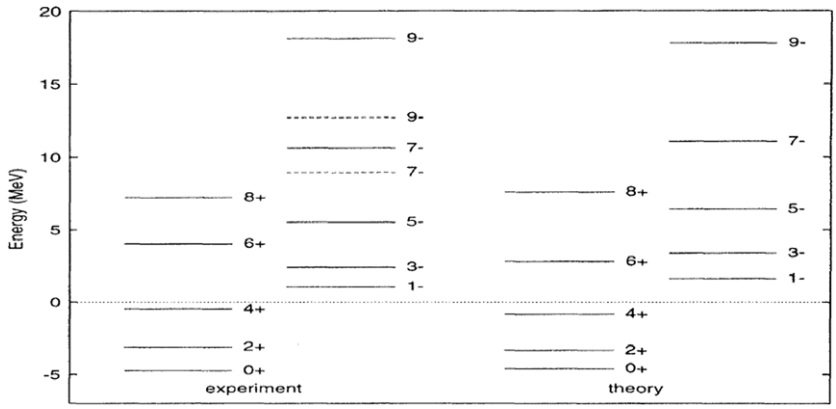

Figure 11. The positive and negative parity experimental rotational bands in ^{20}Ne, compared with the α+core potential model predictions [33]. The reference point for the comparison is the α-decay threshold, 4.73 MeV, shown by the horizontal dotted line. Reprinted with permission from [33]. Copyright 1995 by the American Physical Society.

$J^{\pi} = 2^+, 4^+$ and 6^+ were found to have narrow widths (20–70 keV). It could be argued that the widths were narrow due to their very special character which reduces their α-decay probability to the ^{12}C ground state. However, it is also possible that the states are narrow because they reside close to the top of the ^{8}Be + ^{8}Be Coulomb + centrifugal barrier. Other measurements of states which decay into two ^{8}Be nuclei in this region show that there is a very broad spectrum of states [29,30]. Thus, the definitive identification of the chain-states in ^{16}O remains a challenge.

3.2. ^{20}Ne

The cluster structure of the nucleus ^{20}Ne has often been cited as the best example of clustering in light nuclei (e.g. [31,32]). This is not, perhaps, surprising given that two closed shell nuclei are involved—the α cluster resides outside the ^{16}O core. Indeed, the simple core + α potential model of Buck *et al* [33] produces a rather excellent description of the energy levels α-decay widths and $BE(2)$ values for the low-lying positive and negative parity bands (figure 11). This $\alpha + {}^{16}$O cluster structure of the ground state is intrinsically mass asymmetric. Such an intrinsic structure does not possess good parity which in turn gives rise to an octupole parity doublet of $K^{\pi} = 0^{\pm}$ bands [34, 35]. The energy splitting between the two components has been interpreted in terms of the probability for the α-particle to tunnel between the two sides of the ^{16}O-core. This asymmetric cluster structure of ^{20}Ne is also well reproduced within the AMD framework [36], a prescription which, importantly, is essentially free from any constraints on the arrangement of the 20 nucleons (i.e. *a priori* no clustering). From the experimental perspective the level structure of ^{16}O+α states in ^{20}Ne has been characterized in terms of bands by both Bromley [32] and Tomoda and Arima [37]. These states have very large α-reduced widths which clearly mark out their cluster parentage [38].

Close to the 2α-decay threshold, 11.9 MeV, the ^{12}C + ^{8}Be cluster structure should appear. A detailed set of measurements of the ^{12}C(^{12}C,^{20}Ne)α reaction, performed by Hindi *et al* [39], characterized simultaneously the α and ^{8}Be partial decay widths of states close to this region and as a consequence identified the states with ^{12}C + ^{8}Be, 8p–4h, character, figure 12. This characterization of bands in the ^{20}Ne system permitted Hindi *et al* to form a direct connection between the associated structures and the Ikeda diagram, also shown in figure 12. This is a rather powerful vindication of the underlying concepts.

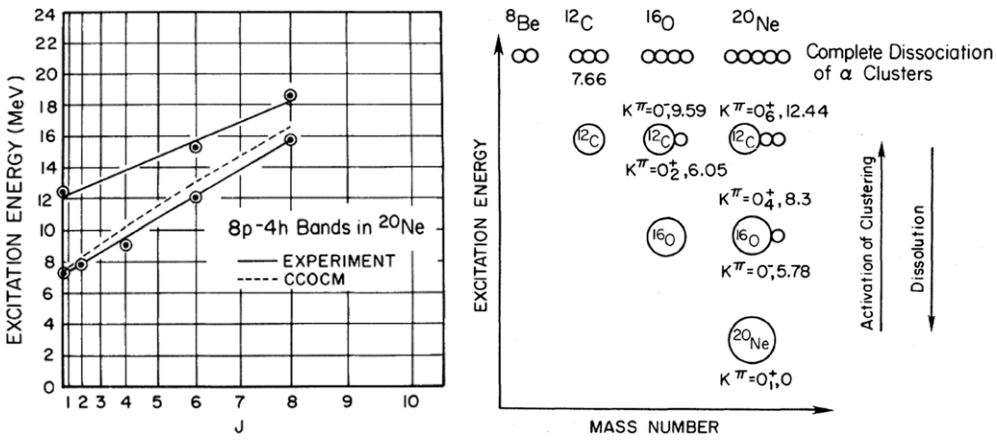

Figure 12. (Left) The 8p–4h, $^{12}C + 2\alpha$ states in ^{20}Ne found in the measurements of the $^{12}C(^{12}C,^{20}Ne)\alpha$ performed by Hindi *et al* [39]. (Right) The modified Ikeda diagram, to include the assignment of rotational bands in ^{20}Ne and ^{16}O. Reprinted with permission from [39]. Copyright 1983 by the American Physical Society.

3.3. Heavier systems: ^{40}Ca

There are of course many columns to the right of the Ikeda description of ^{20}Ne. The next nucleus illustrates an important new development and that is the potential appearance of large scale clusters, that is to say $^{12}C + ^{12}C$ clustering. In terms of shear theoretical and experimental effort ^{24}Mg has been the focus for a tremendous amount of intellectual effort. The experimental evidence for such cluster structures dates back to the 1960s and has been reviewed extensively, for example by Erb and Bromley [40], Cormier [41] and Eberhard [42]. This topic is covered in section 7.3. Similar large scale clustering is found in the nuclei ^{28}Si and ^{32}S (see section 7.3.2).

At the end of the sd-shell lies ^{40}Ca. At low energies, 3.35 and 5.21 MeV, there exist two 0^+ states, 0^+_2 and 0^+_3. These have been associated with 4p–4h ($^{36}Ar + \alpha$) and 8p–8h ($^{32}S + 2\alpha$) configurations, respectively [43, 44]. Measurements using GAMASPHERE have shown that the 0^+_3 state is associated with a superdeformed band extending up to high spin; $J^\pi = 16^+$ [45, 46]. The stability of this rotational structure is not matched by the theoretical situation. In Skyrme–Hartree–Fock calculations a close degeneracy is found between the 4p–4h and 8p–8h configurations is found [47], but that the superdeformed state should have a 8p–8h character. However, in Nilsson–Strutinsky type calculations [50] only the 4p–4h and 12p–12h structures were found to be stable. The instability of the 8p–8h configurations being linked to the influence of octupole degrees of freedom. In this instance unanimous agreement between the various approaches does not emerge. The fact that a stable superdeformed band is an experimental observable prompted Kanada–En'yo and Kimura to observe that 'there might be some mechanism beyond the mean-field' which stabilizes the superdeformation [51]. It was postulated that it is some underlying cluster structure which provides this mechanism. An analysis within the AMD framework led to the conclusion that the 8p–8h configurations should dominate, but that the intrinsic structure had a large overlap with the mass-asymmetric $^{12}C + ^{28}Si$ cluster structure. This result shows that in this instance physics beyond that of the HF mean-field is required. Moreover, the strong influence of cluster structures on the appearance of superdeformed bands is emphasized. It should be noted that a similar result is found, theoretically, in the case of ^{32}S, where $^{16}O + ^{16}O$ cluster states are important in the AMD calculations of superdeformed ^{32}S states [52].

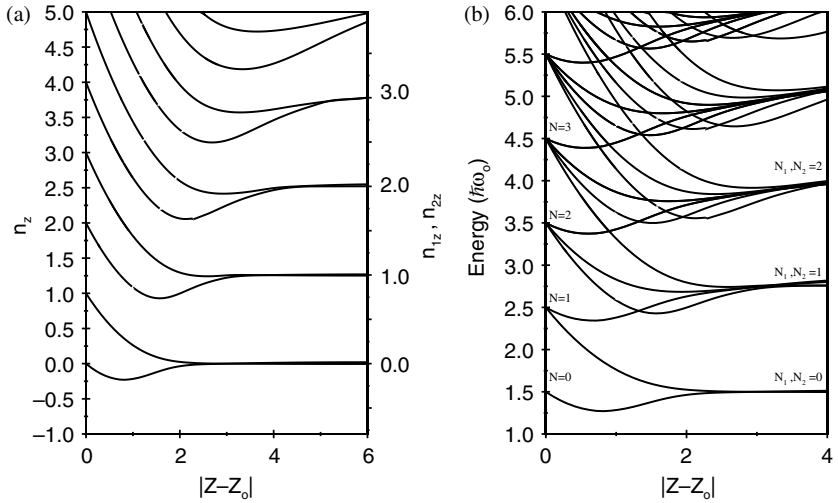

Figure 13. The energy levels (*b*) and n_z quantum numbers (*a*) of the two-centre oscillator. The splitting of the n_z oscillator quantum numbers as the two potentials overlap is shown in (*a*). The final quantum numbers of the fused system are given by $2n_z$ and $2n_z+1$. The corresponding energy levels are shown in (*b*), where the energy levels of the initially separate potentials merge into those of the fused system.

4. Separation of cluster states into clusters

The transition from cluster state to the point at which the fragments are separated, or vice versa the fusion of clusters to form a composite state, provides an important link between the experimental and theoretical perspectives. For example, an ability to predict the types of cluster structures which can be accessed through a particular reaction may then be used to experimentally identify states with a particular character. The two-centre shell model allows this connection to be made [54]. Here the Schrödinger equation is solved for two shell-model potentials as a function of their separation. In order to illustrate the main features of this model the much simpler two-centre oscillator is first examined, where the solutions for two HO potentials are considered as a function of their separation. In the two infinitely separated potentials there are a sequence of harmonic oscillator levels given by equation (1). In the two-centre case the potential is given by

$$V = \frac{m}{2}(\omega_x^2 x^2 + \omega_y^2 y^2 + \omega_z^2(|z| - z_0)^2), \tag{12}$$

where the two potentials are centred at $\pm z_0$. For two infinitely separated potentials, the degeneracies will be twice that observed in figure 7 for zero deformation. As the potentials begin to overlap then this degeneracy must be lifted and, in the limit of zero separation, the energy levels of the spherical harmonic oscillator must be produced. In fact, in the final approach, when the two overlapping potentials are merging towards the spherical limit, an energy level scheme approximating the prolate deformed ($\epsilon_2 > 0$) HO would be expected. The levels of the two-centre HO are shown in figure 13. The energy levels of the fused system are determined by the oscillator quanta in the x, y and z directions. In particular, it is the evolution of the n_z quantum number which is important. Figure 13 shows how n_z changes from large values of z_0, to $z_0 = 0$. It can be seen that the value of n_z in the fused system takes on two values; $2n_z$ and $2n_z+1$. These two combinations correspond to the linear combinations

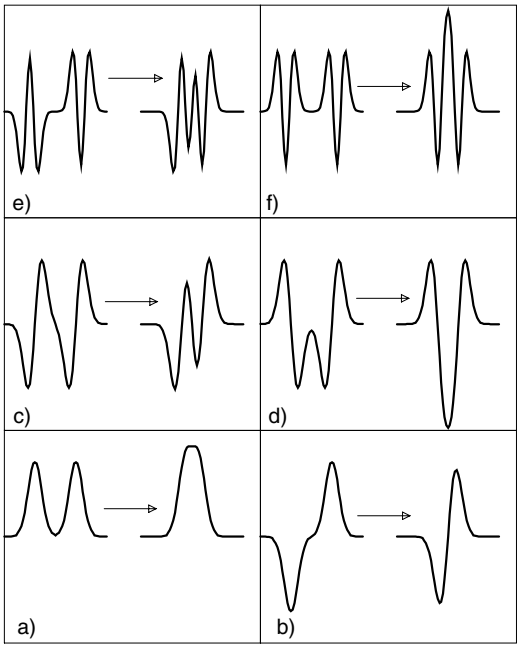

Figure 14. The wave-functions of the two-centre oscillator. The various parts to the figure illustrate the *fusion* of the single-centre wave-functions to those of the composite system. (*a*) and (*b*) show the two linear combinations ($\pm$) of $(n_\perp, n_z) = (0, 0)$ orbits, where in (*a*) the number of nodes is preserved and in (*b*) an additional one is created. (*c*) and (*d*) represent the same behaviour for (0, 1) states, giving rise to (0, 2) and (0, 3) levels. Same for (*e*) and (*f*) where the fusion of two (0, 2) levels produces (0, 4) and (0, 5) final states.

of the two-centre wave-functions,

$$\psi_{1,2} = \frac{1}{\sqrt{2}}(\phi_- \pm \phi_+) \tag{13}$$

the additional node along the z-axis for one of the two combinations (see figure 14) is associated with the $2n_z + 1$ fused wave-function, whilst the other combination conserves the number of nodes.

Having developed the energy level schemes it is possible to place neutrons and protons into the single-particle orbits in the two separate potentials in order to monitor which configuration is produced in the fused nucleus. Of course, this process can be performed in reverse, i.e. going from composite to clusters. The full two-centre shell-model solution is shown in figure 15, and qualitatively the structure is similar to that found in figure 13(*b*).

In an important innovation, Harvey developed a simplification of the two-centre result [53]. He noted that for the most part the complexity of the solutions in the region between zero and infinite separation was unimportant and it was possible to consider only the initial and final quantum numbers. These are, in essence, the initial and final state n_x, n_y and n_z quantum numbers. The Harvey diagram is shown in figure 16.

The observance of the Harvey prescription produces some interesting results. If for example, two α-particles are fused, each with $(n_x, n_y, n_z) = (0, 0, 0)$ then the levels $(0, 0, 0)$ and $(0, 0, 1)(\equiv (n_\perp, n_z) = (0, 0)$ and $(0, 1))$ result. It has also been observed that the population of these two levels results in a double humped structure (figures 8 and 9). It is possible to extend these ideas to the *fusion* of three α-particles along the z-axis. Then the

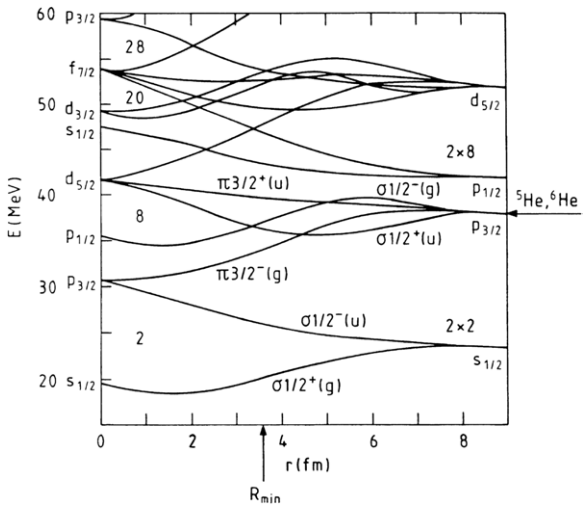

Figure 15. The energy levels of the two-centre oscillator shell model from [18]. The separation of the two potentials is defined in terms of the distance r. The present calculation corresponds to the energy levels associated with the fusion of two ^{4}He nuclei. The separation at which the interaction potential reaches a minimum is marked, $R_{\min}$—this would correspond to the ^{8}Be ground state.

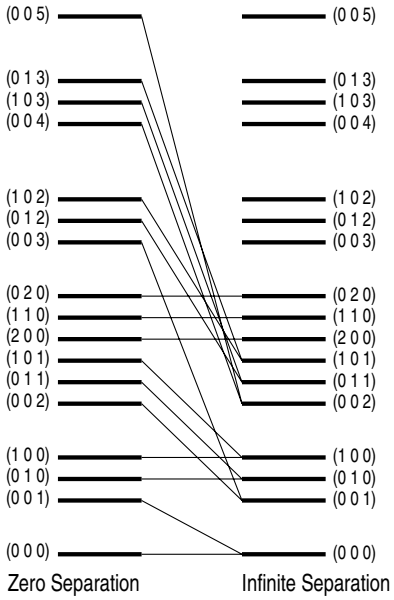

Figure 16. The Harvey diagram. The connection between the oscillator levels of the initially separate (infinite separation) and fused systems (zero separation) is shown. Particles follow these trajectories in cluster fusion or fission [53].

oscillator quanta which result from the merging of the levels with n_z quanta are $3n_z$, $3n_z$+1 and $3n_z$+2. Hence, the fusion of three α-particles, (0, 0, 0), produces levels (0, 0, 0), (0, 0, 1) and (0, 0, 2). This again leads to the same 3α structure which is observed in figures 8 and 9. In this way it can be observed that the application of the conditions of the two-centred, or N-centred, oscillator preserves the asymptotic cluster structure in the fused system.

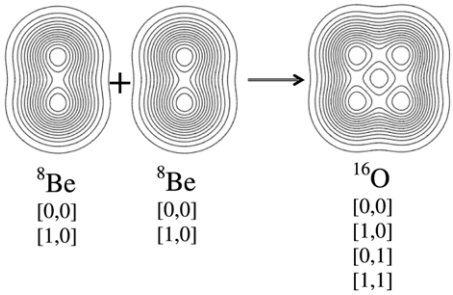

Figure 17. Fusion of ^{8}Be + ^{8}Be to form a square-like arrangement of 4 α-particles. The oscillator configurations, $[n_{\perp}, n_{z}]$, are shown.

Importantly, these concepts also extend beyond the fusion of single α-particles to the fusion of two or three dimensional systems. The application to the hypothetical fusion of two ^{8}Be nuclei to form ^{16}O shows that the four α-particles can be found in the final system, which respects the initial arrangement by forming a square arrangement of the four clusters (see figure 17).

It should be noted that it is possible to relate such structures to those in figure 1. Each of the alpha-cluster structures which appears in the figure can be traced to a harmonic oscillator configuration, and thus a particle-hole structure. If the case of ^{16}O is taken as an example, then the structure shown in figure 17 corresponds to an α-particle promoted to the $N = 2$ (sd) shell, a 4p–4h state. This structure has a close similarity to the 'kite' or 'rhombus' structures found in figures 1 and 10. Similarly, the linear structure found in figures 9 and 10 corresponds to the promotion of α-particles to the $N = 2$ and $N = 3$ shells (sd and fp), which would correspond to an 8p–8h configuration.

5. Beyond α-clusters—valence neutrons

Cluster structure beyond α-conjugate nuclei is, by and large, strongly influenced by the closed shell ^{4}He nucleus. For example, ^{6,7}Li possess $\alpha + d$ and $\alpha + t$ structures, respectively. The first significant attempt to deal with the additional degrees of freedom that valence nucleons bring to systems was that of Hafstad and Teller [5]. This seminal piece of work set the ground rules for this field. They considered the sequence of nuclei, ^{5}He, ^{9}Be, ^{13}C and ^{17}O. The binding energies of these $4n + 1$ nuclei depend on the α–α interaction energy, but also the character of the valence neutrons. The binding energy of the ^{5}He nucleus reflects the α–n interaction, whereas the $\alpha + n + \alpha$ nucleus ^{9}Be whilst containing similar terms in the Hamiltonian was recognized as having a contribution from an *exchange* interaction. Here, the systems were described in terms of the covalent exchange of neutrons between the α-cores. This piece of work demonstrated tremendous insight, but was largely forgotten for a period of about 50 years.

The exchange of neutrons between α-particle cores is a rather important concept which allows a detailed understanding of the structure of the beryllium isotopes to be developed [16–19]. The nucleus ^{9}Be demonstrates this beautiful piece of physics rather well. The $N = Z$ isotope ^{8}Be is unstable against α-decay, held together only by the Coulomb barrier for a period of $\sim 10^{-16}$ s. The only stable beryllium isotope is ^{9}Be. Given the highly clustered nature of ^{8}Be an appropriate description of ^{9}Be would be $\alpha + n + \alpha$. The additional neutron is exchanged between the cores just as electrons are exchanged between atoms in covalent atomic

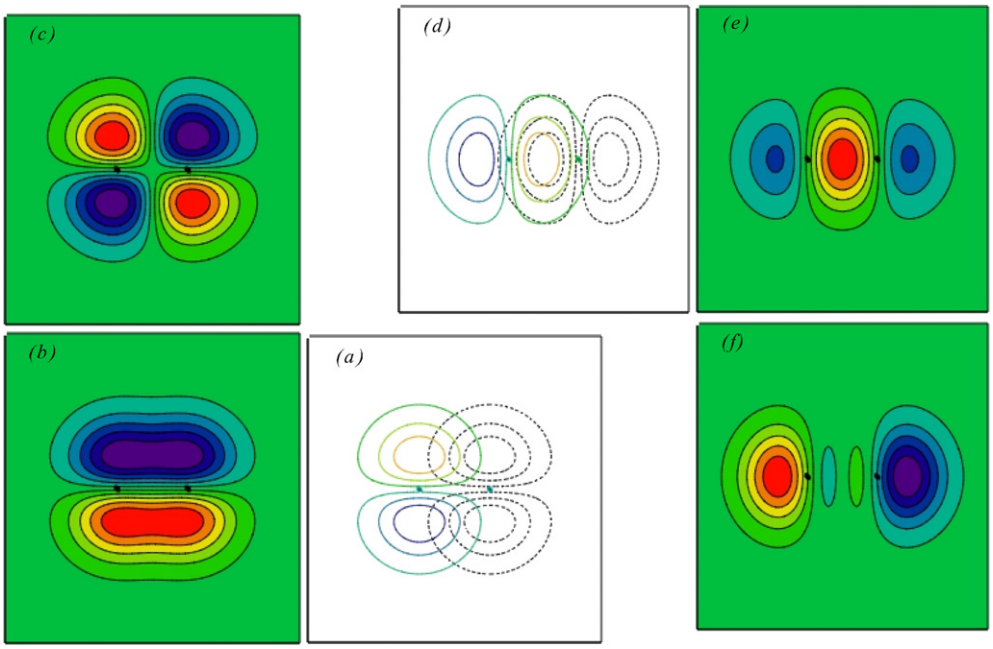

Figure 18. Molecular orbitals associated with linear combinations of HO orbitals $[n_\perp, n_z] = [1, 0]$ and $[0, 1]$ orbits, equivalent to p-states. Here the z-direction is aligned with the separation axis of the two centres indicated by the black dots. (*a*) shows the overlap of the two individual wavefunctions. Diagrams (*b*) and (*c*) the result of forming linear combinations: (*b*) corresponds to the binding π-state, and (*c*) to the anti-binding state. Diagram (*d*) shows the overlap of the two (0, 0, 1) orbits, forming the σ-configurations, and (*e*) and (*f*) the two linear combinations, from [55].

molecules. Thus, such states have been coined *nuclear molecules*. It is the delocalization of the neutron which lowers its kinetic energy giving an enhanced binding energy for the ^{9}Be system compared to ^{8}Be. It is possible to infer from the neutron separation energy in ^{9}Be that the magnitude of the binding is approximately 1.6 MeV [17]. It was recognized by Hafstad and Teller [5] that in the formation of such molecular states that the $p_{3/2}$ single-centre orbital should characterize the exchange, given the spin and parity of the ground state of ^{5}He. Thus, one might expect the neutron to reside in covalent orbits, which are the analogues of those observed in carbon and oxygen molecules, namely σ and π-orbits, which are formed in the exchange of p-electrons.

The possible linear combinations (equation (13)) of the equivalent HO orbitals $[n_\perp, n_z] = [1, 0]$ and $[0, 1]$ are shown in figure 18. Note that these are two possible orientations of the dumbbell-like orbitals—either parallel or perpendicular to the axis separating the α-particles. The linear combination shown in (*b*) of this figure corresponds to the π-type structure for the valence neutron, and (*e*) to the σ-orbital. One, of course, should be able to recognize these orbitals in solutions of the two-centre shell model—a so-called correlation diagram. An examination of figure 15 shows the energy evolution of the energy levels from infinite separation to the point at which the separation is appropriate for the description of the separation of the two α-particles in the ground state of ^{8}Be (marked $R_{\rm min}$—the point at which the α–α potential attains its minimum; $\sim$3.5 fm). At this separation the two lowest energy orbits available for the neutron to follow are marked $\pi 3/2^-$ and $\sigma 1/2^+$. In fact the two levels are almost degenerate. These two orbits are analogues of the Nilsson orbitals from the $1p_{3/2}$ and $1d_{5/2}$ levels, with

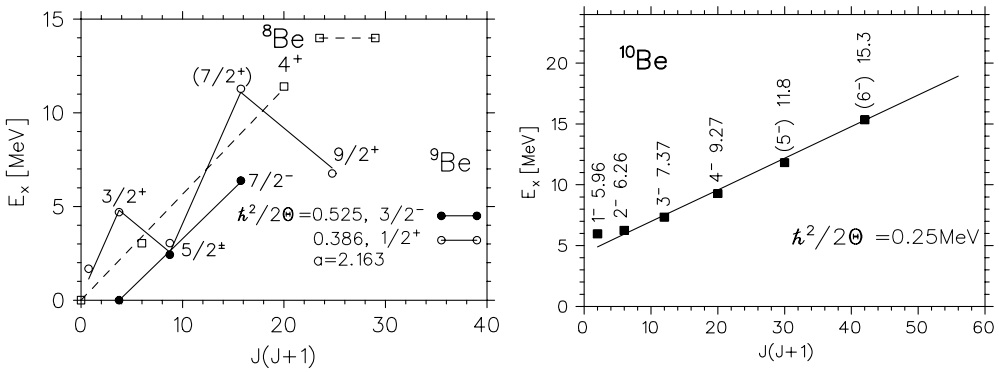

Figure 19. Rotational bands of ^{8}Be, ^{9}Be (left panel) and ^{10}Be (right panel). The excitation energies are plotted as a function of angular momentum $J(J+1)$. The Coriolis decoupling parameter, a, for the $K = 1/2$ band is indicated, from [56].

projections of the total angular momentum $K^{\pi} = 3/2^{-}$ and $1/2^{+}$, respectively (a point to be explored later, see section 6.4).

The notation σ and π corresponds to the projection of the angular momentum of the molecular orbit onto the symmetry axis of the molecule. If the linear combination of the p-orbits is considered, then for the orientation shown in figure 18(a), then this would correspond to $l = 1$ components along the the separation axis and hence π-type orbits. For the alternate case, figure 18(d), the projection of the orbital angular momentum of the two p-orbitals is perpendicular to the separation axis and thus the σ association.

A natural conclusion of this connection is that if such a description of ^{9}Be is correct then the ground state of ^{9}Be should be the head of a rotational band associated with $K^{\pi} = 3/2^{-}$. There should also be a second band linked with a $K^{\pi} = 1/2^{+}$ configuration and both bands should have a similar rotational gradient as that of the ^{8}Be ground state. In fact one would expect the $K^{\pi} = 1/2^{+}$ band to be slightly more deformed than the ground state band as the valence neutron in the σ-configuration intercedes between the two α-particles enhancing the deformation. Figure 19 shows the experimental situation for the nuclei ^{9}Be and ^{10}Be. The data indeed confirms the prediction, aside from the fact that the $K = 1/2$ band suffers from coriolis decoupling. For such bands, an additional term is introduced with an associated coriolis decoupling parameter a,

$$E_J = \frac{\hbar^2}{2\mathcal{I}}[J(J+1) + (-)^{J+1/2}a(J+1/2)], \tag{14}$$

$\mathcal{I}$ being the moment of inertia. It should be noted that the experimental moment of inertia for the $K = 1/2$ band is indeed larger than for the $K = 3/2$ ground state band. The molecular bands of ^{10}Be forms part of the discussion contained in section 7.2.

5.1. Multi-centre calculations using the Hückel approach

Given that the systems described above behave as molecules, it is natural to adapt a mathematical framework used to describe atomic molecules to the nuclear case. The Hückel method is a general approach to describe the wave-functions of valence particles (and their binding effects) in a multi-centre system. The technique has been widely applied to the calculation of atomic molecular systems. In many ways there are very strong parallels between the results of this approach and the symmetries already explored in the case of the deformed harmonic oscillator.

In outline, the wave-functions of the molecular orbits (ψ) may be expressed as linear combinations of n single-particle nuclear wave-functions (χ_n), in the present case these will correspond to neutrons within p-orbitals, χ_i,

$$\psi = C_1\chi_1 + C_2\chi_2 + \cdots + C_n\chi_n. \tag{15}$$

Here the C_n are the coefficients to be evaluated, which determine the relative contribution of each single-centre orbital. The molecular wave-function must satisfy the relation for the energy E and the total Hamiltonian H

$$H\psi = E\psi. \tag{16}$$

E is obtained using a variational method (see also [58]).

If, as an example, we take the two-centre system the energy of the system may be written as

$$E = \frac{C_1^2H_{11} + 2C_1C_2H_{12} + C_2^2H_{22}}{C_1^2 + 2C_1C_2S_{12} + C_2^2}, \tag{17}$$

where the notation $\int \chi_i^* H \chi_j d\tau = H_{ij}$ and $\int \chi_i^* \chi_j d\tau = S_{ij}$ has been used. The final wave-functions are determined by the coefficients C_1 and C_2. The solutions for the values of E are found from the secular determinant

$$\begin{vmatrix} H_{11} - E & H_{12} - ES_{12} \\ H_{12} - ES_{12} & H_{22} - E \end{vmatrix} = 0.$$

Using symmetry arguments for equal cores (as in the case of ^{9}Be) $H_{11} = H_{22} = \alpha$. The value of H_{12}, the resonance integral, is set to β if the two clusters are neighbouring, and to zero if they are not (e.g. in longer chains). This latter condition is often used for more complex systems with many centres and restricts the neutron exchange to be with nearest neighbours only. Furthermore, the simplifying approximation is that the corresponding wave-functions will have 'zero overlap' such that S_{12} is set to zero. The secular determinant, subject to these conditions, then becomes

$$\begin{vmatrix} \alpha - E & \beta \\ \beta & \alpha - E \end{vmatrix} = 0.$$

We will use $(\alpha - E)/\beta = x$. In this specific case we have the molecular wave-functions

$$\psi = \frac{1}{\sqrt{2}}(\chi_1 \pm \chi_2). \tag{18}$$

Following this approach with the harmonic oscillator potential ($V = 1/2m\omega^2$) the molecular orbits of the valence neutron in ^{9}Be can be modelled in an analytical form (e.g. using HO wave-functions, see [57]).

This process can be repeated for more complex nuclei. For example, the secular determinants for the prolate (linear—figure 9) and oblate (triangular) configurations these are, respectively:

$$\begin{vmatrix} x & 1 & 0 \\ 1 & x & 1 \\ 0 & 1 & x \end{vmatrix} = 0 \qquad \text{and} \qquad \begin{vmatrix} x & 1 & 1 \\ 1 & 1 & x \\ 1 & x & 1 \end{vmatrix} = 0,$$

or for ^{16}O with the 4α-particles in a line or a square (figures 9 and 17)

$$\begin{vmatrix} x & 1 & 1 & 0 \\ 1 & x & 0 & 1 \\ 1 & 0 & x & 1 \\ 0 & 1 & 1 & x \end{vmatrix} = 0 \qquad \text{and} \qquad \begin{vmatrix} x & 1 & 0 & 0 \\ 1 & x & 1 & 0 \\ 0 & 1 & x & 1 \\ 0 & 0 & 1 & x \end{vmatrix} = 0.$$

Table 2. The coefficients of the single-particle wave-functions in the molecular orbits of *prolate* nuclei. The magnitude of the coefficients determine the relative contribution of the wave-function to the particular molecular orbit, from [57].

Orbit (i)	C_i	^{9}Be	^{13}C	^{17}O	^{21}Ne	^{25}Mg
1	1	0.707	−0.5	0.372	−0.289	0.232
	2	0.707	−0.707	0.602	−0.5	0.418
	3		−0.5	0.602	−0.577	0.521
	4			0.372	−0.5	0.521
	5				−0.289	0.418
	6					0.232
2	1	0.707	0.707	−0.602	0.5	−0.418
	2	−0.707	0	−0.372	0.5	−0.521
	3		−0.707	0.372	0	−0.232
	4			0.602	−0.5	0.232
	5				−0.5	0.521
	6					0.418
3	1		−0.5	0.602	−0.577	0.521
	2		0.707	−0.372	0	0.232
	3		−0.5	−0.372	0.577	−0.418
	4			0.602	0	−0.418
	5				−0.577	0.232
	6					0.521
4	1			−0.372	0.5	−0.521
	2			0.602	−0.5	0.232
	3			−0.602	0	0.418
	4			0.372	0.5	−0.418
	5				−0.5	−0.232
	6					0.521
5	1				−0.289	0.418
	2				0.5	−0.521
	3				−0.577	0.232
	4				0.5	0.232
	5				−0.289	−0.521
	6					0.418
6	1					−0.232
	2					0.418
	3					−0.521
	4					0.521
	5					−0.418
	6					0.232

The roots of the polynomial solution of the secular determinant give the relative energies between the molecular orbits in terms of the parameter β. Table 2 shows the coefficients for the linear configurations for $N\alpha$-particles plus a single covalent neutron, delocalized along the length of the chain. It should be noted that the solution for three centres corresponds to the equations used to describe the three centre system ^{12}C (equation (11)).

Figure 20 shows result for the density contours for σ and π configurations for a two-centre system ((*a*) and (*b*)). Further, the π-bonding states in three- and four-centres using the Hückel approach are illustrated. The lowest energy configurations are those in the first column. The introduction of nodes along the molecule centres creates higher energy configurations.

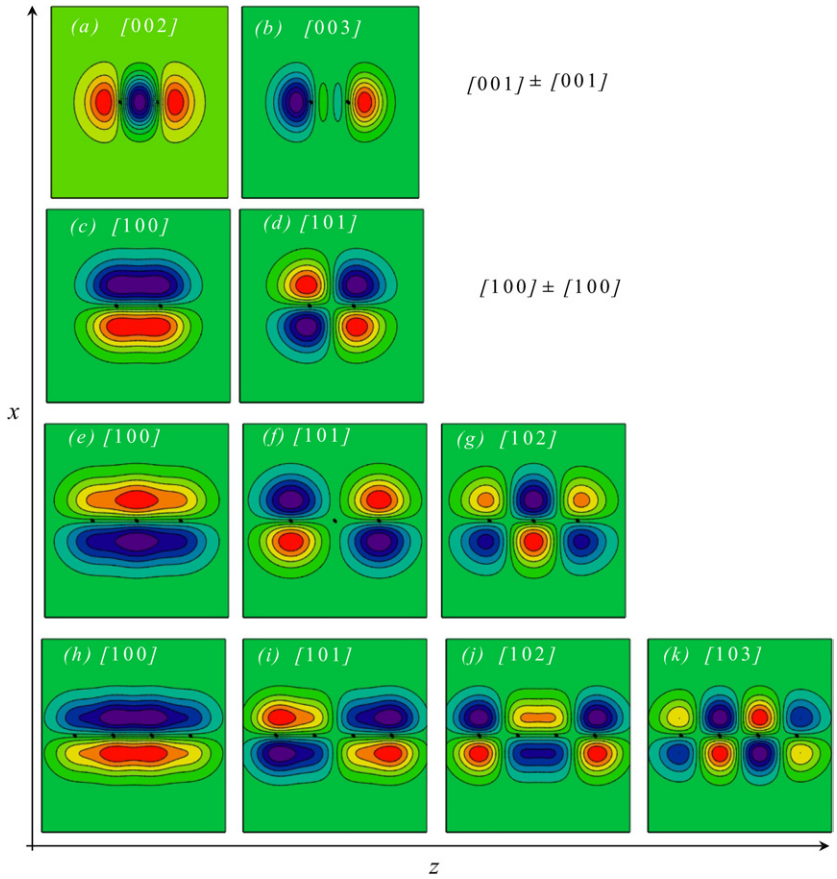

Figure 20. Contour plots of the densities for valence neutrons in chain-like α-particle configurations for up to four-centre systems using the Hückel-method. In the panels (*a*) and (*b*) the linear combinations corresponding to $[n_x, n_y, n_z] = [0, 0, 1]$ HO wave functions (for two centres), with σ-type bonds are shown. In all of the other plots for two-,three- and four-centres, the [1, 0, 0] orbit is used for the valence particle, which generates π-configurations. The labels on each panel refer to the HO-orbit classification indicating a significant overlap with the molecular orbit, see [57].

5.2. Link to HO

In order to tie together the strands of the multi-centred systems to those associated with the single centre, we search for the molecular type structures appearing in the harmonic oscillator. In principle, this allows a prediction of which kind of molecular structures will appear either in the ground state or excited states.

Figure 21 shows the deformed harmonic oscillator scheme from figure 7 augmented with the associated harmonic oscillator densities for the selected levels. If we search above the levels that would be occupied by the eight nucleons associated ^{8}Be nucleus, the next unoccupied levels correspond to the [1,0,0] (which is degenerate with [0,1,0]) and [0,0,2] levels. These are associated with the symmetries of the molecular orbits (b) π and (e) σ in figure 18. In other words, not only are the σ and π configurations predicted to be close to degenerate in the two-centre shell model (figure 15) but also in the HO. Another thing certainly worthy of note is that if we consider all of the linear α structures (corresponding to the full occupancy of the n degeneracy 2 orbits at a deformation of $n : 1$), then the next available orbit for the neutron

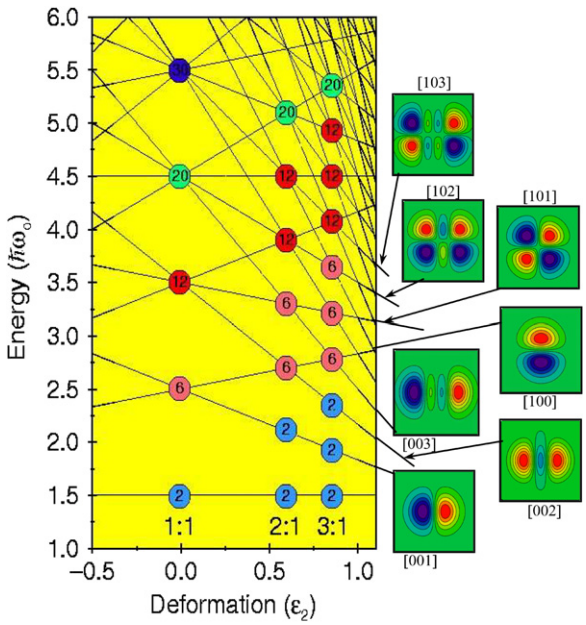

Figure 21. The energy levels of the deformed harmonic oscillator. As deformation increases the spherical shell-model degeneracies are removed until the deformation becomes $n:1$, where n is an integer. At these deformations new shell closures appear which have occupation numbers equal to n times the spherical shell closure's. The plots on the right show the wave-functions of each level calculated in a harmonic oscillator potential, see [57].

corresponds to the $[1, 0, 0]/[0, 1, 0]$ orbits, which are associated with the π-type structure. This orbit can be found in the first column of figure 20 for all centres. In other words the lowest energy molecular structure for the linear structures should be associated with a π-type neutron delocalized along the entire length of the 'chain'. Further examination of figure 21 leads to additional conclusions for the oblate type structures, see [57]. The link between these molecular orbitals and the single-particle equivalents in the deformed shell model is explored in section 6.4.

6. More sophisticated models of clustering

The foregoing discussion is largely based upon the ideas which emerge from an examination of the harmonic oscillator. Though the HO form is not a realistic reproduction of the nuclear potential the results that it produce offer a realistic first approximation. For this reason, the HO wave-functions are often used as trial wave-functions in HF calculations. Nevertheless, more realistic treatments are required to produce a refined understanding of clustering in nuclei. There are a variety of theoretical approaches which have been used with this in mind, these range from those in which the clustering is explicitly defined to those in which the clustering naturally emerges from the details of the nucleon–nucleon interaction.

6.1. Bloch–Brink alpha cluster model (ACM)

The ACM was the original inception of Margenau [59] and was further developed by Brink [6] strongly influenced by the ideas of Bloch. The principle construction of the model is that

quartets are particles are produced from pairs of protons and neutrons which are coupled to a total angular momentum of zero, i.e. they may be represented 0s-state. A collection of such quartet states may be modelled within the harmonic oscillator framework using

$$\phi_i(\boldsymbol{r}) = \sqrt{\frac{1}{b^3\pi^{3/2}}}\exp\left[\frac{-(\boldsymbol{r}-\boldsymbol{R}_i)^2}{2b^2}\right]. \tag{19}$$

Here $\boldsymbol{R}_i$ is the vector describing the location of the ith quartet, and rather crucially $b = (\hbar/m\omega)^{1/2}$ is a scale parameter which determines the size of the α-particle. The $N\alpha$ wave-function is then created using a Slater determinant

$$\Phi_\alpha(\boldsymbol{R}_1, \boldsymbol{R}_2, \ldots, \boldsymbol{R}_N) = K\mathcal{A}\prod_{i=1}^{N}\phi_i(\boldsymbol{R}_i) \tag{20}$$

$\mathcal{A}\prod_{i=1}^{N}\phi_i(\boldsymbol{R}_i)$ being the Slater determinant wave-function ($\mathcal{A}$ is the antisymmetrization operator accounting for the Pauli principle) and K a normalization constant. The Hamiltonian describing the total energy of the $N\alpha$-system is governed by

$$H = \sum_{i=1}^{A} T_i + \frac{1}{2}\sum_{i\neq j}[v(\boldsymbol{r}_i - \boldsymbol{r}_j) + v_c(\boldsymbol{r}_i - \boldsymbol{r}_j)] - T_{\text{c.m.}} \tag{21}$$

$T_{\text{c.m.}}$ is the centre of mass energy and the α–α interactions are governed by the effective nucleon–nucleon potential $v(\boldsymbol{r}_i - \boldsymbol{r}_j)$ and Coulomb interaction $v_c(\boldsymbol{r}_i - \boldsymbol{r}_j)$. The optimal arrangement of the α-particles is arrived at variationally, where the parameters which are optimized are the locations and size of the α-particles. This model has been applied extensively to light cluster systems by for example Brink [6], to the nucleus ^{16}O [22], a series of rather comprehensive set of calculations of the structure of ^{24}Mg by Marsh and Rae [60] (figure 26), linear arrangements of α-particles by Merchant [61] and finally a series of wide ranging calculations by Zhang *et al* [3, 62], some of which are shown in figure 1. Many of these calculations involved the using of *cranking* terms such that the rotational characteristics of the various structures could be tracked. As was observed in figure 1 many of the cluster structures are crystalline in nature, and some of the structures interpreted by Brink are shown in figure 5.

6.2. Microscopic cluster models

The ACM produces a rather good picture of the nature of states within $A = 4n$ nuclei which condense out into collections of α-particles. However, although it antisymmetrizes the α-particles, their individual constituents are ignored, i.e. the internal excitations of the cluster. For clusters such as α-particles this may be good approximation, but for other clusters this is not the case. Such shortcomings are addressed within the generator coordinate method (GCM) (also within the RGM) [64–73]. Moreover, this approach permits reactions between the asymptotic clusters to be studied, as has been performed extensively by Baye and Descouvement (e.g. [74–77]).

Within the RGM the formalism the wave-function describing the A nucleons, separated into two clusters with A_1 and A_2 constituents, may be written as,

$$\Psi(\boldsymbol{r}_1, \boldsymbol{r}_2, \ldots, \boldsymbol{r}_A) = F(\boldsymbol{R}_{\text{c.m.}})\hat{A}\{\phi_1(\xi_1)\phi_2(\xi_2)g(\boldsymbol{R})\} \tag{22}$$

here $F(\boldsymbol{R}_{\text{c.m.}})$ describes the motion of the centre of mass of the nucleus, ϕ_i represent antisymmetrized internal states of the two clusters (whose internal coordinates are described by ξ_i), $g(\boldsymbol{R})$ is a function of the relative motion of the two clusters (so that the relative coordinate $\boldsymbol{R}$ is given by $(1/A_1)\sum_{i=1}^{A_1}\boldsymbol{r}_i - (1/A_2)\sum_{j=1}^{A_2}\boldsymbol{r}_j$) and $\hat{A}$ is the antisymmetrization operator which exchanges nucleons between the two clusters. The great advantage of this approach is that the

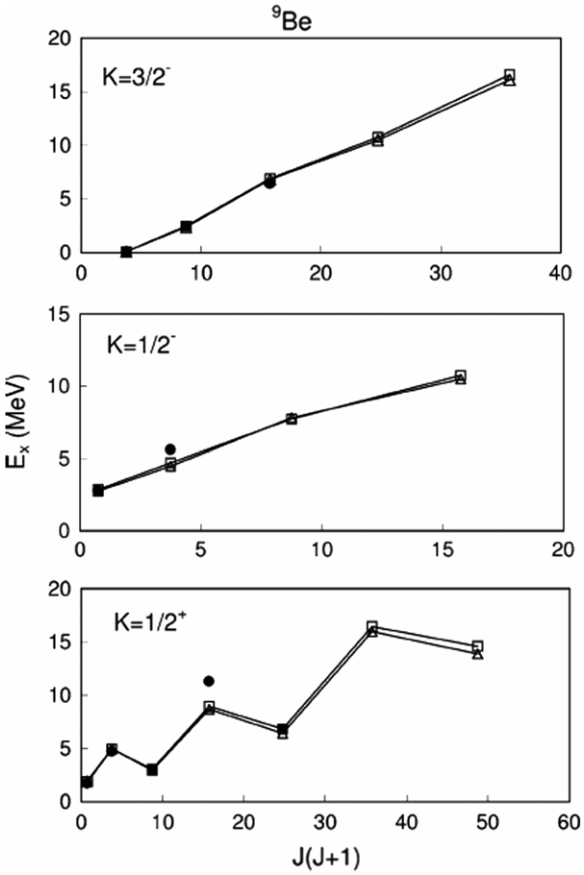

Figure 22. The GCM calculations for ^{9}Be showing the three rotational bands associated with the $K^{\pi} = 3/2^{-}$ (π-configuration), $K^{\pi} = 1/2^{+}$ (σ-configuration) and $K^{\pi} = 1/2^{-}$ bands, from [78]. The experimental data are the filled circles and the squares and circles are the calculations for two different types of interaction.

fact that the constituents of the clusters are fully antisymmetrized and that the centre-of-mass of the system is correctly treated so that the quantum numbers produced have a realistic meaning in terms of the asymptotic fragments. The above corresponds to the single-channel form of the RGM, if excitations of the cluster cores are required then so is a multi-channel approach.

An impressive demonstration of the GCM can be found in the calculations of the structure of the microscopic structure of ^{9,10,11}Be isotopes using $2\alpha + X$n configurations by Descouvement [78]. The calculations for ^{9}Be reproduce almost perfectly the rotational bands in this system. In particular, the coriolis decoupling of the $K^{\pi} = 1/2^{+}$ band is found (see figure 22). These GCM calculations reproduce the characteristics of the molecular states in the nuclei ^{9,10,11}Be. In this instance the neutrons reside in molecular orbits whereby they are exchanged between the two α-particle cores—π-orbit for the ground state band and σ for the excited states.

In recognition of this molecular behaviour, some approaches employ such orbitals explicitly in defining the basis states for the calculation of the structural properties. For example, this molecular orbit (MO) approach has been used to calculate the properties of the neutron-rich beryllium [80–82] and carbon isotopes [79]. Here the molecular orbits are formed

from linear combinations of p-orbitals based around α-particle centres. The MO framework also allows collisions between two nuclei to be considered, for example in the generalized two-center cluster model (GTCM), using a basis function of the form

$$\Phi^{J^\pi K}_{m,n} = \hat{P}^{J^\pi}_K \cdot \mathcal{A}\{\psi_{\rm L}(\alpha)\psi_{\rm R}(\alpha)\phi(m)\phi(n)\}, \tag{23}$$

the formation of resonances in ^{10}Be from ^{6}He + ^{4}He has recently been considered [83]. Here $\psi_{\rm L,R}(\alpha)$ is the wave-function of the left/right (L/R) α-particle and $\phi(m, n)$ are the molecular wave-functions of the neutrons. $\hat{P}^{J^\pi}_K$ and $\mathcal{A}$ are the parity projection and antisymmetrization operators ensuring states have good angular momentum (J), angular momentum projection (K) and parity (π). Rather interestingly, these calculations indicate that in the inelastic scattering ^{4}He + ^{6}He $\Rightarrow$ ^{4}He + ^{6}He(2^+) that at an avoided crossing which takes place between different molecular configurations that a Landau–Zener type transition [86] is responsible for the inelastic scattering in the $L = 1$ channel. In other words the formation of molecular configurations in the scattering process can have a marked impact on the elastic and inelastic scattering processes.

6.3. Antisymmetrized molecular dynamics (AMD)

The AMD approach, which has been comprehensively reviewed recently by Kanada–En'yo and Horriuchi [87], has many important advantages over microscopic cluster models, but the most significant is that there are no assumptions made about the cluster or the relative coordinates between clusters. The model is one which the nucleonic degrees of freedom are explicitly included and the A-nucleon wave-function is then antisymmetrized again via a Slater determinant;

$$\Phi_{\rm AMD}(\boldsymbol{Z}) = \frac{1}{\sqrt{A!}}\mathcal{A}\{\varphi_1, \varphi_2, \ldots, \varphi_A\} \tag{24}$$

In this way the model resembles the Bloch–Brink cluster model, but contains as degrees of freedom the nucleons and releases the constraint that α-particles be preformed. Consequently, clusters emerge without being imposed. The φ_i are Gaussian wave-packets in space, $\phi_{\boldsymbol{X}_i}(\boldsymbol{r}_j) \propto \exp(-\nu(\boldsymbol{r}_j - \boldsymbol{X}_i/\sqrt{\nu})^2)$, but also possesses spin (χ_i) and isospin character (τ_i); $\varphi_i = \phi_{\boldsymbol{X}_i}\chi_i\tau_i$. The wave-function is parameterized in terms of a complex set of variables $\boldsymbol{Z}$ describing the spin and geometry of the wave-function. The energy of the system is computed, variationally, utilizing an *effective* nucleon–nucleon interaction (see [87] for more details). The flexibility of this approach allows a suitable description of cluster and shell-model type systems, alike, and the structure emerges naturally from the details of the nucleon–nucleon interaction under the guidance of the Pauli exclusion principle.

An example of the appearance of the precipitation of clusters from the nucleon–nucleon interaction within the framework of the AMD is shown in figure 23 for the beryllium isotopes $^{6-14}$Be. All isotopes possess a proton distribution which is prolate and clustered. The role of the neutrons is clear. When the neutron number is the same as that of the protons (^{8}Be) the separation of the proton-cores is maximal (maximum clustering), whereas neutrons in more spherical distributions cause the separation of the proton centres to be reduced. This model has been widely applied, but with a particular focus on the Li, Be, B and C isotopes, see [87]—and references therein. In general the model reproduces well both experimental binding energies, transition rates, radii and moments. Figure 24 shows some examples of the rather close agreement between the AMD calculations and the experimental electric quadrupole moments and electromagnetic transition rates.

An alternate approach to AMD which contains an additional degree of freedom, namely the width parameter of the Gaussians, is fermionic molecular dynamics (FMD) [100]. The

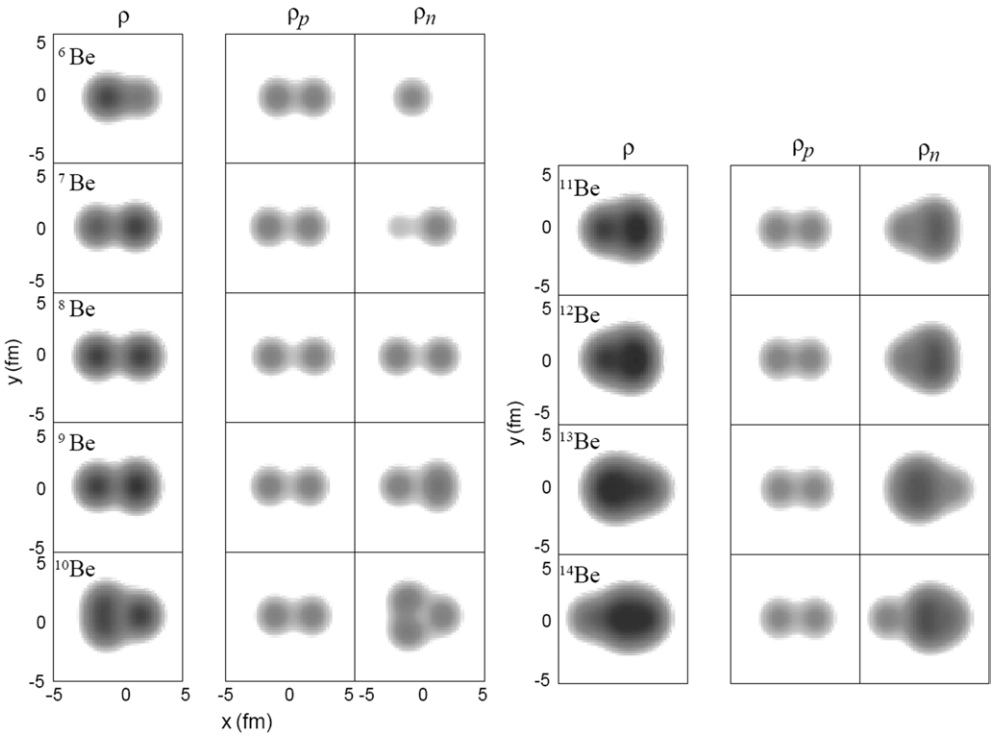

Figure 23. The density distributions of the ground states of the beryllium isotopes calculated within the framework of the AMD. The first column shows the total nucleon density (ρ) and the middle and right-hand columns the proton (ρ_{p}) and neutron densities (ρ_{n}), from [87].

features of these calculations essentially coincide with those of the AMD, but the variable Gaussian width should allow, in principle, a better description of shell-model like states. The recent calculations for the structure of the 7.65 MeV state in ^{12}C are of particular note [99].

6.4. Clusters in the deformed mean-field—Nilsson Strutinsky

The calculation of the energy levels of the deformed shell model gives rise to the Nilsson level scheme [89]. Given that the original basis for this was the deformed harmonic oscillator with additional l^2 and $l \cdot s$ terms, then one would expect that the symmetries present within the deformed harmonic oscillator would also propagate to the Nilsson level scheme. The Nilsson energy levels are shown in figure 25. Many of the deformed magic numbers present in the scheme of figure 7 are found in deformed shell-model. For example, at a deformation close to $2:1$ ($\epsilon = 0.6$) the deformed magic numbers 4, 10 and 16 appear which would be associated with the nuclei ^{8}Be, ^{20}Ne and ^{32}S and the cluster partitions $\alpha + \alpha$, $^{16}\mathrm{O} + \alpha$ and $^{16}\mathrm{O} + {}^{16}\mathrm{O}$, just as appeared in table 1. Thus, for moderate deformations and numbers of nucleons (up to and including the sd-shell) the symmetries present in the HO are retained.

One approach to calculate the variation in energy of a nucleus as a function of the shape would be to adopt a liquid drop and evaluate the change in potential energy as a function of the deformation parameters. However, the Nilsson scheme demonstrates that there is a second contribution to the energy of the system and that is associated with the rise and fall in energy of the Fermi surface as the potential is deformed. The Nilsson–Strutinsky approach

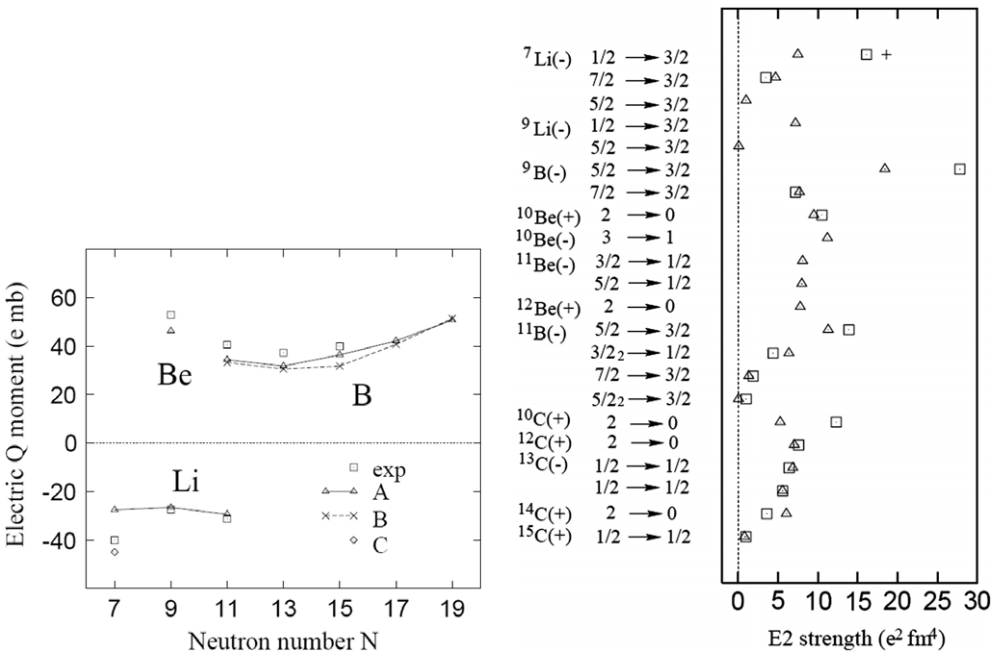

Figure 24. (Left) Electric quadrupole moments for Li, Be and B isotopes. The squares are experimental data and other symbols are the AMD calculations with slightly different interactions or constructions. (Right) $E2$ transition strengths for Li, Be, B and C isotopes. The squares are the experimental data points, the other symbols are the AMD calculations. See [87] for further details.

combines a macroscopic liquid-drop energy term with a microscopic contribution derived from the variation is the shell structure as a function of deformation. This has the effect in creating local minima, or pockets, in the smoothly evolving liquid drop energy. These secondary minima are thus associated with shell closures and also correspond to quasi-stable configurations—shape isomers.

Examples of such features appear in a wide number of systems, but are particularly striking in the calculations of α-conjugate systems. In this regard the calculations of Leander and Larsson provide a seminal contribution. They charted the potential energy surfaces for systems from ^{12}C to ^{44}Ti. The properties of the various minima found in these calculations are listed in table 3. Figure 26 shows the calculation for ^{24}Mg. Also shown in this figure are the ACM calculations for this system [60], generated using the Bloch–Brink approach. As observed in [88], there is an exact correspondence between minima in the potential energy surface and the cluster structures. This connection strongly reinforces the intimate relationship that has already been established between shell structure and clustering. This connection appears to be a universal feature given that such cluster structures may also be found in other structural calculations. For example, the HF predictions for the same nucleus, ^{24}Mg [90, 91], produce structures which are very similar to those found in the ACM [92].

The connection between the Nilsson and harmonic oscillator descriptions allows a further link between the Nilsson levels and those of the two-centre shell model. For example, if figure 15 is consulted for the separation which coincides with $R_{\min}$, then the sequence of levels corresponding to the molecular orbitals (projection of the orbital angular momentum and total angular momentum onto the molecular axis) is $\sigma 1/2^+$, $\sigma 1/2^-$, $\pi 3/2^-$, $\sigma 1/2^+$, $\pi 1/2^-$ and $\pi 3/2^+$. The corresponding Nilsson orbits are (shell-model state: angular momentum

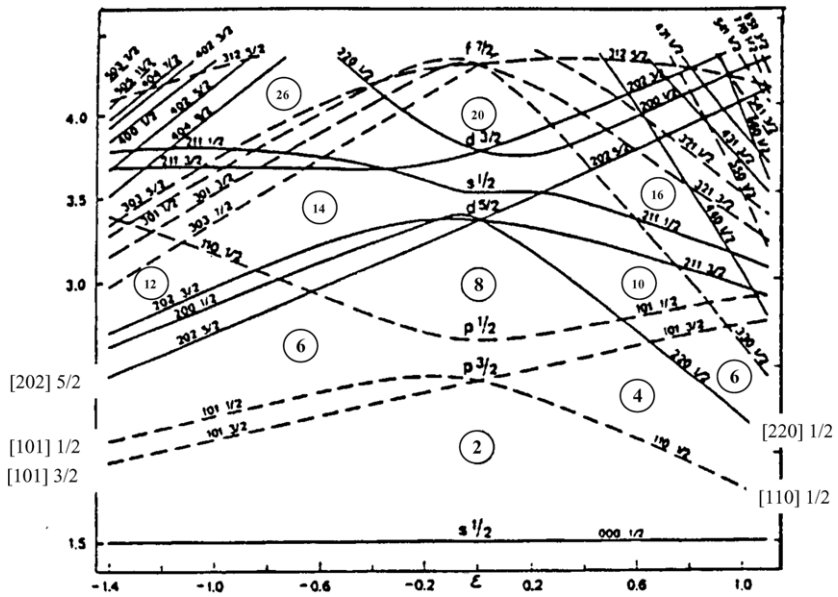

Figure 25. The Nilsson single-particle energy levels. The parameter ϵ corresponds to the deformation of the potential. The magic numbers are labelled as are some of the key Nilsson orbits [89].

projection onto the deformation axis) at a deformation of 2 : 1 are; $s_{1/2} : 1/2^+$, $p_{3/2} : 1/2^-$, $p_{3/2} : 3/2^-$, $d_{5/2} : 1/2^+$, $p_{1/2} : 1/2^-$ and $d_{5/2} : 3/2^+$.

For the first Nilsson orbit, l=0 and thus its projection is also zero, this clearly is associated with the σ-case. The second orbit originates from the $1p_{3/2}$ shell model orbit and has Nilsson quantum numbers $[n, n_z, \Lambda]K^\pi = [1, 1, 0]1/2^-$, in other words again no angular momentum component along the z-axis—and thus a $\sigma\, 1/2^-$ state. The $\pi 3/2^-$ and $\pi 1/2^-$ molecular orbits can be linked with the $[1, 0, 1]3/2^-$ $[1, 0, 1]1/2^-$ Nilsson orbits, where the $l = 1$ projection on the deformation axis couples with the nucleon spin as $l \pm 1/2$ to given total angular momentum projections $3/2^-$ and $1/2^-$. The connections between other orbits follows similarly.

These ideas allow an extension to other numbers of centres. The molecular orbitals for 2, 3, 4 centre linear arrangements were shown in figure 20. The lowest energy configuration ((*c*), (*e*) and (*h*)) is always the one in which the valence neutron is delocalized along the entire chain. This orbital can be seen to possess negative parity (since a reflection through the origin reverses the sign of the wave-function). For the two-centre case the molecular orbital is $\pi 3/2^-$—which corresponds to the ^{9}Be ground state. We see from figure 21 that the energy level for this structure is the first available orbital for all the $n : 1$ linear configurations. Thus all of the linear structures should have a lowest energy state which corresponds to K^π=$3/2^-$. The next lowest level shown in figure 20((*d*), (*f*) and (*i*)) all possess the same symmetry, and positive parity. From figure 21 a similarity with the [1, 0, 1] HO orbit is observed which is associated with the $[2, 1, 1]3/2^+$ Nilsson orbit, and thus this structure should be associated with $K^\pi = 3/2^+$.

The $K^\pi = 3/2^\pm$ configurations should give rise to two rotational bands with very similar moments of inertia. It can be seen from figure 25 that the two levels in question come closer together the larger the prolate deformation. Thus, for the linear structure in ^{13}C the two bands should be closer together than in ^{9}Be. Two rotational bands with this

Table 3. Properties of minima found in the NS calculations of Leander and Larsson [50]. ϵ_3 is the degree of octupole deformation.

Nucleus	ϵ	ϵ_3	γ (°)	Configuration	$\omega_x : \omega_y : \omega_z$
^{12}C	0.83	0	60	$(1)^{-4}$	2 : 1 : 1
	1.11	0	0	$(1)^{-8}(2)^4$	3 : 3 : 1
^{16}O	0.00	0	0		1 : 1: 1
	1.04	0	43	$(1)^{-4}(2)^4$	4 : 2 : 1
	1.2	0	0	$(1)^{-8}(2)^4(3)^4$	4 : 4 : 1
^{20}Ne	0.40	0	0	$(2)^4$	2 : 2 : 1
	1.17	0	50	$(1)^{-4}(2)^8$	8 : 3 : 2
	1.25	0	0	$(1)^{-8}(2)^4(3)^4(4)^4$	5 : 5 : 1
^{24}Mg	0.45	0	20	$(2)^8$	4 : 3 : 2
	1.0	0.3	0	$(2)^4(3)^4$	
	1.23	0	60	$(1)^{-4}(2)^{12}$	3 : 1 : 1
	1.26	0	42	$(1)^{-4}(2)^8(3)^4$	5 : 2 : 1
	1.25	0	0	$(1)^{-8}(2)^4(3)^4(4)^4(5)^4$	6 : 6 : 1
^{28}Si	0.49	0	60	$(2)^{12}$	2 : 1 : 1
	0.45	0	0	$(2)^{12}$	3 : 3 : 2
	1.0	0.3	0	$(2)^4(3)^4(4)^4$	
	1.35	0	60	$(1)^{-4}(2)^{12}(3)^4$	
	1.32	0	35	$(1)^{-8}(2)^8(3)^4(4)^4$	6 : 3 : 1
^{32}S	0.21	0	20	$(2)^{-8}$	5 : 4 : 3
	0.68	0	0	$(2)^{-12}(3)^4$	2 : 2 : 1
	1.42	0	54	$(1)^{-4}(2)^{-12}(3)^4$	10 : 3 : 2
	1.0	0.3	0	$(2)^8(3)^4(4)^4$	
	1.30	0	30	$(1)^{-4}(2)^8(3)^8(4)^4$	
^{36}Ar	0.29	0	60	$(2)^{-4}$	3 : 2 : 2
	0.74	0	7	$(2)^{-12}(3)^8$	
	1.45	0	55	$(1)^{-4}(2)^{-12}(3)^{12}$	
	1.33	0	47	$(1)^{-4}(2)^{-12}(3)^8(4)^4$	
^{40}Ca	0.00	0	0		1 : 1 : 1
	0.45	0	50	$(2)^{-4}(3)^4$	7 : 5 : 4
	0.84	0	5	$(2)^{-12}(3)^8(4)^4$	
	1.50	0	60	$(1)^{-4}(2)^{-12}(3)^{16}$	
^{44}Ti	0.18	0	0	$(3)^4$	3 : 3 : 2
	0.52	0	38	$(2)^{-4}(3)^8$	
	0.86	0	0	$(2)^{-12}(3)^{12}(4)^4$	
	1.50	0	60	$(1)^{-4}(2)^{-12}(3)^{16}(4)^4$	

character have been identified were identified by Milin and von Oertzen in ^{13}C [93] (see section 7.2).

6.5. No-core shell model

Sometimes indirect evidence is just as powerful as direct. The structure of ^{12}C has long been the subject of intense study. In particular, the structure of the 7.65 MeV 0^+, Hoyle, state has drawn great attention. This state is believed to possess a rather remarkable cluster structure, which is explored in section 7.1. Such a structure can be probed within the framework of a cluster model, but a well-developed cluster structure would be difficult to reasonably represent within the shell-model basis.

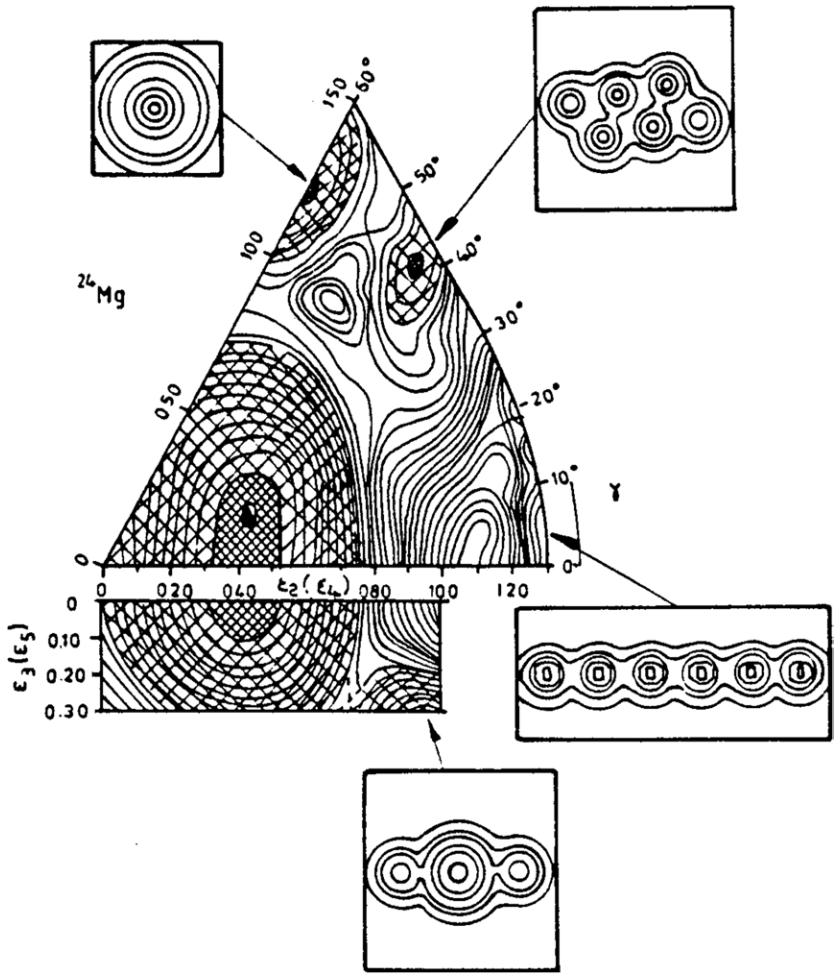

Figure 26. Nilsson–Strutinsky and α-cluster model calculations for ^{24}Mg [50, 88]. The potential energy is shown as a contour plot for the deformation parameters ϵ_2 and γ. Minima are found at particular deformations. For some of the potential minima the shapes obtained with the α-cluster model are indicated. The lower part shows the potential energy for the extension to octupole shapes with the parameter ϵ_3.

Shell-model calculations of the ^{12}C nucleus are shown in figure 27, taken from [94]. The calculations reproduce, rather well, the excitation of the first 2^+ excitation, but in the region of the second state, the 0_2^+ excitation, there is a void in the calculations, and even the inclusion of orbits very high up in the shell-model space ($>4\hbar\omega$) the energy of this state cannot be reproduced. This in itself points to the rather unusual structure of the state, possibly indicating the cluster structure.

The AMD and FMD calculations described in section 6.3, on the other hand, can reproduce the excitation of this state and, moreover, confirm its dramatic cluster character [95, 99].

It is rather interesting that the no-core shell model fails to find an accurate description of the 7.65 MeV state without the inclusion of high $\hbar\omega$ contributions, whereas the structure of a 3α-cluster state can be found within the harmonic oscillator description (figure 8) with only the inclusion of the $N = 2$ levels. It should be noted that in both the AMD and FMD

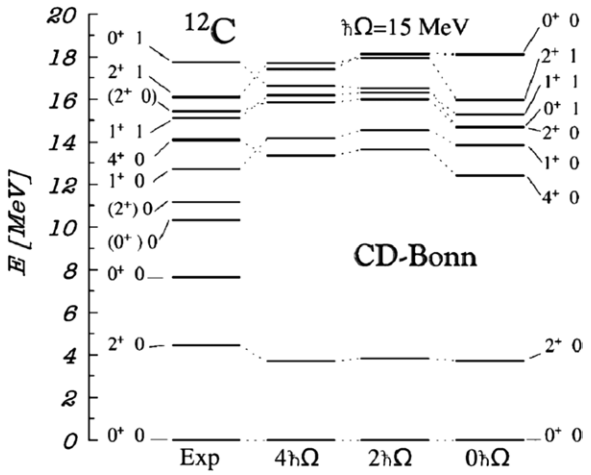

Figure 27. The no core shell-model calculations for the nucleus ^{12}C. The left hand part of the figure shows the experimental results. The calculations using the CD Bonn N–N interaction with increasing numbers of oscillator orbits are shown on the right. Reprinted with permission from [94]. Copyright 2000 by the American Physical Society.

calculations the resulting structure of this state is not the linear arrangement found in the HO description. In order to produce a state which has some large bending angle then certainly higher HO components would be required. This piece of evidence, alone, argues against the 7.65 MeV having a linear arrangement of α-particles, but something more akin to a bent chain. This is a topic explored in section 7.1.

7. Selected topics

7.1. The structure of ^{12}C—the Hoyle state

The structure of the nucleus ^{12}C remains one of the most important questions in nuclear physics. The ground state possesses the triangular 3α symmetry, but resides so far below the α-decay threshold (7.27 MeV) that the cluster structure is strongly suppressed. The ground state does, however, possess an oblate deformation and the first excited state at 4.44 MeV (2^+) and the 14.08 MeV (4^+) would be the corresponding rotational excitations. The state which is of greatest interest is the 7.65 MeV, 0^+, state. This is the portal for the synthesis of ^{12}C in stellar nucleosynthesis, and is named after Hoyle who proposed its existence [101]. In stars the nucleus ^{12}C is formed in a two-step process; the first involves the formation of ^{8}Be which has a fleeting existence, surviving for only $\sim 10^{-16}$ s before decaying. Before decay it is necessary that ^{8}Be captures a further α-particle, and then decay to the ^{12}C ground state proceeds via either sequential gamma-emission or pair production. Hoyle realized that the reaction rate was approximately 8 orders of magnitude too small to account for the known abundance of carbon—if this process were to occur through direct capture. He thus proposed the existence of a s-wave ($l = 0$) resonance through which the capture should proceed. Since reaction rates change exponentially with temperature in stars, as does barrier penetration, Hoyle was able to make a rather precise prediction for the energy of the proposed 0^+ resonance. The state was, of course, found at 7.65 MeV with 0^+ character, as predicted. This was a triumph for anthropic science—since the existence of the resonance was a requisite for human life. The importance of this state is arguably unparalleled in nuclear science. As a

consequence one would anticipate that the level of knowledge of the structure of the state would also be well documented. This is far from the case and the structure remains an open question.

For many years it was believed, in accordance with the Ikeda picture and the ideas of Morinaga [7] and Brink [6], that the 7.65 MeV should correspond to a linear chain structure. This interpretation was always problematic as a 2^+ member of the rotational band built on the 3 α-chain, is predicted by the ACM to lie at $\sim$8.4 MeV [61]. The closest 2^+ candidate is some 3 MeV higher in energy, and thus cannot be rotationally linked with the 7.65 MeV state if the configuration possesses a significant deformation. This feature alone casts considerable doubt on the connection of this state with the 3 α-chain. The energy 8.4 MeV lies between the 7.65 MeV state and a 3^- state at 9.64 MeV. In this region, a further state can be unambiguously excluded. However, the same is not true above the 3^- state. Thus, an extended configuration with a large moment of inertia, perhaps a bent chain [102–104], cannot be excluded.

There is, however, a rather intriguing possible alternative. Stimulated by developments in the field of cold-atom physics it has been speculated that the Hoyle-state corresponds to a dilute gas of α-particles. The α-particle possesses a bosonic nature and the proposed large radial extent of the excited state would in principle permit the internal fermionic degrees of freedom to be neglected. This invites the possibility that the three α-particles condense into the lowest (s-state) of their interaction potential—a Bose-Einstein condensate (BEC). In order to describe such a possibility, the Bloch–Brink wave-function (section 6.1) has been adapted to reflect the possible character of the state [105–107]. The condensed wave-function has the form

$$\langle \boldsymbol{r}_1, \ldots \boldsymbol{r}_N | \Phi_{n\alpha} \rangle = \mathcal{A}[\phi_\alpha(\boldsymbol{r}_1, \boldsymbol{r}_2, \boldsymbol{r}_3, \boldsymbol{r}_4)\phi_\alpha(\boldsymbol{r}_5, \boldsymbol{r}_6, \boldsymbol{r}_7, \boldsymbol{r}_8)\phi_\alpha(\boldsymbol{r}_{N-3}, \ldots, \boldsymbol{r}_N)]. \tag{25}$$

Here the construction is for N nucleons grouped into quartets described by ϕ_α. The wave-function of the α-particle is given by

$$\phi_\alpha(\boldsymbol{r}_1, \boldsymbol{r}_2, \boldsymbol{r}_3, \boldsymbol{r}_4) = \mathrm{e}^{-\boldsymbol{R}^2/B^2}\phi(\boldsymbol{r}_1 - \boldsymbol{r}_2, \boldsymbol{r}_1 - \boldsymbol{r}_3, \ldots), \tag{26}$$

where $[\boldsymbol{R} = \boldsymbol{r}_1{+}\boldsymbol{r}_2{+}\boldsymbol{r}_3{+}\boldsymbol{r}_4]/4$ is the c.o.m. coordinate of one α-particle and $\phi(\boldsymbol{r}_1{-}\boldsymbol{r}_2, \boldsymbol{r}_1{-}\boldsymbol{r}_3, ...)$ is a Gaussian wave-function

$$\phi(\boldsymbol{r}_1 - \boldsymbol{r}_2, \boldsymbol{r}_1 - \boldsymbol{r}_3, \ldots) = \exp([\boldsymbol{r}_1 - \boldsymbol{r}_2, \boldsymbol{r}_1 - \boldsymbol{r}_3, \ldots]/b^2) \tag{27}$$

Importantly, b is the size parameter of the *free* α-particle and B ($\gg b$) is the parameter which describes the size of the common Gaussian distribution of the three α-particles. In the limit that $B \to \infty$ then the antisymmetrization operator $\mathcal{A}$ ceases to be important and the wave-function (25) becomes the product of Gaussians, i.e. a wave-function describing a free α-particle gas [108].

One of the main successes of this model is that it manages to reproduce the form factor for the electron elastic excitation to the Hoyle-state without any arbitrary normalization [109] (see figure 28). These calculations reveal that the spatial extent of the 0_2^+, 7.65 MeV, excited state is such that the volume of the Hoyle-state is $\sim$3–4 times that of the ground state. It is this large volume which permits the realization of the clustering and the liberation of the α-particle gas. The recent FMD calculations of this state, indicate that the level of overlap with a 3α condensate is of the order of 70% [99]—which is a very large fraction for the individual α-particles. In [111] the statistics that such states were examined. It was demonstrated that for finite systems, as with the three α-case, all particles cannot aggregate into a single level, and thus the statistics are not entirely Bose–Einstein (BE). However, with increasing system size the BE description improves.

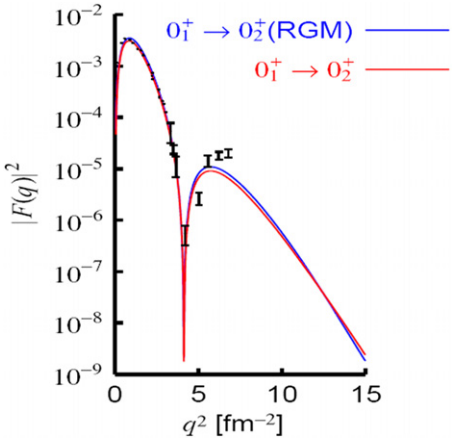

Figure 28. The calculated inelastic form factor for electron inelastic scattering from the 0^+ ground state to the 0_2^+ excited state [109], compared with the experimental data from [110].

The question then arises as to the nature of the excitations of the 0_2^+ state. If it is a condensate then the next level in the potential containing the 3α-particles would be a d-state, and thus the promotion of an α-particle from the s- to d-state would result in a 2^+ excitation. The model predicts this to lie $\sim$2.5 MeV above the 0_2^+ state, i.e. close to 10 MeV. From an experimental perspective this is a very challenging region to untangle. Aside from the narrow 9.64 MeV 3^- and 10.84 MeV 1^- states, there is a well-documented broad 0_3^+ resonance close to 10.3 MeV. The width is such ($\Gamma \sim 3$ MeV) that it extends across the whole region of interest. The experimental situation remains unclear at present. Measurements at RCNP using the ^{12}C(α, α') reaction indicate the possibility of a 2^+ component close to the 9.64 MeV 3^- state [112]. On the other hand, $\beta^{\pm}$-decay studies suggest that the 2^+ strength in this region is small [113]. The latter may be the consequence of a small FT value for the decay.

If a 2^+ excitation does exist then is there a collective 4^+ excitation also? If a vibrational model is employed then the 4^+ should lie close to $7.65 + 2 \times 2 = 11.65$ MeV (taking the energy of the 2^+ state to lie under/close to the 9.64 MeV state). There is no known state of this character close to this energy. If, however, a rotational model is used then the energy of the 4^+ would reside at $7.65 + 3.33 \times 2 = 14.31$ MeV. This could place the 4^+ state beneath the 4^+ collective excitation of the ground state. This would make detection difficult. Thus, it is possible that the collective excitations of the Hoyle-state is the best hidden secret in nature.

An alternative strategy might be to develop an understanding of similar states in the 4α-system ^{16}O. Some progress has been made from the theoretical perspective [109, 114], though again this is not matched entirely by experimental progress. There is some indication, again from the theoretical perspective, that the exotic structure of the Hoyle-state should have structural implications for other neighbouring nuclei. For example, AMD calculations suggest that states with a dilute nature and a well-developed $2\alpha + t$ structure exist in ^{11}B [115]. Inelastic scattering measurements, ^{11}B(d, d') [115], suggest there is a very large monopole strength for the excitation of the $3/2^-$ state at $E_x = 8.65$ MeV which is taken as a signature of the well-developed cluster structure. It is possible that measurements of the analogs of the Hoyle-state will provide key information as to the nature of the cluster structure of this all important state. One question which remains unclear is if the creation of the mixed boson-fermion cluster system $2\alpha + t$ changes in some way the essence of what makes the 3α state special.

7.2. Nuclear molecules—advances and perspectives

Nuclear molecules are a class of systems which can be described in terms of the exchange of valence particles between stable cluster cores. This is a topic which has been the subject of a recent, and detailed, review [85] and the reader is referred also to [55, 116] and references therein. The main advances in this field are considered here.

As has been demonstrated earlier, the ingredients required for the formation of nuclear molecules may be found within the symmetries of the deformed harmonic oscillator, figure 21. The full realization of the molecular structure is found when the potential is permitted to reflect the underlying cluster symmetry which is the two-centre shell-model limit, figure 15. At the limit of infinite separation, the two potentials describe the cluster cores, usually α-particles, and the valence nucleons (usually neutrons) reside in the next available orbits associated with each core. In the case of α-cores then the neutrons reside in the $p_{3/2}$ orbit corresponding to the $3/2^-$ ^{5}He ground state. As the two potentials overlap then the linear combinations of the $p_{3/2}$ orbits must be considered. As illustrated in figure 15, this then corresponds to molecular orbitals with σ and π character, depending on the orientation of the orbital angular momentum with respect to the symmetry axis of the 'molecule'. These two molecular orbitals are associated with total angular momentum projections $1/2$ and $3/2$, i.e. $J^\pi = 1/2^+$ and $3/2^-$. The rotational bands of the nucleus ^{9}Be clearly demonstrate the $\alpha + n + \alpha$ structure of this nucleus and the two molecular orbitals (figure 22).

The molecular analogue extends beyond the deformation of intrinsic structure associated with the rotational bands, but also to the concept of molecular binding. The ^{8}Be nucleus is unbound to decay into two α-particles, whereas ^{9}Be is stable. Similarly, the H_2^+ molecule consists of two protons which are individually unbound, but forms the molecular state when the single electron is introduced. Here, the important point is that the electron orbital is highly delocalized when it is covalently exchanged—reducing its kinetic contribution to the total energy and thus enhancing the stability. Similarly, the covalent neutron binds the two α-cores, in this case by 1.67 MeV (for the π-bond). A detailed discussion of these points is found in the seminal contributions by von Oertzen on this topic [17, 18].

Several questions arise from the observation that the nucleus ^{9}Be can be described in terms of a molecular structure: *(i)* are molecular structures observed in heavier beryllium isotopes? *(ii)* can longer structures be formed, e.g. from 3α-particles and valence neutrons, in carbon isotopes and *(iii)* do molecular structures exist for cores other than α-particles? The answers to many of these is, more or less, yes, though in several instances more experimental work is required to produce the definitive proof.

7.2.1. Beryllium isotopes: 2 centre molecules. The addition of a neutron to the ^{9}Be ground state can produce a number of configurations. The lowest energy state corresponds to the $(p_{3/2})^2$ configuration, in other words two neutrons in the π-molecular orbital. Rather interestingly, this state is bound with respect to 2n removal by ~8.5 MeV and to 1n removal by 6.8 MeV. Thus, the ground state lies a long way below the associated cluster decay thresholds. For this reason, it is unlikely that the molecular structure is strongly developed in the ground state, just as the 3α-cluster structure is not strongly represented in the ^{12}C ground state—even though the symmetry exists.

There are four states which lie much closer to the cluster decay thresholds: 5.9583 MeV $[2^+]$, 5.9599 MeV $[1^-]$, 6.1793 MeV $[0^+]$ and 6.2633 $[2^-]$. These potentially would have a cluster structure which is much more strongly developed. The negative parity states correspond to an excitation of a neutron from the p-shell to the sd-shell. Within the two-centre shell model the lowest lying sd-orbital corresponds to the $\sigma 1/2^+$ state, which is associated with

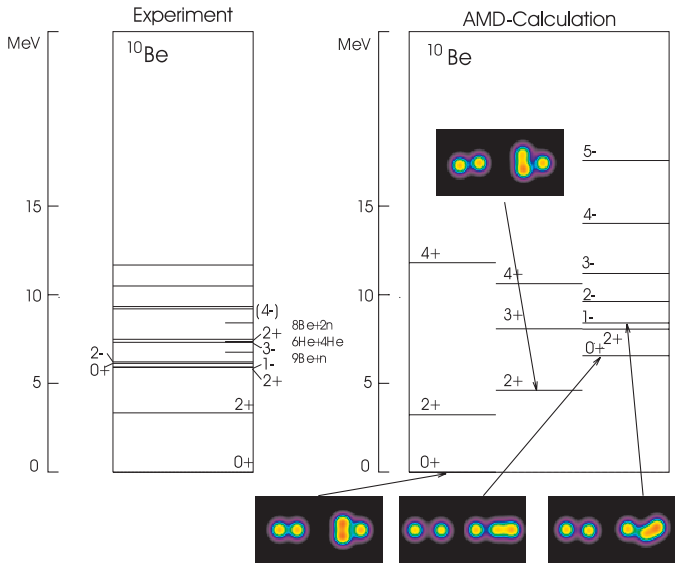

Figure 29. (Left) Experimental level scheme of ^{10}Be. (Right) The calculated level scheme using the AMD framework [118]. The contour plots illustrate the densities of the protons (left part) and neutrons (right part) for the various configurations. Of particular note are the structures associated with the 1^- and 0^+_2 states. The cluster-cluster separation, as evidenced by the proton density, is found to be largest for the 0^+_2 state.

the $1/2^+$ first excited state in ^{9}Be. The geometry of the σ and π orbitals is characteristically different. In the σ-case the neutron(s) lie between the α-cores and by virtue of the Pauli-repulsion promote the α–α separation. The 1^- and 2^- states have been interpreted as being members of a $K^\pi = 1^-$ rotational band [17, 18, 117] with a σ-π configuration for the two valence neutrons. That is to say the band should possess a large deformation and an underlying molecular structure. The negative parity states require both the breaking of the neutron pair and an excitation to the next major shell. Thus, the 2n excitation to the sd-shell should have a very similar excitation energy. The 0^+_2 state has thus been associated with a σ^2 molecular configuration.

This interpretation is consistent with that found within the AMD calculations for ^{10}Be [118, 119], shown in figures 29 and 30. In these calculations the cluster structure in the ground state, as judged by the separation of the protons, is less pronounced than in the excited states located close to the cluster decay threshold. Moreover, the molecular configurations of the 0^+_1, 1^- and 0^+_2 states is confirmed.

The 0^+_2 state should thus be the most deformed of the three. The gamma-decay of this state is suppressed (it possesses a lifetime of the order of 1 ps). This isomeric behaviour may be understood in terms of the small overlap of its structure and that of the more compact ground state. The excited state at 7.542 MeV (2^+) is believed the first rotational member of the associated band. This state lies very close to the α-decay threshold (7.409 MeV) and thus its decay to this channel is strongly suppressed by the Coulomb and centrifugal barriers. Nevertheless, the α-decay has been found to correspond to a very large reduced width [120], representative of the large degree of clusterization associated with the state. The 4^+ member of the band would lie in the region of 10–11 MeV. There are a number of possible states which could correspond to the molecular band; 10.15 and 10.57 MeV. The spin of the latter state is unknown (it has a tentative assignment of 3^- from [117]), whereas the former has

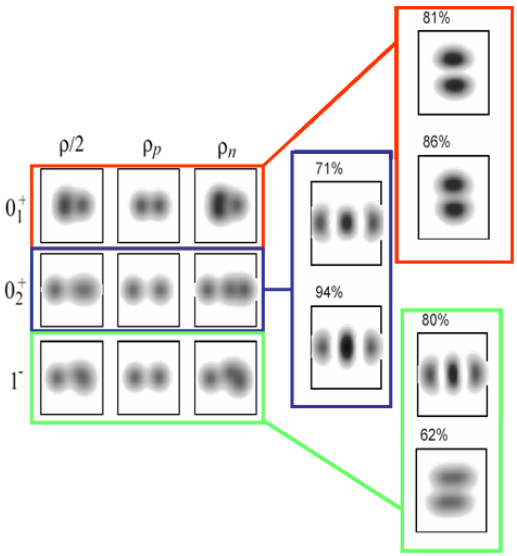

Figure 30. (Main part) The densities of protons (middle), neutrons (right) and total (left) for the three states 0^+_1 (ground state), 0^+_2 and 1^- states. The dominant components of the densities of the two valence neutrons for the three states are shown on the right-hand part of the figure. Note that for the ground state the neutrons have dominant π-components, 1^- mixed π and σ and 0^+_2 just σ. Adapted from [119].

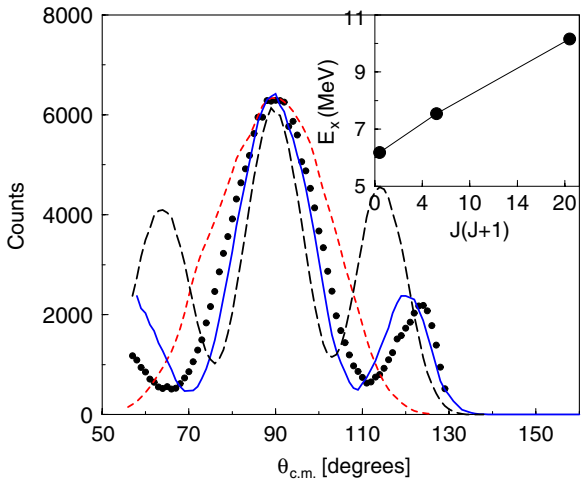

Figure 31. Experimentally determined center-of-mass distribution (data points) compared with simulations for the decay of a spin 4 (solid line), 2 (dashed line) and 6 (long-dashed line) resonance. The inset shows the energy-spin systematics of the rotational band of which the present 4^+ state is a member, from [123].

been associated with spins 3^- [121] and 4^+ [122]. The latter assignment was also found in a measurement of the resonant scattering of ^{6}He + ^{4}He [123] (figure 31). The resonance appears to be the 4^+ member of a rotational band built on the 6.18 MeV (0^+_2) state (the inset in figure 31). The rotational gradient ($\hbar^2/2I$, I being the moment of inertia) of the band is 0.20 MeV. This may be compared with that for the ^{8}Be and ^{9}Be ground state bands of 0.57 MeV and 0.53 MeV,

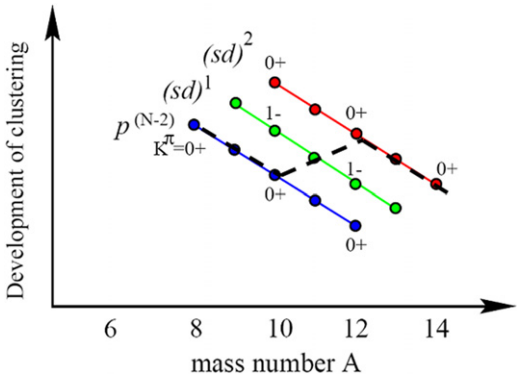

Figure 32. The development of clustering in the beryllium isotopes according to the filling of the molecular orbitals. p^{N-2} corresponds to the π-orbit, $(sd)^1$ and $(sd)^2$ correspond to 1 or 2 neutrons in the σ-orbital, respectively. The dashed line indicates the configuration of the ground states. Adapted from [87].

respectively. In other words the separation of the two α-clusters is greatly enhanced in ^{10}Be a feature which is seen in the AMD calculations for the ^{10}Be 6.18 MeV (0^+) state [95] and which, as noted earlier, arises from the presence of the *molecular* neutrons between the two α-cores. The measurement of the 4^+ state indicates, as was found for the 2^+ state, that reduced α-width was very large compared with the Wigner limit.

The proposed ^{10}Be negative parity band was shown in figure 19. This possesses a very similar rotational gradient ($\hbar^2/2I$) to that found for the $K^\pi = 0^+$ band. However, the moment of inertia is slightly less than for the σ^2 band—consistent with the images in figures 29 and 30.

The question of if such structures persist to heavier beryllium isotopes, even to the point of the drip-line is intriguing. As indicated in [85] (and references therein) it is also possible to find evidence for molecular structures in ^{11}Be. For example, the $1/2^+$ ground state is associated with a coriolis decoupled band with a large moment of inertia and the $3/2^-$ excited band with $\hbar^2/2I = 230$ keV. The $K^\pi = 1/2^+$ configuration is associated with the ^{10}Be ground state (π^2) with a σ neutron, whereas the excited band is related to the ^{10}Be(1^-) structure coupled to a σ neutron ($\sigma^2\pi$). Here the molecular structures appear to play a dominant role in the low-lying deformed configurations of ^{11}Be. It is worth observing that these conclusions are broadly matched by those reached in the resonant ^{10}C + p scattering measurements populating states in ^{11}N [124]. In that instance the ground state was found to be associated with a $2s_{1/2}$ proton and a narrow $3/2^-$ resonance with the $(1p_{3/2})(2s_{1/2})^2$ proton structure. It was further noted that there were anomalous Coulomb energy shifts which indicated that these states were associated with larger radii than say the $1/2^-$ shell-model like state. This larger radius would in the present picture be associated with the well-developed molecular structure, particularly in the $3/2^-$ band.

This evolution of the molecular structures across the beryllium isotopes is illustrated in the figure 32, which is taken from the review in [87]. The development of clustering is strongly related to the relative number of σ (sd) and π (p) neutrons. The σ-neutrons tend to drive the α-cores apart, whilst those of π character tend to produce a more spherical structure. So if the case of ^{10}Be is considered, the expected ordering in terms of increasing clusterization, 0^+_1, 1^- and 0^+_2, is found. The dashed line shows the location of the ground states. For ^{9}Be this corresponds to the π configuration whereas the ground state is the σ-configuration for ^{11}Be. The $3/2^-$ band being associated with σ^2 neutrons and has the largest deformation.

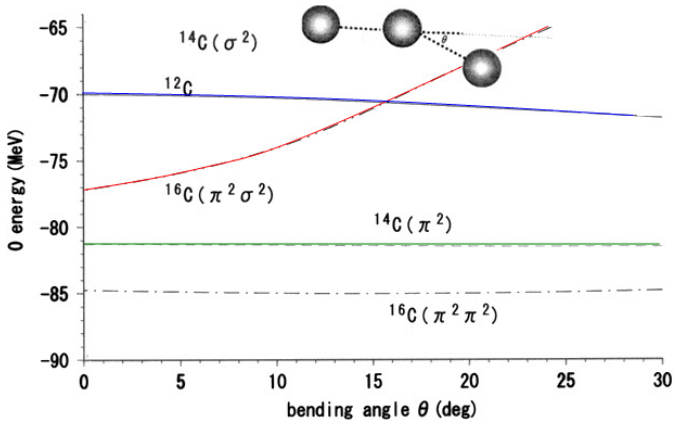

Figure 33. The energy of the 0^+ states associated with various molecular configurations in ^{14}C and ^{16}C, together with the 3α-system ^{12}C as a function of the bending angle of the chain of α-particles. Reprinted with permission from [79]. Copyright 2001 by the American Physical Society.

In ^{12}Be the ground state is the $\pi^2\sigma^2$ valence neutron structure and the first excited 0^+ state (2.24 MeV) π^4. This corresponds to a compact structure whose small overlap with the ground state ensures its isomeric behaviour [125]. The more pronounced cluster states appear at higher energies. For example, a band of resonances which decay into two ^{6}He nuclei were observed in the inelastic scattering of a ^{12}Be projectile above an excitation energy of 12 MeV [126,127]. Similar measurements suggest there may be a series of cluster states in ^{14}Be which decay into ^{8}He + ^{6}He above the cluster decay threshold [128].

7.2.2. Carbon isotopes: 3 centre molecules. The apparently reasonable description of nuclei such as ^{9}Be and ^{10}Be in terms of the molecular picture leads to a natural extension—can three centre systems be constructed and do these form linear structures? Calculations based on the molecular orbit framework (see section 6.2), where molecular orbits are constructed around three α-particles produced some interesting results. The energy of 0^+ states in the carbon isotopes ^{12,14,16}C were calculated as a function of the bending angle of the underlying linear configuration of three α-particles (see figure 33). As might be expected, the three α-particles in ^{12}C were found to unstable against collapse into the more compact triangular structure. However, in ^{16}C where the 4 valence neutrons occupied the $\pi^2\sigma^2$ molecular configurations (where the neutrons are exchanged between two centres) the energy of the 0^+ state rises with increasing bending angle. This was attributed to the effect of the Pauli-principle—as the chain bends the wave-functions of the molecular orbitals begin to overlap with those in the core giving rise to Pauli repulsion [79]. Thus, it might be anticipated that although the linear structure is unlikely to exist in ^{12}C, it might in ^{16}C, where it is stabilized by the molecular structure. A similar effect is observed for ^{14}C, though the increase in energy occurs for larger bending angles than displayed in figure 33. Such a molecular structure might exist in ^{13}C also.

The $3\alpha + n$ structure in ^{13}C has an intrinsic asymmetry as illustrated in figure 34. The neutron, be it in a σ or a π orbital, must reside on either side of the central α-particle in the intrinsic frame. This asymmetry means that in order to find a quantum representation then both odd and even parity states are required, just as with octupole nuclei [35]. This may alternatively be viewed in terms of the probability for the neutron to tunnel from one side of the central α-particle to the other. The overlap of the two corresponding wave-functions gives

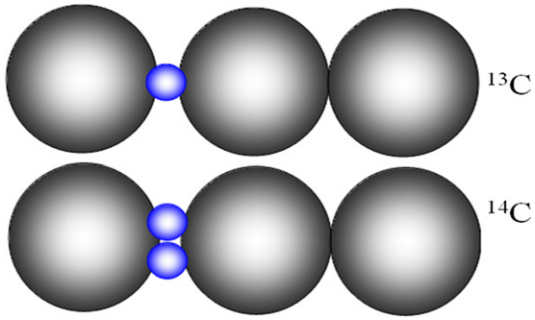

Figure 34. The 3α + n and 3α + 2n structures in ^{13}C and ^{14}C, respectively.

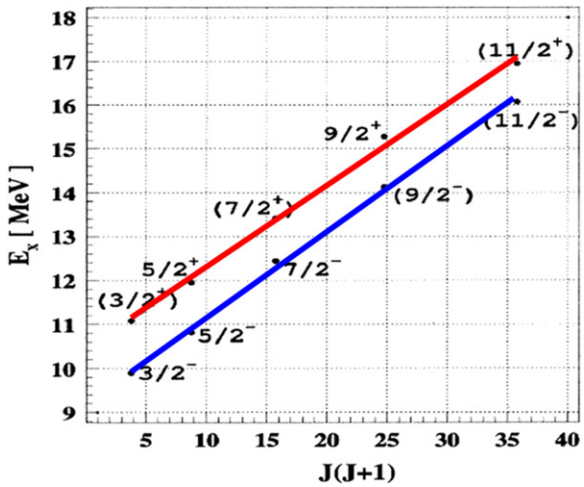

Figure 35. The proposed rotational bands in ^{13}C with a molecular structure, from [93].

rise to two new states (with $2N$ and $2N$+1 nodes; N being the number of nodes in the one centre wave-functions) the energy splitting depends on the tunnelling probability. The two new states have opposite parity.

As discussed in sections 6.4 and 5.1, the lowest energy configuration formed from the linear combination of p-orbitals has negative parity and is of π-type character (figure 20(e)). This was associated with the orbital derived from the $1p_{3/2}$-orbital with the projection of the angular momentum on the deformation axis of $K^\pi = 3/2^-$. Similarly, the second highest level corresponds to a positive parity state (figure 20(f) associated with the $K^\pi = 3/2^+$ component of the $1d_{3/2}$ shell-model orbital. Thus, the signature for such a molecular structure in ^{13}C would be two rotational bands built on bandheads with spin and parity $3/2^-$ and $3/2^+$. Milin and von Oertzen [93] analysed the tabulated energy levels of ^{13}C to search for two bands of the requisite character (see figure 35). The two bands, shown in figure 35, appear to possess the same moment of inertia and have a splitting of the magnitude that is anticipated—however, many of the spin and parities remain uncertain and further experimental measurements are required to confirm the systematics. A similar analysis was performed for ^{14}C [129] where candidates for positive (0^+) and negative (1^-) parity bands were identified. In this case the two neutrons are paired in the lowest energy intrinsic molecular structure and so both reside

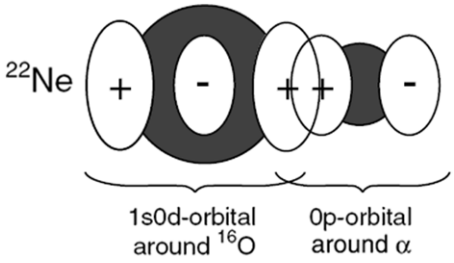

Figure 36. The covalent exchange of a neutron between the ^{16}O and α cores that occurs in the neon isotopes. Reprinted with permission from [132]. Copyright 2007 by the American Physical Society.

on one side of the central α-particle (figure 34). The moments of inertia ($\hbar^2/2I$) of the two bands were found to be 120 and 130 keV which compare with the 190 keV extracted for the ^{13}C bands shown in figure 35. The case for these structures is further developed in [85] and is compelling, but much more experimental work is required to fully characterize these states.

One experimental complexity is that at a very similar excitation energy exist a series of molecular states which, rather than possessing prolate character, are oblate. In this instance the neutrons could reside within the plane of the 3α triangular structure—in which case they intercede between the α-particles increasing the radius and lowering the binding energy. As an alternative the neutron orbitals can be delocalized above and below the plane of the α-particles—with a change in phase of the wave-function across the plane [57]. In this instance the lowest energy molecular orbital is associated with the Nilsson orbital $[110]1/2^-$ and thus the oblate molecular structure in ^{13}C should have $J^\pi = 1/2^-$ [57]. The oblate states in ^{14}C are discussed in [85, 129, 130].

7.2.3. Asymmetric cores. The production of molecular structures in the case of asymmetric cores introduces additional concepts. This is the case when one considers the cluster structure of the neutron-rich neon isotopes. The nucleus ^{20}Ne is known to have a well-developed $\alpha + ^{16}$O cluster structure [34, 133], the asymmetric structure giving rise to two rotational bands of $K^\pi = 0^\pm$ character [35]. The question as to what happens to valence neutrons introduced into this system was addressed by von Oertzen [131]. When the neutron orbits the α-particle its lies in a p-orbital (negative parity), when orbiting the closed shell ^{16}O it resides in the sd-shell (positive parity, associated with the $5/2^+$ ground state). The two orbitals which will be aligned with the intrinsic deformation of the α-^{16}O system are the harmonic oscillator levels $[n_x, n_y, n_z] = [0, 0, 1]$ and $[0, 0, 2]$ (see figure 21). These are associated with the Nilsson orbitals with projections $K^\pi = 1/2^-$ and $1/2^+$; both have σ-character. The strong overlap of these two orbitals in the region between the cores gives rise to the molecular binding effect, illustrated in figure 36. The resulting hybridized orbital gives rise to parity doublet bands [131], just as was explored in the case of three centre molecules (section 7.2.2), and in detail in [85]. A rather beautiful demonstration of the molecular behaviour of the last two neutrons in ^{22}Ne is displayed in figure 37 [132]. Here the densities of the neutron pairs (1–6) in ^{22}Ne are plotted against the core background as calculated within an extension of the AMD framework. The orbitals 1–5 are localized within the ^{16}O core or α-particle, as expected, but for the last two valence neutrons are delocalized between the cores. They have a density distribution which coincides with that expected from the two harmonic oscillator orbitals discussed above. In

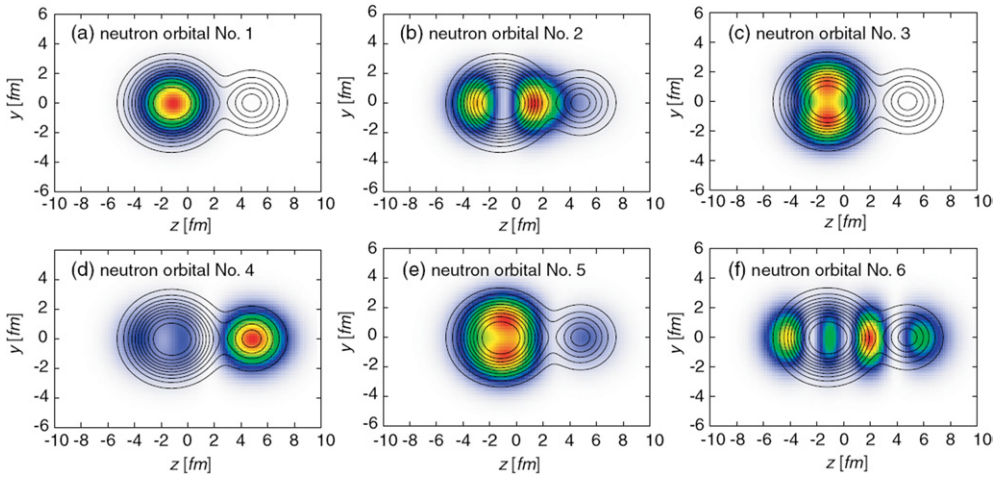

Figure 37. The density distributions of the core and the neutron single-particle orbitals. Contour lines show the density distribution of the core and are common to all figures. The colour plots show the density distribution of the neutron orbitals lowest: 1 (*a*) to highest: 6 (*f*). Reprinted with permission from [132]. Copyright 2007 by the American Physical Society.

this particular configuration, the presence of the σ-molecular neutrons between the two cores serves to enhance the clusterization, just as was found with the 0^+ excited state in ^{10}Be.

7.3. Large di-nuclear clusters

The ideas developed in section 4, which allowed composite structures to be formed from large (i.e. non-α) clusters, invite some interesting predictions. For example, it is possible to ask what kind of cluster structures might be formed in ^{32}S via the fusion of two ^{16}O nuclei? Or, and slightly more complicated, the fusion of two ^{12}C nuclei? The answers to these and other questions may be found in figure 38. Here the Harvey prescription is employed to chart the evolution of the nucleons in the constituents (pairs of protons and neutrons are represented by black dots) to those in the composite system. So for example, it can be seen that the fusion of two ^{16}O nuclei produce a state in ^{32}S which corresponds to a 4p–4h excitation, where an α-particle is promoted to the fp-shell. This is exactly the configuration which appears in the deformed HO at the 2 : 1 shell gaps (figure 7). This shell gap correspondingly appears as a minimum in the Nilsson-Strutinsky calculations [50]. Again, it can be seen that the application of the Harvey prescription preserves the cluster structure in the fused system—a dumbbell type structure is observed. In other words, it should be possible to populate such a structure in, for example, ^{16}O + ^{16}O resonant scattering.

Since the nucleus ^{12}C has an intrinsic oblate deformation, there are three possible relative orientations that the deformation axes of the two ^{12}C nuclei might take. These are also shown in figure 38. The different orientations result in different ^{24}Mg structures—all of which have counterparts in figure 26. Again, one might expect that such structures can be observed in ^{12}C + ^{12}C resonant scattering.

Of course, there is a wealth of evidence to suggest that indeed it is possible to for di-nuclear systems in collisions of ^{12}C and ^{16}O nuclei (amongst others). These observations date back to the earliest days of heavy ion science (the 1960s) and have since those days intrigued

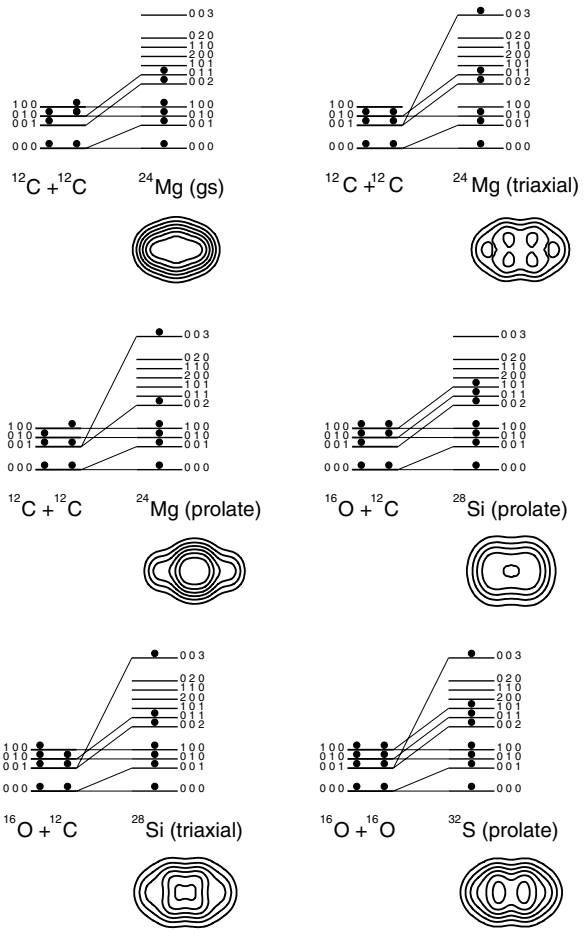

Figure 38. Cluster structures produced in the fusion of ^{12}C and ^{16}O nuclei predicted using the Harvey prescription [92]. Each black dot represents an α-particle—a pair of protons and a pair of neutrons with their total angular momentum coupled to zero. For the fusion involving the oblate nuclei there are several possibilities due to the differing orientations of the deformation axis. Thus, in the fusion of ^{12}C with ^{16}O there are two non-degenerate possibilities and with ^{12}C there are three.

the field. The experimental evidence has been reviewed extensively, for example by Erb and Bromley [40], Cormier [41] and Eberhard [42]. Cindro also produced an extensive compilation of resonant systems [134, 135].

7.3.1. $^{12}C + {}^{12}C = {}^{24}Mg?$ Despite there being such a vast scientific commitment to the study of the resonances the subject never found complete closure. Part of the reason for this can be traced to the complexity of the data. Unlike superdeformed structures in heavier nuclei, where an intrinsic structure may be characterized by a single rotational band, or for octupole deformed systems two interleaving bands of opposing parity, di-nuclear rotational bands do not have a simple structure. This is best illustrated by the data for the ^{12}C + ^{12}C system which is by far the most complete. The energy spin-systematics of the resonances are shown in figure 39. Rather than being characterized by a single set of rotational states, there are many states of the same spin. This multiplicity has in the past been interpreted as evidence for

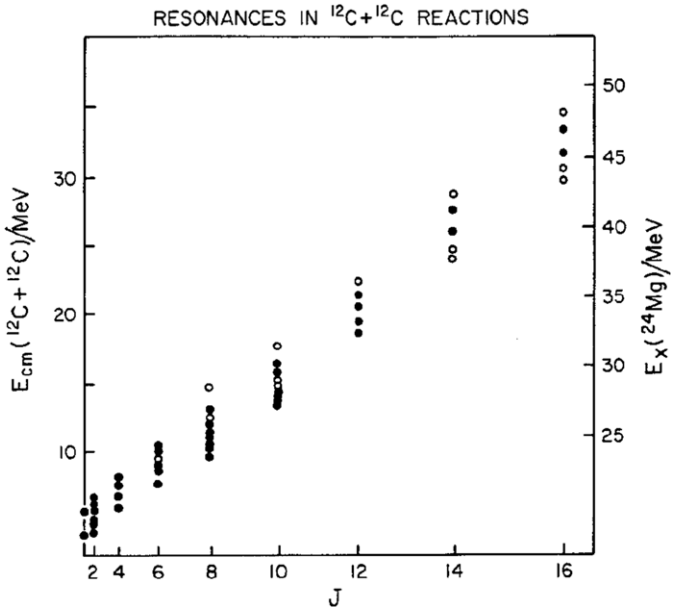

Figure 39. Energy-spin systematics of $^{12}C + ^{12}C$ resonances, from [138].

vibrational modes coupled to the rotational one [137]. This explanation is probably less likely than others which relate the superdeformed cluster states to those in the normal deformed minimum, as in the case of the fission isomers [136]. With the fission isomers, broad states in the second minimum are fragmented into a series of narrow resonances through the coupling to configurations associated with the ground state well. Fission then proceeds from the ground state well via coupling of states with the same spin and parity in the normal and superdeformed minima. Thus, a sequence of states with common J^{π} are produced modulated by the envelope of the broad superdeformed resonances. The spectrum of resonances observed in figure 39 would appear to possess the same character. In this case the fission probability is enhanced by the coupling between the wells. However, this coupling also serves to fragment the states in the second minimum. A recent theoretical analysis of the superdeformed states in ^{32}S within the AMD framework, suggested that there was such a fragmentation of the strength in the superdeformed well via coupling to the normal deformed states, much as described above [52]. This type of behaviour is also observed in scattering of a range of heavy-ions on α-particles, using helium gas 'targets' in inverse kinematics [139, 140]. For example, the multitude of resonances observed in these incredibly detailed measurements for the composite systems ^{28}Si and ^{32}S demonstrates that they, on the whole, follow a rotational trajectory with each rotational state being fragmented into a large number of narrow states. By extension of the ideas developed in, for example, section 6.4 the broad structures would be associated with the secondary minima which appear in the potential energy surfaces of the Nilsson–Strutinsky calculations (figure 26).

Before exploring the link between the experimental data and the possible cluster configurations, it should be observed that clustering appears in two limits. These correspond to strong and weak coupling. In strong coupling, the clusters are strongly coupled and give rise to rotational structures associated with a rigid intrinsic cluster configuration. In this way rotational bands are generated by cranking the cluster structure. In the other, weak coupling,

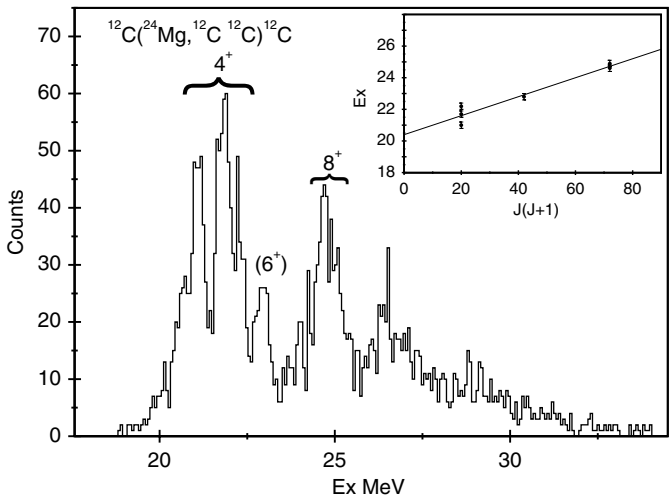

Figure 40. The excitation energy spectrum of ^{24}Mg corresponding to the breakup into two ^{12}C nuclei, from the ^{12}C(^{24}Mg,^{12}C^{12}C)^{12}C reaction. The energy-spin systematics of the break up states are shown in the inset, from [143].

limit the clustering arises from the dynamics of the interaction, i.e. a pocket in the cluster–cluster potential and there is no rigid cluster structure. The strong coupling limit may be associated with the types of cluster structures and bands produced by the ACM, whilst the weak coupling limit is associated with the resonances which are produced by, for example, the RGM. The scattering resonances observed in ^{12}C + ^{12}C collisions could in principle be associated with either picture. The question as to where the experimental data lie, between these two limits, could in part be probed by adopting an alternative experimental approach. If, rather than scattering two ^{12}C nuclei, inelastic scattering of a ^{24}Mg projectile is employed then some overlap with the ^{24}Mg ground state would be expected. This was the approach employed in measurements of the ^{12}C(^{24}Mg,^{12}C^{12}C)^{12}C breakup reaction, in which the decay of the excited ^{24}Mg states into two ^{12}C clusters is probed. This work is extensively reviewed in [88,92]. The spectrum of states observed in the breakup reaction is shown in figure 40. The spins of a number of the resonances were measured using angular correlation techniques [143] and were found to roughly lie on a rotational trajectory (shown as an inset in figure 40). The associated moment of inertia was consistent with that found for the scattering resonances, shown in figure 39, suggesting a common origin. A higher resolution measurement of the ^{12}C(^{24}Mg,^{12}C^{12}C)^{12}C breakup reaction reaction was reported by Curtis *et al* [144] (figure 41). This showed that the region of the excitation energy spectrum associated with the 4$^+$ states is further fragmented into a finer structure. These narrower resonances correlated well with the, so-called, barrier resonances observed in reactions proceeding from the ^{12}C + ^{12}C entrance channel [145, 146], reinforcing the idea of a common origin.

One of the limitations of the ^{12}C(^{24}Mg,^{12}C^{12}C)^{12}C reaction is that the probability for exiting higher spin states diminishes. In this respect the alternative reaction ^{12}C(^{16}O,^{12}C^{12}C)α has been extremely productive. The spectrum in figure 42(*a*) shows the measurements of the breakup of ^{24}Mg to two ground state ^{12}C nuclei at incident ^{16}O energies of 115 MeV (Freer *et al* [147]) and 160 MeV [148]. The excitation energy spectrum extends from about 20 MeV up to 55 MeV, and provides evidence for resonant structures persisting to extremely high excitation energies in the ^{24}Mg system, a remarkable result as complexity might be expected to increase exponentially with excitation energy. Given that the resonances decay by the emission of two

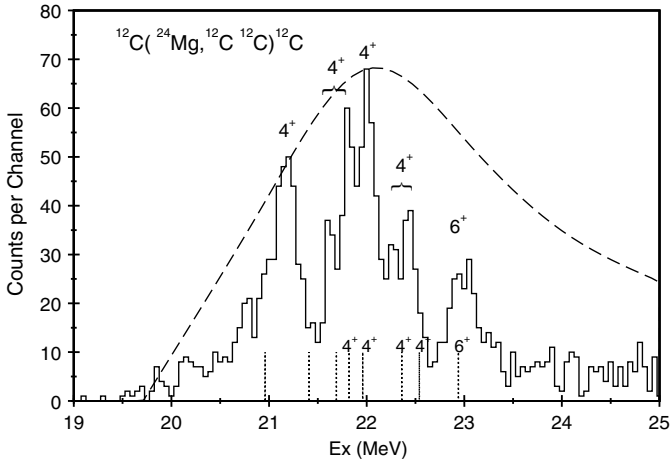

Figure 41. The ^{24}Mg excitation energy spectrum from [144], showing the fragmentation of the structures close to 22 MeV into narrower, ∼100 keV, resonances. The vertical lines indicate the energies of barrier resonances observed in the same energy region from [145, 146]. The dashed line represents the magnitude of the detection efficiency in the measurement.

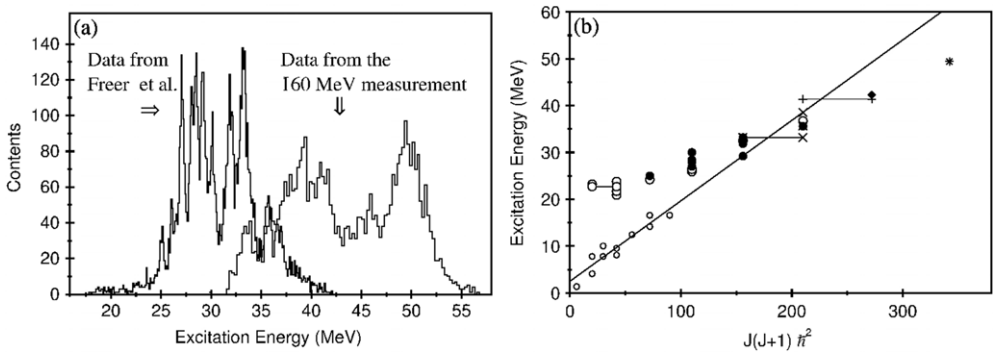

Figure 42. (*a*) Resonances observed in the ^{12}C(^{16}O,^{24}Mg*) breakup reaction [147, 148]. (*b*) The energy-spin systematics of the breakup resonances, from [148]. The smaller symbols and the solid line indicates the trend of the yrast states in ^{24}Mg.

spin-zero fragments, then the spin of the resonance is carried by the orbital angular momentum of the two particles. Thus, it is possible to utilize angular correlation techniques to extract the spins of the decaying states. Figure 42(*b*) shows the energy-spin systematics of the resonances observed in this particular reaction. The resonances occupy a rotational locus and extend up to a maximum spin of $J^\pi = 18^+$. For comparison the locus of the yrast ^{24}Mg states at low excitation is shown. It is clear that the moment of inertia of the higher energy 'band' is considerable, i.e. corresponds to a structure with a large deformation, and thus is a candidate for being one of the deformed cluster structures identified in figure 26. Figure 43 is a comparison between the high energy breakup data and resonances observed in ^{12}C + ^{12}C inelastic scattering. The lower part of the figure, figure 43(*b*), shows the breakup data, using a slightly different experimental cut to the data in figure 42, and demonstrates that the resonance at 50 MeV is actually the terminating state in the rotational band in figure 42(*b*). Figure 43(*a*) shows a compilation of the inelastic scattering data from [149, 150, 153]. The inelastic scattering to the ^{12}C(2^+) + ^{12}C(2^+) final

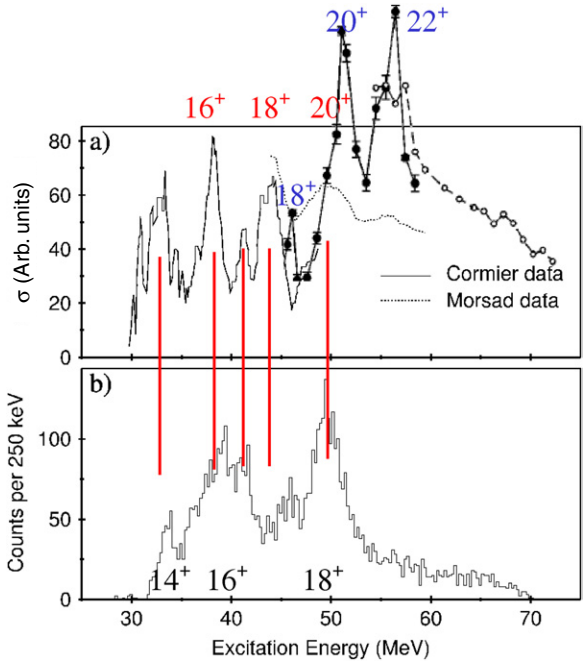

Figure 43. (*a*) Compilation of high energy resonances observed in inelastic scattering measurements; $^{12}C(2^+) + {}^{12}C(2^+)$ (Cormier [150] and Morsad [153] data), $^{12}C(3^-) + {}^{12}C(3^-)$ are the data points from [149, 154]. (*b*) Resonances observed in the $^{12}C(^{16}O,^{24}Mg^*)$ breakup reaction [148].

state (Cormier data [150] and Morsad data [153]), shows a number of resonance-like structures which extend up to about 56 MeV. These are echoed in the excitation function corresponding to the scattering to the $^{12}C(3^-) + {}^{12}C(3^-)$ final state (both in terms of the energy and the deduced spins). High energy measurements of the $^{12}C + {}^{12}C$ inelastic scattering, with center-of-mass energies up to 60 MeV (^{24}Mg excitation energies of 74 MeV) show that there are no further narrow resonant structures in the inelastic scattering reaction [149]. Thus, these resonances terminate at an excitation energy of 56 MeV with a spin of 22 $\hbar$. The figure is organized such that it is possible to compare the ^{24}Mg resonances populated in the two reactions. The first thing to note is that the resonances observed in the $^{12}C(2^+) + {}^{12}C(2^+)$ and $^{12}C(3^-) + {}^{12}C(3^-)$ channels agree both in terms of energy and spin. So it would appear that the same states are sampled by the two reaction channels. Secondly, the resonance spins are different for the 50 MeV resonance populated in the inelastic scattering and the $^{12}C(^{16}O,\ ^{24}Mg^*)$ reaction, and the 18^+ resonance observed in the inelastic scattering data appears to have no counterpart in the breakup data. Thus, there would appear to be very real differences between the resonances populated in the breakup and inelastic scattering reactions.

On the other hand, a comparison between the breakup states populated in the $^{12}C(^{16}O,\ ^{24}Mg^*)$ and $^{12}C(^{20}Ne,\ ^{24}Mg^*)$ reactions shows remarkable agreement [151]. This comparison is shown in figure 44. As discussed in [151] the agreement between the states populated in the two reactions is almost exact, i.e. the number of states, their energies and spins. Of course the strengths with which the two sets of states are populated are different, but this is a reflection of differences in the reaction mechanism. There is, however, one crucial difference between the two sets of data, and that is the appearance of the 14^+ states in the $^{12}C(^{16}O,^{24}Mg^*)$ reaction, which are absent in the $^{12}C(^{20}Ne,^{24}Mg^*)$ measurement.

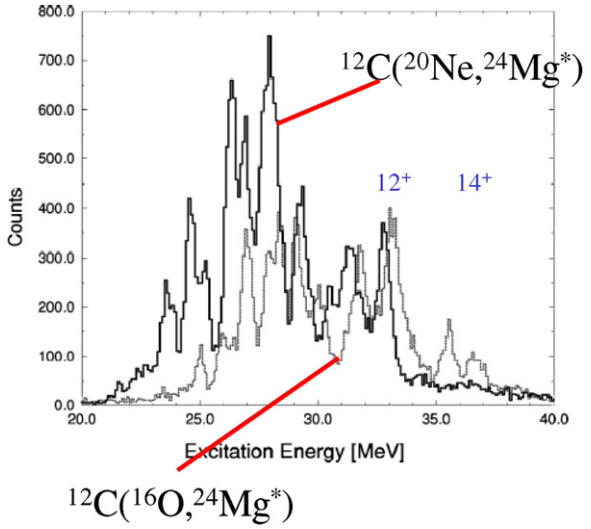

Figure 44. Comparison between resonances observed in the $^{12}C(^{16}O,^{24}Mg^*)$ and $^{12}C(^{20}Ne,^{24}Mg^*)$ reactions. The spins of the highest energy resonances, populated in the two reactions, are indicated.

This difference can be understood if it is assumed that in the $^{12}C(^{20}Ne,^{24}Mg^*)$ reaction the alpha-particle is transferred to the fp-shell ($N = 3$), in which case the maximum angular momentum that can be generated (assuming the ^{20}Ne core remains inert) is $12\,\hbar$. If, however, the starting point is a ^{16}O core, then the transfer of one alpha-particle to the fp-shell and the other to the sd-shell can generate higher spins (up to a maximum of $20\,\hbar$). This would be consistent with the description of the prolate ^{24}Mg configuration shown in figure 38, which has a $(0)^4(1)^{12}(2)^4(3)^4$ harmonic oscillator structure. It should be observed at this point that it is not possible to populate the trixial configuration in ^{24}Mg (in this picture) using either ^{16}O or ^{20}Ne cores as starting points. Thus, it might be concluded that the states populated in the two breakup reactions are associated with the prolate minimum/cluster configuration.

The question then arises as to the nature of the resonances that appear in the inelastic scattering measurements. In [152] it was shown that the resonances in the $^{12}C(2^+) + ^{12}C(2^+)$ were associated with an aligned configuration, that is to say with the spins of the two ^{12}C nuclei aligned with their orbital angular momentum, the same conclusion was reached in [154] concerning the $^{12}C(3^-) + ^{12}C(3^-)$ final state. In other words, the oblate planes of the two ^{12}C nuclei are themselves co-planar which would strongly resemble the triaxial structure that appears in figures 26 and 38, and as already noted in [152]. Thus, the inelastic scattering resonances appear to be associated, largely, with the triaxial minimum.

If the present interpretation is correct and the two sets of rotational bands are associated with the prolate and triaxial shape-isomeric minima, then at least one questions remains; why is it the inelastic scattering preferentially samples the triaxial minimum? The coupled channels analysis discussed in [155] suggests that dynamical properties of the scattering of the deformed ^{12}C nuclei, serves to enhance the scattering of the aligned ^{12}C nuclei, such an effect would result in the preferential formation of the triaxial states.

An alternative technique to probe the nature of the resonances and their overlap with structures in ^{24}Mg is via radiative capture; $^{12}C(^{12}C,\gamma)$. The capture reaction was studied extensively by Sandorfi, and others, in the 1980s [157–160]. Gamma-decay to the ^{24}Mg was

recorded and the capture was found to proceed via a number of resonances which can be linked to those found in the spectrum of barrier resonances. The overlap between the structure of the shape isomer and the ground state is likely to be small and thus such decays do not proceed readily. These measurements were performed with low resolution scintillator detectors, but more recently the radiative capture process has been explored with high resolution germanium detectors [161]. These measurements indicate that the $K = 2$ band in ^{24}Mg is more strongly populated than the ground state band in the radiative decay, which can be traced to the larger deformation of the $K = 2$ structure. This is consistent with the suggested large deformation of the cluster band populated in the entrance channel.

Now returning to the discussion of strong and weak coupling. The above picture is what is termed the strong coupling picture, in which the structure of the molecular state is strongly linked to the underlying ^{24}Mg cluster configuration. It should be noted that, for example, the inelastic scattering associated with the $^{12}C_{gs} + ^{12}C(2^+)$ and $^{12}C(2^+) + ^{12}C(2^+)$ final states that the broad structures ($\Gamma = 2$–3 MeV) are fragmented into a series of narrow states. This may be understood in terms of the coupling of the broad quasimolecular band—doorway states—to excited states of the scattering system. In the weak coupling picture the doorway states are associated with a pocket in the potential of the scattering system, and thus the two ^{12}C nuclei couple only weakly to ^{24}Mg. Such ideas form the basis of the band-crossing model [141]. In this description the resonances associated with the pocket in the scattering potential couple most strongly with the aligned inelastic molecular band. Such an approach provides a good description of the experimental data [142]. In the preceding discussion, the broad resonances were associated with a secondary minimum in the ^{24}Mg deformed potential, and the alignment is associated with the intrinsic structure, and the decay channels populated would be those with a strong structural link, i.e. $^{12}C(2^+)$ and $^{12}C(3^-)$.

The appearance of the barrier resonances in the $^{12}C(^{16}O,^{24}Mg^*)$ and $^{12}C(^{20}Ne,^{24}Mg^*)$ reactions links them strongly to an intrinsic ^{24}Mg cluster structure. On the other hand, the series of resonances observed in the inelastic scattering data could exist in either the strong or weak coupling limit. To draw a distinction it would be necessary to observe the resonances in an alternative *reaction* channel. There is of course an experimental difficulty here, in that it is difficult to populate planar states in reactions in which the participants are not planar themselves. Thus, the nature of of the inelastic resonances remains an open question, though the link with the triaxial ^{24}Mg shape isomer is inviting.

As an aside, there was an interesting contribution to the saga of the $^{12}C + ^{12}C$ scattering resonances from Pauling [156]. The nature of structure predicted is one which is described by a point symmetry group (4^-2m) and corresponds to two ^{12}C triangles with their planes orientated at 90° to one another, forming a central *bisphenoid*. In other words, the structure (shown in figure 45) can either be described by two ^{12}C nuclei. Alternatively, it can also be described in terms of a central ^{16}O nucleus with an α-particle located on either side. This is identical to the prolate structure with which the resonances have been identified. This was a prediction which demonstrated a remarkable piece of insight.

7.3.2. Scattering and clusters. The ideas of the two-centre shell model suggest that in principle it should be possible to provide a unified description of both the scattering properties of the cluster-cluster system and from the same interaction potential generate the cluster states of the composite system (see for example the recent review [162]). Such a unification was rather beautifully achieved in the case of the $\alpha + ^{40}$Ca system [163]. In this instance it is important to exclude states in the resultant potential which are forbidden for reasons of Pauli exclusion. In this approach, all states in the common potential are labelled by the quantum number $N = 2n_l + l$. Thus, for ^{40}Ca all of the states up to the closure of the sd-shell are

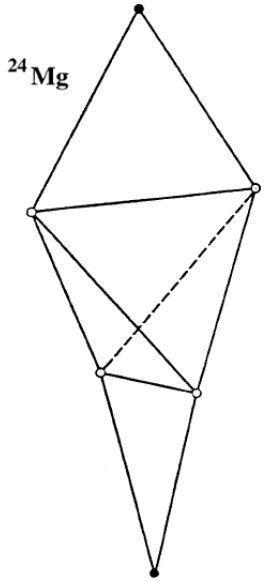

Figure 45. The structure of ^{24}Mg predicted by Pauling [156] to be associated with the ^{12}C + ^{12}C scattering resonances. Reprinted with permission from [156]. Copyright 1973 by the American Physical Society.

occupied ($N = 2$) and consequently states in which 4 nucleons (an α-particle) are added to the sd-shell ($N = 8$) are Pauli-forbidden. The α-particle must thus reside in the fp-shell ($N = 12$). This would then correspond to the ^{44}Ti ground state. The great success of this model was to predict an excited $N = 13, 0^-$, cluster band which was subsequently observed [164]. Such a description is appropriate as both ^{40}Ca and ^{4}He are closed shell nuclei, and thus good cluster candidates. Similarly, good reproduction of experimental properties are found for the $^{8}\mathrm{Be} = \alpha + \alpha$ [167], $^{20}\mathrm{Ne} = {}^{16}\mathrm{O} + \alpha$ [168–171] systems.

In a whole series of experimental measurements (e.g. [165, 166]) of the $^{16}\mathrm{O} + {}^{16}\mathrm{O}$ elastic scattering over a wide range of energies (75–1120 MeV) it has been possible to characterize in detail the scattering potential. This has subsequently permitted the calculation of the properties of the $^{16}\mathrm{O} + {}^{16}\mathrm{O}$ cluster bands within this potential [172]. Once again, the states which are Pauli-forbidden must be excluded which provides the lower limit of $N = 24$ (twice the value of N for ^{16}O ground state—conserving the number of oscillator quanta in the two clusters). Higher nodal bands then correspond to $N = 26, 28, \ldots$, noting that odd values are excluded by the symmetry of the $^{16}\mathrm{O} + {}^{16}\mathrm{O}$ system. The results of these calculations are shown in figure 46. The calculations are compared with the experimental data, and reasonable agreement is found (see [172] for details). The evidence for the superdeformed $N = 24$ is, however, sparse. This band lies close to $E_x = 10$ MeV where there are many candidate states, but no clear identification of a superdeformed band. It should be noted that a similar structure is produced in the AMD calculations [52]. In addition to the scattering resonances, there are a number states observed in cluster breakup reactions, for example $^{12}\mathrm{C}(^{24}\mathrm{Mg},{}^{32}\mathrm{S}[{}^{16}\mathrm{O},{}^{16}\mathrm{O}])\alpha$ [173], which are associated with a $N = 28$ configuration, i.e. a higher nodal excitation of the superdeformed $^{16}\mathrm{O} + {}^{16}\mathrm{O}$ cluster state (figure 47).

In principle, it should also be possible to extend these ideas to scattering systems involving ^{12}C nuclei, though the relatively low-lying first excited state implies that this nucleus is not such an ideal cluster producing a more complex behaviour.

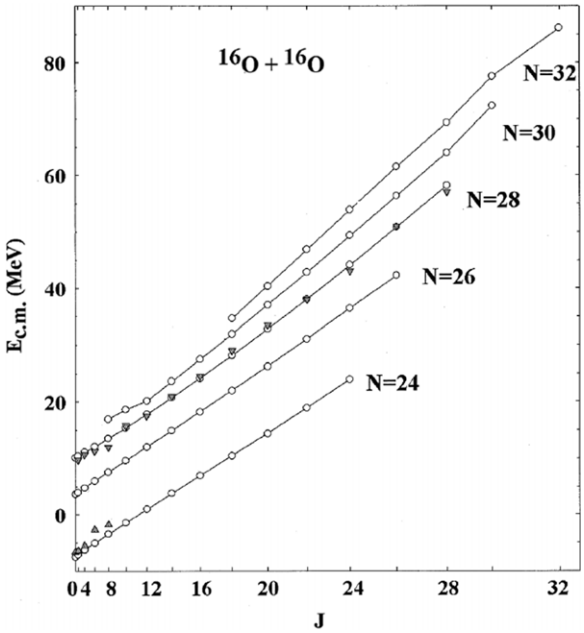

Figure 46. Bands in ^{32}S predicted using the complex scaling method from a ^{16}O + ^{16}O scattering potential. Reprinted with permission from [172]. Copyright 2002 by the American Physical Society.

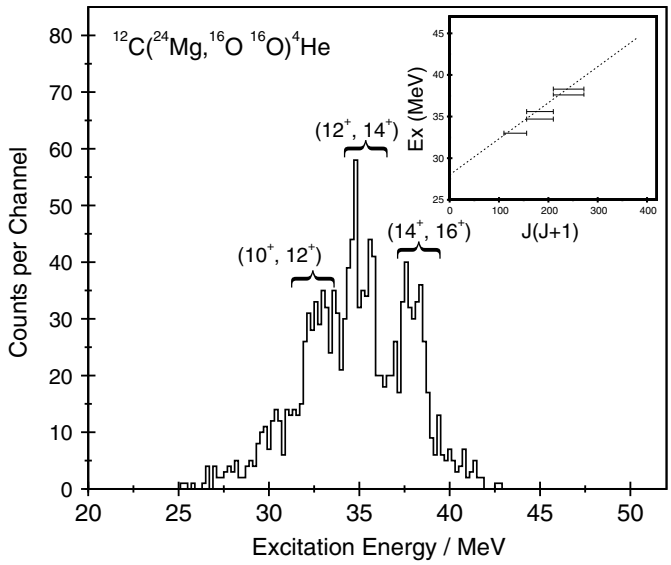

Figure 47. Excitation energy spectrum of states in ^{32}S which decay into two ^{16}O nuclei [173]. These are members of the higher nodal, $N = 28$, band found in figure 46.

7.4. Clustering at the drip-line—cluster islands

The long established traditions of clustering have left some *golden rules*. One of these is that cluster structure typically occurs close to cluster decay thresholds—the Ikeda picture.

Table 4. Neutron and helium cluster decay thresholds in the boron isotopes. Note, the lowest helium decay threshold is given.

	Neutron decay threshold (MeV)	Cluster decay threshold (MeV)	Cluster
^{10}B	8.436	4.459	α
^{11}B	11.453	8.663	α
^{12}B	3.370	10.000	α
^{13}B	4.878	10.816	α
^{14}B	0.969	12.600	α
^{15}B	2.765	13.576	^{6}He
^{16}B	−0.099	14.292	^{6}He
^{17}B	1.901	13.242	^{8}He
^{18}B	−0.899	13.158	^{8}He
^{19}B	0.991	13.138	^{8}He

However, the adventure the field has embarked upon into the territory of neutron-rich nuclei, particularly at the limits of stability—the neutron drip-line, has thrown up some exceptions to these rules. These signal a new type of cluster structure which is yet to be probed, and awaits the development of sufficiently intense beams of nuclei such as ^{19}B. In order to illustrate this point, the decay thresholds for the boron isotopes are listed in table 4. The table shows that, as expected, for more neutron-rich nuclei the neutron decay threshold decreases and at some points becomes negative. The helium cluster decay thresholds, on the other hand, rise, saturating somewhere close to 13–14 MeV. The conclusion that might be reached is that at the drip-line (^{19}B) these nuclei should be well described by the shell model, and that clustering degrees of freedom are only important at higher excitation energies. As has been described earlier, AMD calculations are well suited to describing both the shell model and cluster limits within a single framework. The calculated densities of the odd A boron isotopes are shown in figure 48. The densities, particularly illustrated by those of the protons, reveal that with the addition of neutrons that there is a transition from a compact ^{11}B ground state to one which is highly clustered at the neutron drip-line, ^{19}B. This is a trend which is completely counter intuitive.

Given that the Ikeda picture suggests that clustering should only feature close to the associated cluster decay threshold, which for $^{19}\mathrm{B} = {}^{11}\mathrm{Li}+{}^{8}\mathrm{He}$ [174], then why does clustering appear within the ground state? It is clear that there must be some energetic advantage. The minimization of the energy of such neutron-rich systems is related to two factors [175]. For nuclei with a large neutron excess, e.g. halo nuclei [176, 177], there exists a core of normal nuclear matter with small values of isospin which is embedded in a cloud of less dense valence neutrons which occupy a much larger volume than the core. Neutron matter, on the nuclear scale, is unbound, and thus to maximize the binding of the nucleus the neutron–proton interaction is important. The protons reside within the core, and thus to maximize the n–p overlap the neutrons should spend a significant fraction of their time within the core. However, neutrons within the core Pauli-block occupied orbitals and thus the valence neutrons must occupy higher energy orbits which are energetically unfavoured. Alternatively, if the core deforms, or optimally clusters, then the n–p overlap can be maximized. This process is illustrated by the schematic in figure 49. This is believed to be the driving force in the development of clustering in ^{19}B [175]. It is thus possible that this is the favoured state of nuclear matter close to the neutron drip-line. However, beams of nuclei intense enough to test this hypothesis remain to be developed.

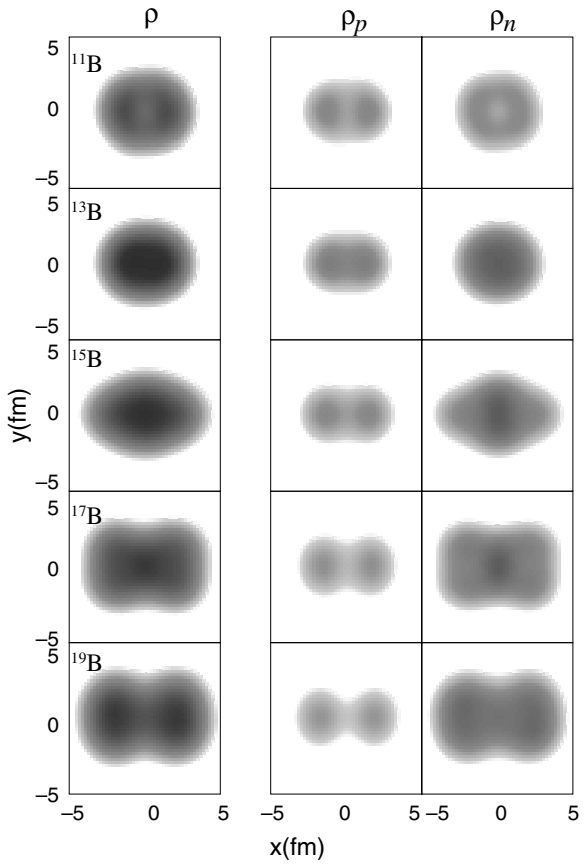

Figure 48. Density distributions of boron isotopes, $^{11-19}$B. The densities of the protons and neutrons as well as their sum, ρ, are shown, from [87].

Nevertheless, some suggestions exist as to how it might be possible to probe the structure of nuclei at the drip-line [174]. AMD calculations in which collisions between ^{13}B and ^{19}B nuclei described by the densities shown in figure 48 and a reaction target show that there is sensitivity to the degree of clustering within the ground states in the coincident breakup cross sections for the two cluster constituents [174]. Motivated by this, a series of measurements of the cluster breakup cross-sections of beryllium, boron and carbon isotopes have been reported [178, 179, 180].

Figure 50 shows the measured cross-sections for the breakup of the isotopes ^{10,11,12,14}Be, from [178]. These are those associated with the neutron decay and cluster (helium) decay. In each case the cross-section is plotted against the number of nucleons detected [A]. What is observed is that the neutron removal cross-sections dominate close to the projectile mass, but the cluster decay increases in importance close to the point at which only two α-particles remain. In these reactions the highest cluster-decay probability is for the system to shed all of its valence neutrons and then the remaining ^{8}Be nucleus decays. The probability that the system cluster decays in the first step (first chance) is comparatively small—corresponding to the much higher decay threshold. The second part of the figure compares the first chance cluster decay cross-sections for the even mass systems (^{11}Be decays to ^{6}He + ^{5}He and is thus not possible to measure the first chance breakup). These cross-sections are, following from

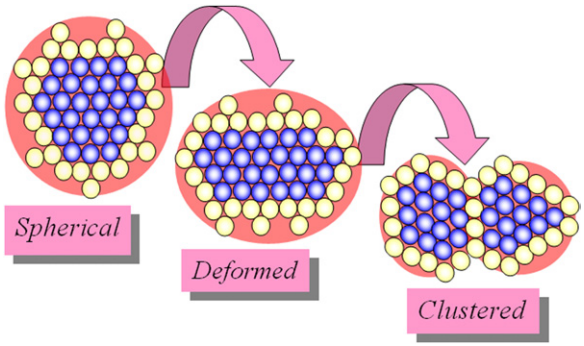

Figure 49. A schematic of the evolution of cluster structure in the ground states of drip-line nuclei. The darker spheres represent nucleons associated with nuclear matter of *normal* isospin, whereas the lighter spheres are the excess valence neutrons. The transition from spherical through deformed to clustered permits a more even distribution of the valence neutrons.

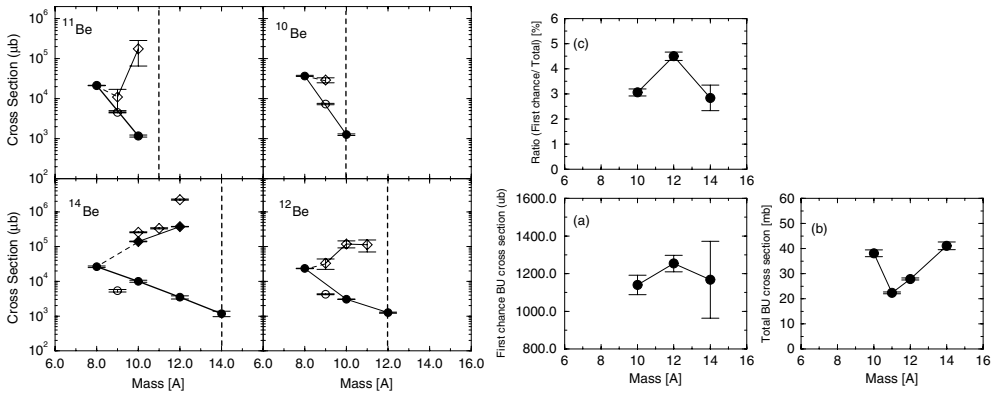

Figure 50. (Left) Neutron removal (◊) and cluster breakup (●) cross-sections for the neutron-rich Be isotopes versus the sum of the mass of the decay fragments [A]. The neutron cross-sections are normalized by dividing by the difference in the number of neutrons between the observed fragment and the projectile. The vertical dotted lines indicate the mass of the projectile. (Right) (*a*) The first-chance cluster breakup cross-sections, i.e. ^{14}Be → ^{6}He + ^{8}He, ^{12}Be → (^{6}He + ^{6}He and ^{4}He + ^{8}He) and ^{10}Be → ^{6}He + ^{4}He, (*b*) the total He + He breakup cross-sections and (*c*) the ratio of the first-chance breakup cross-sections to the total breakup cross-section, versus the mass of the projectile [A], from [178].

the ideas developed for ^{19}B, in principle sensitive to the degree of clustering in the ground state. They appear to demonstrate that the clusterization remains approximately constant from ^{10}Be through to ^{12}Be. In fact, it can be seen that all of the cross-sections for the three systems present the same message.

It is thus interesting to then compare this behaviour with the breakup cross-sections for a nucleus which is not clustered. Figure 51 compares the trends in the cross-sections for the two nuclei ^{14}Be and ^{14}B [179]. From the systematics presented in figure 48 ^{14}B should not have a strongly clustered ground state. For the most part, the cross-sections follow a rather linear relationship between the reaction Q-value and the natural logarithm of the cross-sections. There is one notable exception and that is the breakup of ^{14}Be into ^{8}He + ^{6}He. By comparison, the breakup of ^{14}B into ^{8}Li + ^{6}He is suppressed. This points to the fact that indeed the ^{14}Be nucleus is clustered in the ground state and that there should be an important influence from

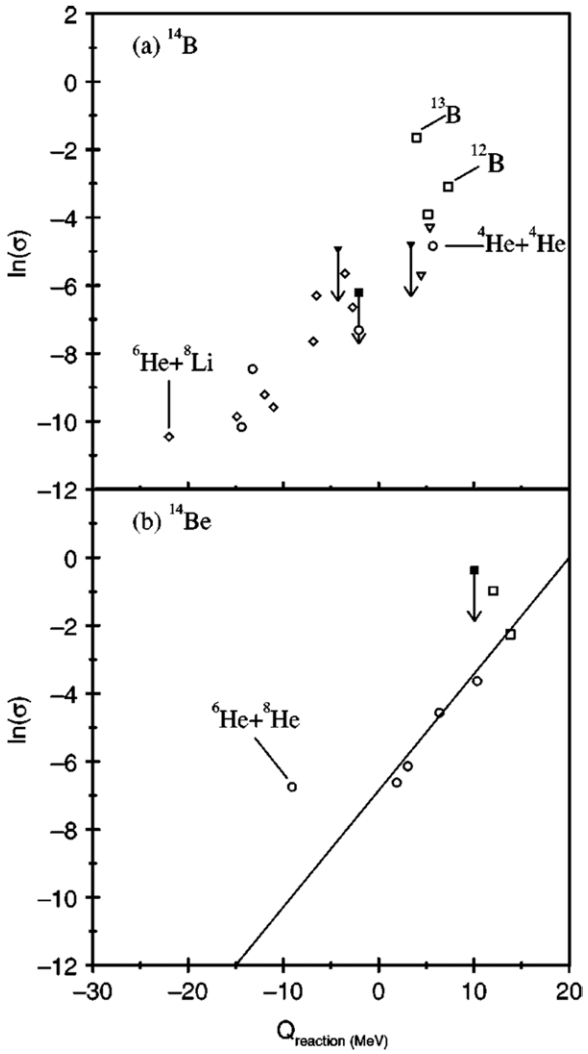

Figure 51. Plot of $\ln(\sigma)$ versus the reaction Q-values for the (*a*) ^{14}B and (*b*) ^{14}Be data. In (*a*) the squares show the neutron removal cross-sections and the triangles the 1p + Xn removal cross-sections. The breakup into ^{x}Li + ^{y}He is indicated by diamonds, and circles represent the ^{x}He + ^{y}He breakup. In (*b*) the neutron removal is shown by squares and the ^{x}He + ^{y}He breakup by circles. Closed symbols indicate cross-section limits with arrows indicating whether the cross-section should lie above or below the limits, from [179].

the $\alpha + 6\mathrm{n} + \alpha$ structure. This is an area which requires further measurements to furnish a better understanding.

The above discussion relates to the neutron drip-line, but there are some intriguing possibilities for proton-rich systems also. The nucleus ^{10}C occupies a rather unique position in the chart of nuclides, as illustrated in figure 52. It resides at the top of a loop of particle-stable nuclei, caused by the presence of two nuclei which are particle unstable in the ground state; ^{9}B and ^{6}Be. The removal of a proton from ^{10}C results in the formation of ^{9}B, which proton decays into ^{8}Be, which in turn decays into two α-particles. In other words, the removal of the proton causes the dissembly of the whole nucleus. Similarly, the

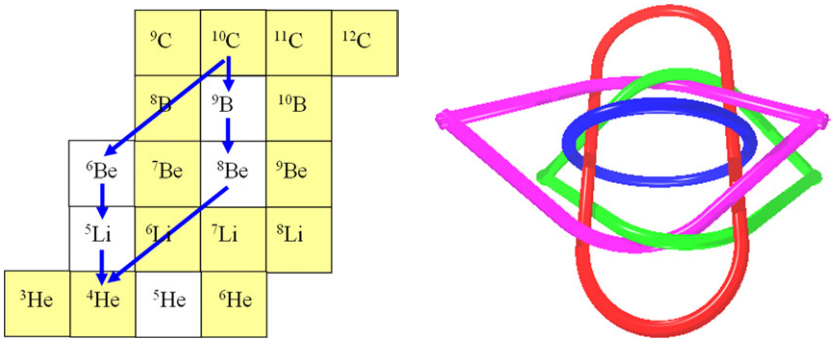

Figure 52. Illustration of the decay properties of excited, unbound, states of ^{10}C. The white squares indicate nuclei which are particle unstable in the ground state, others correspond to either stable nuclei, or those which undergo weak decays. The right-hand part shows the four interlocking rings of the super-Borromean, Brunnian system.

removal of an α-particle produces ^{6}Be, which then decays into 2p + α via an intermediate unbound ^{5}Li ground state. The removal of p–p, α–α or p–α pairs also results in the system 'falling apart'. Nuclei which are composed of three constituents which are all required to bind the system have become known as Borromean, after the symbolic three interlocking Borromean rings [176, 177]. Thus, the ^{10}C nucleus should be termed a super-Borromean nucleus since it has four constituents all of which are required to produce a particle-stable ground state. In fact the Borromean rings are a member of a set of non-trivial mathematical knots which become trivial if any link is broken. These are known as Brunnian knots after the mathematician Brunn [181]. Thus, ^{10}C nucleus corresponds to a class of Brunnian nuclei. The symbolic four interlocking rings representing the structure of ^{10}C are shown in figure 52.

Studies of the cluster structure of this system are likely to be extremely important in constraining many-body components of the nuclear force. More broadly, our understanding of the structure of nuclear matter at and beyond the drip-lines is likely to grow dramatically over the coming years with the new radioactive beam facilities in Japan and Europe coming on-line. It is probable that the ideas relating to clustering, developed here, will play an important role in determining the nature of of matter in the extremes where dilute states will feature large.

8. Outlook—the future

Although the topic of clustering is a rather mature one, it still is one which presents many future challenges. As noted throughout the review there are many open questions and topics which require both experimental and theoretical resolution. Among these are the question as to the nature of the Hoyle-state. It appears to be a cluster state, but what is the structure (traditional cluster or condensate) where is the 2^+ state, does a collective excitation exist? Another vital topic relates to molecular structures. The existence of hyperdeformed chain-structures in the carbon isotopes stabilized by covalent neutrons needs to be clearly experimentally demonstrated. The structure of matter at the drip-lines is a topic which concerns not only nuclear clustering but excites the field in general. However, it is entirely possible that clustering plays a central role in the subject—this remains to be demonstrated at future radioactive beam facilities. Then there is always the possibility at such facilities that some completely unexpected cluster modes will be discovered.

Acknowledgments

The ideas developed in this review were strongly influenced by many people I have had the great fortune to work with over the years, in particular Bill Rae and Wolfram von Oertzen. Many of the experimental developments are the result of the efforts of my collaborators within the Charissa and DEMON collaborations and thus they are owed a large debt of gratitude.

References

[1] Peacock J A *et al* 2001 *Nature* **410** 169
[2] Brink D M and Castro J J 1973 *Nucl. Phys.* A **216** 109
[3] Zhang J and Rae W D M 1993 *Nucl. Phys.* A **564** 252
[4] Wiringa R B, Pieper S C, Carlson J and Pandharipande V R 2000 *Phys. Rev.* C **62** 014001
[5] Hafstad L R and Teller E 1938 *Phys. Rev.* **54** 681
[6] Brink D M 1966 *Proc. Int. School of Physics 'Enrico Fermi' (Varenna, 1965)* Course 36, ed C Bloch (New York: Academic) p 247
[7] Morinaga H 1956 *Phys. Rev.* **101** 254
[8] Ikeda K, Tagikawa N and Horiuchi H 1968 *Prog. Theor. Phys.* (Suppl.) extra number, 464
[9] Bohr A and Mottelson B R 1975 *Nuclear Structure* vol 2 (Reading, MA: Benjamin)
[10] Nazarewicz W and Dobaczewski J 1992 *Phys. Rev. Lett.* **68** 154
[11] Ripka G 1968 *Advances in Nuclear Physics* ed M Baranger and E Vogt (New York: Plenum) vol 1 p 183
[12] Mottelson B 1958 *The Many Body Problem* (New York: Wiley)
[13] Bengtsson T, Faber M E, Leander G, Moller P, Ploszajczak M, Ragnarsson I and Aberg S 1981 *Phys. Scr.* **24** 200
[14] Rae W D M 1988 *Int. J. Mod. Phys.* **3** 1343
[15] Freer M, Betts R R and Wuosmaa A H 1995 *Nucl. Phys.* A **587** 36
[16] Seya M, Kohno M and Nagata S 1981 *Prog. Theor. Phys.* **65** 204
[17] von Oertzen W 1996 *Z. Phys.* A **354** 37
[18] von Oertzen W 1997 *Z. Phys.* A **357** 355
von Oertzen W 1997 *Nuovo Cimento* A **110** 895
[19] Itagaki N and Okabe S 2000 *Phys. Rev.* C **61** 044306
[20] Peierls R E and Yoccoz J 1957 *Proc. Phys. Soc. Lond.* A **70** 381
[21] Blatt J M 1960 *Aust. Math. Soc.* **1** 465
[22] Bauhoff W, Schultheis H and Schultheis R 1984 *Phys. Rev.* C **29** 1046
[23] Aberg S, Ragnarsson I, Bengtsson T and Sheline R 1982 *Nucl. Phys.* A **391** 327
[24] Krieger S J 1969 *Phys. Rev. Lett.* **22** 97
[25] Reid N E, Davison N E and Svenne J P 1974 *Phys. Rev.* C **9** 1882
[26] Buck B, Dover C B and Vary J P 1975 *Phys. Rev.* C **11** 1803
[27] Chevallier P, Scheibling F, Goldring G, Plesser I and Sachs M W 1967 *Phys. Rev.* **160** 827
[28] Brochard F, Chevallier P, Disdier D, Rauch V, Rudolf G and Scheibling F 1976 *Phys. Rev.* C **13** 967
[29] Freer M *et al* 1995 *Phys. Rev.* C **51** 1682
[30] Freer M *et al* 2004 *Phys. Rev.* C **70** 064311
[31] Betts R R 1994 *Proc. 6th Int. Conf. on Cluster in Nuclear Structure and Dynamics (Strasbourg)*
[32] Bromley D A 1985 *Proc. 4th Int. Conf. on Clustering Aspects of Nuclear Structure and Nuclear Reactions (Chester, UK)* vol 1 ed J S Lilley and M A Nagarajan (Dordrecht: Reidel)
[33] Buck B, Johnston J C, Merchant A C and Perez S M 1995 *Phys. Rev.* C **52** 1840
[34] Horiuchi H and Ikeda K 1968 *Prog. Theor. Phys.* A **40** 277
[35] Butler P A and Nazarewicz W 1996 *Rev. Mod. Phys.* **68** 350
[36] Kanada En'yo Y and Horiuchi H 1995 *Prog. Theor. Phys.* **93** 115
[37] Tomoda T and Arima A 1978 *Nucl. Phys.* A **303** 217
[38] Sanders S J, Martz L M and Parker P D 1979 *Phys. Rev.* C **20** 1743
[39] Hindi M M, Thomas J H, Radford D C and Parker P D 1983 *Phys. Rev.* C **27** 2902
[40] Erb K A and Bromley D A 1985 *Treatise on Heavy-Ion Science* vol 3 ed D A Bromley (New York: Plenum)
[41] Cormier T M 1982 *Annu. Rev. Nucl. Part. Sci.* **32** 271
[42] Eberhard K A (ed) 1982 *Resonances in Heavy Ion Reactions* (Berlin: Spinger) p 448
[43] Gerace W J and Green A M 1967 *Nucl. Phys.* A **93** 110
[44] Gerace W J and Green A M 1969 *Nucl. Phys.* A **123** 241

[45] Ideguchi E *et al* 2001 *Phys. Rev. Lett.* **87** 222501
[46] Chiara C J *et al* 2003 *Phys. Rev.* C **67** 041303
[47] Zheng D C, Berdichevsky D and Zamick L 1988 *Phys. Rev. Lett.* **60** 2262
[48] Zheng D C, Berdichevsky D and Zamick L 1988 *Phys. Rev.* C **38** 437
[49] Zheng D C, Berdichevsky D and Zamick L 1990 *Phys. Rev.* C **42** 1004
[50] Leander G and Larsson S E 1975 *Nucl. Phys.* A **239** 93
[51] Kanada-En'yo Y and Kimura M 2005 *Phys. Rev.* C **72** 064322
[52] Kimura M and Horiuchi H 2004 *Phys. Rev.* C **69** 051304
[53] Harvey M 1975 *Proc. 2nd Int. Conf. on Clustering Phenomena in Nuclei (College Park) USDERA Report* ORO–4856–26 p 549
[54] Eisenberg J M and Greiner W 1972 *Microscopic Theory of the Nucleus* vol 3 (North-Holland) p 426
[55] Freer M 2003 *C. R. Phys.* **4** 475
[56] Bohlen H G, von Oertzen W, Blazevic A, Gebauer B, Milin M, Kokalova T, Schulz Ch, Thummerer S and Tumino A 2002 *Proc. Int. Symp. on Exotic Nuclei (Lake Baikal, Russia, 2001)* ed Yu E Penionzhkevich and E A Cherepanov (Singapore: World Scientific) p 453
[57] McEwan P and Freer M 2004 *J. Phys. G: Nucl. Part. Phys.* **30** 1
[58] Feynman R *The Feynman Lectures in Physics* vol 3 (Reading, MA: Addison Wesley) chapter 10 and 11
[59] Marenau H 1941 *Phys. Rev.* C **59** 37
[60] Marsh S and Rae W D M 1986 *Phys. Lett.* B **180** 185
[61] Merchant A C and Rae W D M 1992 *Nucl. Phys.* A **549** 431
[62] Zhang J, Rae W M D and Merchant A C 1994 *Nucl. Phys.* A **575** 61
[63] Brink D M 1967 *Nucl. Phys.* A **91** 1
[64] Wheeler J A 1937 *Phys. Rev.* **52** 1083
Wheeler J A 1937 *Phys. Rev.* **52** 1107
[65] Hill D L and Wheeler J A 1953 *Phys. Rev.* **89** 1102
[66] Griffin J J and Wheeler J A 1957 *Phys. Rev.* **108** 311
[67] Wildermuth K and McClure W 1966 Cluster representations of nuclei *Springer Tracts in Modern Physics* vol 41 (Berlin: Springer)
[68] Wildermuth K and Tang Y C 1977 *A Unified Theory of the Nucleus* (New York: Academic)
[69] Arima A, Horiuchi H, Kubodera K and Takigawa N 1972 *Advances in Nuclear Physics* vol 5 ed M Baranger and E Vogt (New York: Plenum) p 345
[70] Furutani H, Kanada H, Kaneko T, Nagata S, Nishioka H, Okabe S, Saito S, Sakuda T and Seya M 1980 *Prog. Theor. Phys.* (Suppl.) **68** 193
[71] Tang Y C, LeMere M and Thompson D R 1978 *Phys. Rep.* **47** 167
[72] Langanke K and Friedrich H 1987 *Advances in Nuclear Physics* vol 17 ed J W Negele and E Vogt (New York: Plenum) p 223
[73] Langanke K 1994 *Advances in Nuclear Physics* vol 21 ed J W Negele and E Vogt (New York: Plenum) p 85
[74] Baye D and Heenen P-H 1974 *Nucl. Phys.* A **233** 304
[75] Baye D, Heenen P-H and Liebert-Heinemann M 1977 *Nucl. Phys.* A **291** 230
[76] Baye D and Descouvement P 1988 *Proc. 5th Int. Conf. Clustering Aspects in Nuclear and Subnuclear Systems (Kyoto, Japan, 25–29 July 1988)* ed K Ikeda *et al*
Baye D and Descouvement P 1989 *J. Phys. Soc. Japan* (Suppl.) **58** 103
[77] Baye D 1994 *Proc. 6th Int. Conf. on Clusters in Nuclear Structure and Dynamics (Strasbourg, France, 6–9 September 1994)* ed F Haas p 259
[78] Descouvement P 2002 *Nucl. Phys.* A **699** 463
[79] Itagaki N *et al* 2001 *Phys. Rev.* C **64** 014301
[80] Itagaki N, Hirose S, Otsuka T, Okabe S and Ikeda K 2002 *Phys. Rev.* C **65** 044302
[81] Itagaki N and Okabe S 2000 *Phys. Rev.* C **61** 044306
[82] Itagaki N, Okabe S and Ikeda K 2000 *Phys. Rev.* C **62** 034301
[83] Ito M 2006 *Phys. Lett.* B **636** 293
[84] Itagaki N, von Oertzen W and Okabe S 2006 *Phys. Rev.* C **74** 067304
[85] von Oertzen W, Freer M and Kanada En'yo Y 2006 *Phys. Rep.* **432** 43
[86] Landau L D and Lifshitz E M 1958 *Quantum Mechanics* 3rd edn (Amsterdam: Elsevier)
Nakamura H 2000 *Nonadiabatic Transition* (Singapore: World Scientific) and references therein
[87] Kanada-En'yo Y and Horiuchi H 2001 *Prog. Theor. Phys.* **142** 205
[88] Fulton B R and Rae W D M 1990 *J. Phys. G: Nucl. Part. Phys.* **16** 333
[89] Nilsson S G 1955 *Mat. Fys. Medd. Dan. Vid. Selsk.* **29**
[90] Flocard H , Heenen P-H, Krieger S J and Weiss M S 1984 *Prog. Theor. Phys.* **72** 1000

[91] Cugnon J, Dombre H and Flocard H 1979 *Nucl. Phys.* A **331** 213
[92] Freer M and Merchant A C 1997 *J. Phys. G: Nucl. Part. Phys.* **23** 261
[93] Milin M and von Oertzen W 2002 *Eur. Phys. J.* A **14** 295
[94] Navrátil P, Vary J P and Barrett B R 2000 *Phys. Rev. Lett.* **84** 5728
[95] Kanada-En'yo Y 1998 *Phys. Rev. Lett.* **81** 5291
[96] Itagaki N, Masui H, Ito M and Aoyama S 2005 *Phys. Rev.* C **71** 064307
[97] Itagaki N, Aoyama S, Okabe S and Ikeda K 2004 *Phys. Rev.* C **70** 054307
[98] Masui H and Itagaki N 2007 *Phys. Rev.* C **75** 054309
[99] Chernykh M, Feldmeier H, Neff T, von Neumann-Cosel P and Richter A 2007 *Phys. Rev. Lett.* **98** 032501
[100] Roth R, Neff T, Hergert H and Feldmeier H 2004 *Nucl. Phys.* A **745** 3
[101] Hoyle F 1954 *Astrophys. J.* (Suppl.) **1** 12
[102] de Takacsy N and das Gupta S 1970 *Phys. Lett.* B **33** 556
[103] Friedrich H, Satpathy L and Weiguny A 1971 *Phys. Lett.* B **36** 189
[104] de Takacsy N 1972 *Nucl. Phys.* A **178** 469
[105] Tohsaki A, Horiuchi H, Schuck P and Röpke G 2001 *Phys. Rev. Lett.* **87** 192501
[106] Funaki Y, Tohsaki A, Horiuchi H, Schuck P and Röpke G 2003 *Phys. Rev.* C **67** 051306
[107] Yamada T and Schuck P 2004 *Phys. Rev.* C **69** 024309
[108] Röpke G and Schuck P 2006 *Mod. Phys. Lett.* A **21** 2513
[109] Funaki Y, Tohsaki A, Horiuchi H, Schuck P and Ropke G 2006 *Eur. Phys. J.* A **28** 259
[110] Sick I and McCarthy J S 1970 *Nucl. Phys.* A **150** 631
Nakada A, Torizuka Y and Horikawa Y 1971 *Phys. Rev. Lett.* **27** 745
Nakada A, Torizuka Y and Horikawa Y 1971 *Phys. Rev. Lett.* **27** 1102 (erratum)
Strehl P and Schucan Th H 1968 *Phys. Lett.* B **27** 641
[111] Gnilozub I A, Kurgalin S D and Tchuvil'sky Yu M 2007 *Nucl. Phys.* A **790** 687c
[112] Itoh M *et al* 2004 *Proc. 8th Int. Conf. on Clustering Aspects of Nuclear Structure and Dynamics, (Nara, Japan, 2003)* ed K Ikeda *et al Nucl. Phys.* A **738** 268
[113] Fynbo H O U *et al* 2005 *Nature* **433** 136
[114] Funaki Y, Tohsaki A, Horiuchi H, Röpke G and Schuck P 2006 *Mod. Phys. Lett.* A **21** 2331
[115] Kawabata T *et al* 2007 *Phys. Lett.* B **646** 6
[116] von Oertzen W and Bohlen H G 2003 *C. R. Phys.* **4** 465
[117] Bohlen H G *et al* 2007 *Phys. Rev.* C **75** 054604
[118] Kanada-En'yo, Horiuchi H and Dóte A 1998 *J. Phys. G: Nucl. Part. Phys.* **24** 1499
[119] Kanada-En'yo Y, Horiuchi H and Doté A 1999 *Phys. Rev.* C **60** 064304
[120] Liendo J A *et al* 2002 *Phys. Rev.* C **65** 034317
[121] Curtis N *et al* 2001 *Phys. Rev.* C **64** 044604
[122] Milin M *et al* 2005 *Nucl. Phys.* A **753** 263
[123] Freer M *et al* 2006 *Phys. Rev. Lett.* **96** 042501
[124] Axelsson L *et al* 1996 *Phys. Rev.* C **54** 1511
[125] Shimoura S *et al* 2003 *Phys. Lett.* B **560** 31
[126] Korsheninnikov A A *et al* 1995 *Phys. Lett.* B **343** 53
[127] Freer M *et al* 1999 *Phys. Rev. Lett.* **82** 295
[128] Saito A *et al* 2002 *Proc. Int. Symp. on Clustering Aspects of Quantum Many-body Systems (Kyoto, 2001)* ed A Ohnishi *et al* (Singapore: World Scientific) p 39
Saito A *et al* 2001 *RIKEN Accelerator Progress Report* p 55
Saito A *et al* 2002 *Prog. Theor. Phys.* (Suppl.) **146** 615
Saito A *et al* 2004 *Nucl. Phys.* A **738** 337
[129] von Oertzen W *et al* 2004 *Eur. Phys. J.* A **21** 193
[130] Itagaki N, Otsuka T, Ikeda K and Okabe S 2004 *Phys. Rev. Lett.* **92** 014301
[131] von Oertzen W 2001 *Eur. Phys. J.* A **11** 403
[132] Kimura M 2007 *Phys. Rev.* C **75** 034312
[133] Kanada En'yo Y and Horiuchi H 1995 *Prog. Theor. Phys.* **93** 115
[134] Cindro N 1981 *Riv. Nuovo Cimento* **4** 1
[135] Cindro N 1988 *Ann. Phys. Fr.* **13** 289
[136] Pollikanov S M *et al* 1962 *J. Expt. Theor. Phys. USSR* **42** 1464
Pollikanov S M *et al* 1962 *Sov. Phys. JETP* **15** 1016 (Engl. Transl.)
[137] Erb K A and Bromley D A 1981 *Phys. Rev.* C **23** 23
[138] Cosman E R *et al* 1975 *Phys. Rev. Lett.* **35** 265

[139] Goldberg V Z *et al* 2000 *Phys. At. Nucl.* **63** 1518
[140] Källman K-M, Brenner M, Goldberg V Z, Lönnroth T, Manngøard P, Pakhomov A E and Pankratov V V 2003 *Eur. Phys. J.* A **16** 159
[141] Abe Y 1978 Nuclear molecular phenomena *Proc. Int. Conf. on Resonances in Heavy Ion Reactions* ed N Cindro (Amsterdam: North-Holland) p 211
[142] Kondo Y, Abe Y and Matsuse T 1979 *Phys. Rev.* C **19** 1356
[143] Fulton B R *et al* 1991 *Phys. Lett.* B **267** 325
[144] Curtis N *et al* 1995 *Phys. Rev.* C **51** 1554
[145] Erb K A, Betts R R, Hindi M M, Korotky S K, Tung P P, Sachs M W, Willett S T and Bromley D A 1980 *Phys. Rev.* C **22** 507
[146] Voit H, Glaster W, Treu W, Flöhlich H and Dück P 1977 *Phys. Lett.* B **67** 399
[147] Freer M *et al* 1998 *Phys. Rev.* C **57** 1277
[148] Metelko C J *et al* 2003 *Phys. Rev.* C **68** 054321
[149] Bremner C A *et al* 2002 *Phys. Rev.* C **66** 034605
[150] Cormier T M, Jachcinski C M, Berkowitz G M, Braun-Munzinger P, Cormier P M, Gai M, Harris J W, Barrette J and Wegner H E 1978 *Phys. Rev. Lett.* **40** 924
[151] Freer M, Murgatroyd J T, Singer S M, Curtis N, Henderson D J, Hofman D J and Wuosmaa A H 2001 *Phys. Rev.* C **63** 034317
[152] Konnerth D *et al* 1985 *Phys. Rev. Lett.* **55** 588
[153] Morsad A, Haas F, Beck C and Freeman R M 1991 *Z. Phys.* A **338** 61
[154] Chappell S P G and Rae W D M 1996 *Phys. Rev.* C **53** 2879
[155] Boztosun I and Rae W D M 2001 *Phys. Rev.* C **63** 054607
[156] Pauling L 1973 *Phys. Rev. Lett.* **35** 1480
[157] Sandorfi A M 1985 *Treatise on Heavy Ion Science* vol 2 ed D A Bromley (New York: Plenum) section 3 and references therein
[158] Nathan A M, Sandorfi A M and Bowles T J 1981 *Phys. Rev.* C **24** 932
[159] Sandorfi A M and Nathan A M 1978 *Phys. Rev. Lett.* **40** 1252
[160] Dechant B and Kuhlmann E 1988 *Z. Phys.* A **330** 93
[161] Jenkins D G *et al* 2005 *Phys. Rev.* C **71** 041301
[162] Khoa D T, von Oertzen W, Bohlen H G and Ohkubo S 2007 *J. Phys. G: Nucl. Part. Phys.* **34** 111
[163] Michel F, Reidemeister G and Ohkubo S 1986 *Phys. Rev. Lett.* **57** 1215
[164] Yamada T *et al* 1990 *Phys. Rev.* C **42** 1935
[165] Nicoli M P *et al* 1999 *Phys. Rev.* C **60** 064608
[166] Khoa D T *et al* 2000 *Nucl. Phys.* A **672** 387
[167] Buck B, Friedrich H and Wheatley C J 1977 *Nucl. Phys.* A **275** 246
[168] Buck B, Dover C B and Vary J P 1975 *Phys. Rev.* C **11** 1803
[169] Buck B and Rubio J A 1984 *J. Phys. G: Nucl. Part. Phys.* **10** L209
[170] Buck B, Merchant A C and Perez S M 1995 *Phys. Rev.* C **51** 559
[171] Buck B, Johnston J C, Merchant A C and Perez S M 1995 *Phys. Rev.* C **52** 1840
[172] Ohkubo S and Yamashita K 2002 *Phys. Rev.* C **66** 021301
[173] Curtis N *et al* 1996 *Phys. Rev.* C **53** 1804
[174] Takemoto H, Horiuchi H and Ono A 2001 *Phys. Rev.* C **63** 034615
[175] Horiuchi H 2000 *Proc. 7th Int. Conf. on Clustering Aspects of Nuclear Structure and Dynamics* (Singapore: World Scientific) p 405
[176] Riisager K 1994 *Rev. Mod. Phys.* **66** 1105
[177] Jensen A S, Riisager K, Fedorov D V and Garrido E 2004 *Rev. Mod. Phys.* **76** 215
[178] Ashwood N I *et al* 2004 *Phys. Lett.* B **580** 129
[179] Ashwood N I *et al* 2004 *Phys. Rev.* C **70** 064607
[180] Ashwood N I *et al* 2004 *Phys. Rev.* C **70** 024608
[181] Brunn H 1892 Über Verkettung *S.-B. Math.—Phys. Kl. Bayer Akad. Wiss.* **22** 77